

David Francisco Camarena Torres

The tension between global and local
determinations of the Hubble constant in the
presence of a non-standard dark energy

Brasil

2017, v-1.9.6

David Francisco Camarena Torres

**The tension between global and local determinations of
the Hubble constant in the presence of a non-standard
dark energy**

Dissertação apresentada ao Programa de Pós-Graduação em Física da Universidade Federal do Espírito Santo, como requisito para obtenção do grau de mestre em Física.

Universidade Federal do Espírito Santo –UFES

Centro de Ciências Exatas – CCE

Programa de Pós-Graduação em Física – PPGFIS

Supervisor: Valerio Marra

Brasil

2017, v-1.9.6

David Francisco Camarena Torres

**The tension between global and local determinations of
the Hubble constant in the presence of a non-standard
dark energy**

Dissertação apresentada ao Programa de Pós-Graduação em Física da Universidade Federal do Espírito Santo, como requisito para obtenção do grau de mestre em Física.

Orientador

Dr. Valerio Marra

Professor

Dr. Miguel Boavista Quartin

Professor

Dr. Oliver Fabio Piattella

Professor

Dr. Wiliam Hipólito Ricaldi

Brasil

2017, v-1.9.6

The scientist does not study nature because it is useful to do so. He studies it because he takes pleasure in it, and he takes pleasure in it because it is beautiful. If nature were not beautiful it would not be worth knowing, and life would not be worth living.

Henri Poincaré

Abstract

There is a 3.4σ tension between local and global measurements of the Hubble constant H_0 provided by observations of SNe Ia [1] and CMB [2], respectively. This tension cannot be totally explained by the concordance ΛCDM model and could be produced by unknown systematics on the calibration of the cosmic distance ladder or CMB analysis. However, in the absence of these systematics, the tension could be a hint for physics beyond the ΛCDM model. On the other hand, it is well known that the linear perturbation theory predicts a cosmic variance on the Hubble parameter H_0 , produced by peculiar velocities and local structures, which leads to systematic errors on local determinations of H_0 . Here, we consider this cosmic variance, predicted by linear perturbation theory, in a presence of a non-standard dark energy, in order to compute the systematic error on the local Hubble rate. Non-standard dark energy models are represented by the coupled quintessence models and the γ CDM, γw CDM and γ_a CDM parametrizations. Then, we include this systematic error in the Bayesian statistical analysis that uses CMB, BAO, SNe Ia, RSD and H_0^{local} data. Thus, we show the effect of the cosmic variance on the cosmological constraints and the tension problem. Finally, we accomplish the model selection using the AIC and BIC criteria and also show how the systematic error provided for the models of non-standard dark energy could help to alleviate the current tension in determinations of H_0 .

Keywords: dark energy, observational cosmology, Hubble constant, statistical analysis.

Resumo

Existe uma tensão ao redor de 3.4σ entre as determinações globais e locais da constante de Hubble H_0 fornecidas por observações de supernovas de tipo Ia [1] e da radiação cósmica de fundo [2], respectivamente. Esta tensão não pode ser explicada pelo modelo de concordança Λ CDM e ela poderia ser produzida por erros sistemáticos desconhecidos na calibração da escadaria cósmica ou na análise da radiação cósmica de fundo. Contudo, na ausência destes erros, a tensão poderia ser uma sugestão da existência de física além do modelo Λ CDM. Por outro lado, é bem sabido que a teoria linear de perturbações prevê uma variância cósmica sobre o parâmetro de Hubble H_0 , produzida pelas velocidades peculiares e estruturas locais, que conduz a um erro sistemático na determinações locais de H_0 . No presente trabalho, nós consideramos a variância cósmica, prevista pela teoria de perturbações lineares, na presença de uma energia escura não padrão, com o fim de calcular o erro sistemático sobre a taxa de Hubble local. A energia escura não padrão é representada pelo modelo de quintessência e pelas parametrizações γ CDM, γw CDM e γ_a CDM. Logo, nós incluímos o erro sistemático na análise estatística Bayesiana que usa dados da radiação cósmica de fundo, oscilações acústicas dos bárions, supernovas de tipo Ia, distorções no espaço de redshift e H_0^{local} . Assim, nós mostramos o efeito da variância cósmica na determinação de parâmetros cosmológicos e o problema de tensão. Finalmente, nós realizamos a seleção de modelos usando os critérios de seleção AIC e BIC e também mostramos como o erro sistemático, fornecido pelos modelos de energia escura não padrão, poderia ajudar a aliviar a atual tensão nas determinações de H_0 .

Palavras-chave: energia escura, cosmologia observational, constante de Hubble, análise estatística.

List of Figures

Figure 1 – Hubble diagram from [3].	29
Figure 2 – Λ CDM show a good agreement with cosmological data, in this cases data corresponding to SNe Ia, BAO and CMB. One can see that inference about cosmological parameters, $\Omega_\Lambda = \Omega_m$, are in concordance to experiments of different nature. Although this figure does not correspond to recently analysis, it is useful to illustrated concordance in Λ CDM. This figure is from [4].	30
Figure 3 – Background evolution of dark energy Ω_Λ , cold dark matter Ω_c , baryons Ω_b and radiation Ω_r in a Λ CDM universe. Vertical line point out the equivalence redshift, here $z_{eq} \sim 3370$	34
Figure 4 – Left panel: Hubble rate as function of redshift (or scale factor) to Λ CDM model. Right panel: Deceleration parameter on function of z (or a). The vertical and horizontal dashed line indicate when the deceleration becomes negative, in this case is estimated $z \sim 0.643$	35
Figure 5 – Sound velocity c_s^2 and w_{ef} for a matter-radiation fluid. Red dotted lines are the values $w_r = 1/3$ and $w_m = 0$. It is easy to note that during the transition between radiation-dominated and matter-dominated epoch $c_s^2 \neq w$	42
Figure 6 – Top panel: Background dynamics for $\alpha = 0.1$. Solid lines represent the case with weak coupling $\beta = 0.05$, while dashed lines the case with strong coupling $\beta = 0.25$. Bottom panel: Background dynamics for $\alpha = 0.08$. Solid lines represent the case with weak coupling $\beta = 0.05$, while dashed lines the one with strong coupling $\beta = 0.25$. In both cases a vertical line is placed at z_{eq} . See the text for more details.	47
Figure 7 – Left panel: Hubble rate as function of redshift for the CQ model, with $\alpha = 0.08$. Right panel: Deceleration parameter as a function of z for the same CQ model. The vertical and horizontal dashed lines indicate when the deceleration becomes negative, in this case at $z \sim 0.652$ for $\beta = 0.25$ and $z \sim 0.652$ for $\beta = 0.05$. In both cases solid lines correspond to weak coupling $\beta = 0.05$ and dashed lines to strong coupling $\beta = 0.25$	49
Figure 8 – Cosmic growth index γ as a function of w_{de} , see equation (2.24), for different values of Ω_m	51
Figure 9 – Relative difference in γ when using (2.24) with $\Omega_m = 1$ and $\Omega_m = 0.7$	52
Figure 10 – Gaussian distributions for both measurements of the Hubble constant, H_0^{Pl} (CMB) and H_0^{R16} (SNe Ia). The discordance between them is evident.	54

Figure 11 – A historical review of H_0 values and their error bars for different experiments. Note that the large increase in precession has unveiled the tension between local and global measurements. This figure is from [5].	55
Figure 12 – The observer is located at \vec{r}_i . (S)he measures the velocity of a star at \vec{r}_j , which has the peculiar velocity \vec{v}_j . The velocity measured by the observer is always parallel to the line of sight $\vec{r}_j - \vec{r}_i$ and it will be composed by both the recession velocity $H_0 \vec{r}_j - \vec{r}_i $ and the contribution of the peculiar velocity $\vec{v}_j \cdot (\vec{r}_j - \vec{r}_i) / \vec{r}_j - \vec{r}_i $.	58
Figure 13 – Deviation of H_0^{loc}/H_0 as a function of scales (or redshift). One can note that, as expected, the variance decreases at higher redshifts, at which the contribution of peculiar velocities becomes less important.	60
Figure 14 – Deviation of H_0^{loc}/H_0 as a function of scales in the CQ model, with $\alpha = 0.08$, for weak ($\beta = 0.05$) and strong ($\beta = 0.25$) coupling.	62
Figure 15 – Systematic error produced by cosmic variance in the CQ context, with $\alpha = 0.08$, as function of β .	62
Figure 16 – Deviation of H_0^{loc}/H_0 as a function of scales for different values of γ .	63
Figure 17 – Deviation of H_0^{loc}/H_0 as a function of scales for different values of w_{de} .	64
Figure 18 – Systematic error produced by cosmic variance as a function of γ and for different values of w_{de} . Note, that here we have used the common parametrization for the growth rate $f(z)$.	65
Figure 19 – Cartoon illustrating one of the differences between Bayesian and frequentist inference: inclusion of prior. This cartoon is from < https://twitter.com/RevBayes >.	66
Figure 20 – The temperature power spectrum of the CMB. Blue dots are data while the red line is a theoretical prediction according to the Λ CDM model. This figure is from [6].	70
Figure 21 – Correlation function of baryons measured from a sample of 46,748 luminous red galaxies from Sloan Digital Sky Survey. BAO show up as a peak in the correlation function, here it is located at $100h^{-1}$ Mpc. The different lines represent different cosmology. This figure corresponds to first observation of the BAO peak and it is from [7].	72
Figure 22 – Compilation of $f\sigma_8(z)$ data from [8]. Note that current RSD data is quite imprecise as it is shown by the error bars. A dashed red line corresponds to a theoretical prediction of fiducial Λ CDM model.	75
Figure 23 – This picture is from < https://www.nasa.gov/image-feature/goddard/2016/three-steps-to-measuring-the-hubble-constant >	77

Figure 24 – **Top:** Functions $f(z)$ and $f\sigma_8(z)$ predicted for the different cosmologies when the best fit provided by $\chi^2_{H_0}$ without $\sigma_{\delta H}$ is used. **Bottom:** Functions $f(z)$ and $f\sigma_8(z)$ predicted for the different cosmologies when the best fit provided by $\chi^2_{H_0}$ with $\sigma_{\delta H}$ is used. Note that inclusion of the cosmic variance an its error budget changes the functions. See the text for further information.

81

Figure 25 – Cosmological constraints, with the full likelihood, for the Λ CDM model, where the contours are 68.3%, 95.4% and 99.7% confidence levels. One can note that the inclusion of the cosmic variance into the analysis (dashed black contours) shifts the usual constraints (blue contours). Higher values of Ω_{m0} and lower values of H_0 are preferred if the cosmic variance is included. Note the high correlation between $\Omega_{m0} - H_0$

88

Figure 26 – Cosmological constraints, with the full likelihood, for the CQ08 model, where the contours are 68.3%, 95.4% and 99.7% confidence levels. One can note that the inclusion of the cosmic variance into the analysis (dashed black contours) shifts the usual constraint (blue contours). Higher values of Ω_{m0} , lower values of H_0 and non-null couplings β are preferred if the cosmic variance is included. Note the high correlation between $\Omega_{m0} - H_0$

89

Figure 27 – Cosmological constraints, with the full likelihood, for the CQ08 + w_{de} model, where the contours are 68.3%, 95.4% and 99.7% confidence levels. One can note that the inclusion of the cosmic variance into the analysis (dashed black contours) shifts the usual constraint (blue contours). Higher values of Ω_{m0} , lower values of H_0 and non-null couplings β are preferred if the cosmic variance is included. Also, the cosmic variance extends the confidence levels for w_{de} . Note the high correlation between $\Omega_{m0} - H_0$

90

Figure 28 – Cosmological constraints, with full the likelihood, for the CQ10 model, where the contours are 68.3%, 95.4% and 99.7% confidence levels. One can note that the inclusion of the cosmic variance into the analysis (dashed black contours) shifts the usual constraint (blue contours). Higher values of Ω_{m0} , lower values of H_0 and non-null couplings β are preferred if the cosmic variance is included. Note the high correlation between $\Omega_{m0} - H_0$

91

Figure 29 – Cosmological constraints, with full the likelihood, for the CQ10 + w_{de} model, where the contours are 68.3%, 95.4% and 99.7% confidence levels. One can note that the inclusion of the cosmic variance into the analysis (dashed black contours) shifts the usual constraint (blue contours). Higher values of Ω_{m0} , lower values of H_0 and non-null couplings β are preferred if the cosmic variance is included. Also, the cosmic variance extends the confidence levels for w_{de} . Note the high correlation between $\Omega_{m0} - H_0$.

92

Figure 30 – Cosmological constraints, with the full likelihood, for the γ CDM extension, where the contours are 68.3%, 95.4% and 99.7% confidence levels. One can note that the inclusion of the cosmic variance into analysis (dashed black contours) shifts the usual constraint (blue contours). Higher values of Ω_{m0} and lower values of H_0 and γ are preferred if the cosmic variance is included. Note the high correlation between $\Omega_{m0} - H_0$.

93

Figure 31 – Cosmological constraint, with the full likelihood, to the γw CDM extension, where the contours are 68.3%, 95.4% and 99.7% confidence levels. One can note that the inclusion of the cosmic variance into the analysis (dashed black contours) shifts the usual constraint (blue contours). Lower values of H_0 and higher values of Ω_{m0} and w_{de} are preferred if the cosmic variance is included. Here, the cosmic variance does not change markedly constraint on γ . Note the high correlation between $\Omega_{m0} - H_0$.

94

Figure 32 – Cosmological constraints, with the full likelihood, for the γ_a CDM extension, where the contours are 68.3%, 95.4% and 99.7% confidence levels. One can note that the inclusion of the cosmic variance into the analysis (dashed black contours) shifts the usual constraint (blue contours). Higher values of Ω_{m0} and lower values of H_0 , γ_0 and γ_1 are preferred if the cosmic variance is included. Note the high correlation between $\Omega_{m0} = H_0$.

95

Figure 33 – Cosmological constraints, without RSD data, to the Λ CDM model, where the contours are 68.3%, 95.4% and 99.7% confidence levels. One can note that the inclusion of the cosmic variance into the analysis (dashed black contours) shifts the usual constraint (blue contours). Higher values of Ω_{m0} and lower values of H_0 are preferred if the cosmic variance is included. Note the high correlation between $\Omega_{m0} - H_0$. . .

96

Figure 34 – Cosmological constraints, without RSD data, for the γ CDM extension, where the contours are 68.3%, 95.4% and 99.7% confidence levels. One can note that the inclusion of the cosmic variance into the analysis (dashed black contours) shifts the usual constraint (blue contours). Higher values of Ω_{m0} and lower values of H_0 are preferred if the cosmic variance is included. Also, the cosmic variance is able to constraint, weakly, the cosmic growth index γ . Note the high correlation between $\Omega_{m0} - H_0$

97

Figure 35 – Cosmological constraints, with non-marginalized RSD data and without the local determination of H_0 , where the contours are 68.3%, 95.4% and 99.7% confidence levels. Note that in the absence of cosmic variance (red contours) $\gamma = 0.55$ is ruled out at about 99.7% confidence level. The best fit of the cosmic growth index is $\gamma = 0.699$

116

List of Tables

Table 1 – The 6 free parameters of Λ CDM: baryon energy density $\Omega_b h^2$, cold dark matter energy density $\Omega_m h^2$, angular diameter distance to sound horizon at last scattering θ , reionization optical depth τ , amplitude A_s and tilt n_s of primordial scalar fluctuations. We also show the latest constraints by the Planck satellite [6].	31
Table 2 – BAO data sets in old format.	73
Table 3 – BAO data sets in new format.	73
Table 4 – “Gold” RSD data set from [8]	76
Table 5 – Free parameters for each cosmological model. See the text for more details.	79
Table 6 – Best fit parameters obtained by the full likelihood analysis for all parametrizations and models here considered. Note that we show the two cases of $\chi^2_{H_0}$ used in analysis. See the text for further information.	80
Table 7 – Mean and variance of H_0 , computed from the posterior obtained via Bayesian inference. Note that we show the two cases of $\chi^2_{H_0}$ used in the analysis. See the text for further information.	82
Table 8 – Main results of the Bayesian inference with the full likelihood and, therefore, of this work. See the text for further information.	83
Table 9 – Comparison between the absolute error budget due to cosmic variance $\sigma_{\delta H} H_0$ and the error on local measurements σ_{R16} from the analysis with the full likelihood. Note that for all cosmological models $\sigma_{\delta H}$ and σ_{R16} are of the same order.	84
Table 10 – Best fit parameters obtained with the analysis without RSD data for Λ CDM and γ CDM. Note that we show the two cases of $\chi^2_{H_0}$. See the text for further information.	86
Table 11 – Mean and variance of H_0 , computed from $PDF(H_0)$ provided by cosmological constraints without RSD data. Note that we show the two cases of $\chi^2_{H_0}$. See the text for further information.	86
Table 12 – Main results of Bayesian inference without RSD data. See the text for further information.	87
Table 13 – Comparison between the absolute error budget due to cosmic variance $\sigma_{\delta H} H_0$ and the error on local measurements σ_{R16} from the analysis without RSD data.	87

Contents

	INTRODUCTION	14
1	STANDARD COSMOLOGY AND THE CONCORDANCE MODEL	17
1.1	General relativity	18
1.1.1	Geometry of spacetime	18
1.1.2	Equivalence principle	22
1.1.3	Einstein equations	23
1.1.4	Cosmological constant	24
1.2	Standard cosmology	25
1.2.1	Cosmological principle and the FLRW metric	25
1.2.2	Friedmann equations	26
1.2.3	The expanding universe and the Hubble law	27
1.3	The Λ CDM model	30
1.3.1	Radiation	31
1.3.2	Matter	32
1.3.3	Dark Energy	32
1.3.4	Background dynamics	33
1.3.5	Evolution of perturbations	34
1.4	Problems in the standard paradigm	43
2	BEYOND THE COSMOLOGICAL CONSTANT	45
2.1	Coupled quintessence	45
2.1.1	Background dynamics	46
2.1.2	Evolution of perturbations	49
2.2	Λ CDM extensions	50
2.2.1	γ CDM parametrization	51
2.2.2	γw CDM parametrization	51
2.2.3	γ_a CDM parametrization	53
3	THE TENSION ON H_0 AND THE EFFECT OF COSMIC VARIANCE	54
3.1	Tensions, discordances or inconsistencies	56
3.2	Linear perturbation theory and peculiar velocities	57
3.2.1	Cosmic variance	57
3.2.2	Relative systematic error $\sigma_{\delta H}$	61

3.3	The local determination of H_0 and a non-standard dark energy	62
3.3.1	Cosmic variance in Coupled Quintessence	62
3.3.2	Cosmic variance in γ CDM	63
3.3.3	Cosmic variance in γw CDM	64
4	BAYESIAN STATISTICS AND OBSERVATIONAL COSMOLOGY	66
4.1	Bayesian statistics	66
4.1.1	The χ^2 function and likelihood	68
4.1.2	Model selection criteria	69
4.2	Cosmological data	70
4.2.1	Cosmic microwave background	70
4.2.2	Baryonic acoustic oscillations	71
4.2.3	Type Ia Supernovae	74
4.2.4	Redshift space distortions	75
4.2.5	Local H_0	77
4.3	Full likelihood	78
5	BAYESIAN INFERENCE: RESULTS	79
5.1	Results for the full Likelihood	80
5.1.1	Best fit parameters and posteriors	80
5.1.2	Error budget $\sigma_{\delta H}$ and tension	82
5.2	Results without RSD data	85
5.2.1	Best fit parameters and posteriors	85
5.2.2	Error budget $\sigma_{\delta H}$ and tension	86
6	CONCLUSIONS	98
	BIBLIOGRAPHY	100
	APPENDIX A – MAXIMALLY SYMMETRIC SPACE	112
	APPENDIX B – COSMOLOGICAL DISTANCES	114
	APPENDIX C – RSD DATA NOT MARGINALIZED OVER	
	σ_8	116

Introduction

The Hubble parameter, $H(a)$, is one of the most important cosmological parameters. It quantifies the expansion rate of the universe. The value that the Hubble parameter takes today, H_0 , is known as the Hubble constant. Historically, the Hubble constant showed up in 1929 [3], when Edwin Hubble showed that the apparent distances of galaxies and its recession velocities obey the relationship $v = H_0 d$, where v is the recession velocity and d is the apparent distance. The latter expression is often known as the Hubble law and it is a consequence of the expansion of the universe. Measurements of the Hubble constant have been a fundamental topic in the development of cosmology, its value allows us to constrain, for example, the content of the universe [9, 5].

Roughly speaking, there are two ways to measure H_0 : through model-dependent or model-independent methods. For instance, we can use a fiducial cosmological model and observations, such as CMB or GW, to constrain the Hubble constant H_0 , whose value, evidently, will depend on the fiducial model. Also, one could use, for example, the Hubble law in order to obtain a model-independent value of H_0 . Among the model-independent determinations of the Hubble constant we can find the approaches presented in [1, 10, 11, 12, 13]. On the other hand, determinations given by [2, 6, 14, 15, 16] constrain H_0 through a fiducial cosmological model. The values given by [2] and [1] are the most important model-dependent and model-independent determinations of the Hubble constant, respectively.

The value provided by [2] is $H_0 = 66.93 \pm 0.62 \text{ km s}^{-1}\text{Mpc}$ (hereafter H_0^{Pl}) and comes from the most recent analysis of the temperature fluctuations of CMB. Meanwhile, observations of SNe Ia coupled with Cepheid distances to SNe Ia host galaxies [1] provides a measurement $H_0 = 73.24 \pm 1.74 \text{ km s}^{-1}\text{Mpc}$ (hereafter H_0^{R16}). So, it is easy to note that there is a tension between these determinations of H_0 . This tension or discordance, between the global (from CMB) and local (from SNe Ia) determinations, is often characterized as a tension of about 3.4σ [1, 17] and could be generated by both misunderstanding on the astrophysical process used to measure H_0^{R16} and unknown systematics on CMB or cosmic ladder-distance. However, in the absence of these kind of misunderstandings, the tension could be a hint for physics beyond the standard Λ CDM model.

Thus, in this sense, there have been proposed different possible solutions to the tension problem. For example, it has been considered that physics beyond Λ CDM could provide a higher value of H_0 , which would be in agreement with local determinations of H_0 [18, 19, 20, 21, 22, 23, 24, 25]. Also, modifications and systematic errors on the cosmic ladder-distance used to determine H_0^{R16} have been proposed [26, 27, 28, 29, 30, 31, 32].

None of the above proposals have provided a satisfactory explication of the discordance of 3.4σ .

On the other hand, linear perturbation theory predicts a deviation of $H_0^{\text{R}16}$ with respect to H_0^{Pl} . This deviation, produced by the field of peculiar velocities at local scales, could have non-negligible effects on the local determinations of H_0 . Statistically, the deviation, due to peculiar velocities and local gravitationally fields, can be characterized by a variance on the local H_0 . This variance, dubbed cosmic variance, allows us to compute the systematic error produced by peculiar velocities in local measurements of H_0 , which could be fundamental in the study of the tension problem. The cosmic variance has already been considered in order to cure the current tension in the Λ CDM context. Thus, it has been showed that, despite having non-negligible effects, the cosmic variance is not able to explain the whole tension [33, 34].

So, in a attempt to explain the 3.4σ tension, we shall study the effect of a cosmic variance on local determinations of H_0 when a presence of a non-standard dark energy is considered.¹ For that, first, we will compute the cosmic variance and its error budget, using the estimator proposed in [33]. Then, this error budget will be included into the analysis of the current cosmological data, in order to recognize the impact of the cosmic variance on cosmological parameters. Our cosmological data sets will be composed of data coming from CMB, BAO, SNe Ia, RSD and H^{loc} . Also, in order to represent a non-standard dark energy, we will use the coupled quintessence model, which has already considered in order to alleviate the tension [18, 19], and some parametric extensions of Λ CDM, here labelled as γ CDM, γw CDM and γ_a CDM.

Data analysis will be performed in the framework of Bayesian statistics. Using the results of data analysis we will compute the tension value by the simple estimator proposed in [35]. Also, in order to determinate which of all cosmological models here considered provides a better agreement with the data, we will carry out model selection using the AIC [36] and BIC criteria [37].

This dissertation is organized as follows. In Chapter 1 we will discuss the basis of standard cosmology, such as the theory of gravity and the cosmological principle. Besides that, we will also give a brief review of the Λ CDM model, focusing both on its theoretical and observational features. Then, in Chapter 2 we will discuss dark energy models beyond the cosmological constant, Λ . We shall emphasize non-standard dark energy models that could be able to cure the tension. These non-standard dark energy models will be represented by the coupled quintessence model and the three parametrized extensions γ CDM, γw CDM and γ_a CDM. The heart of this work will be discussed in Chapter 3,

¹ When we refer to a non-standard dark energy, actually we refer to any model, different from Λ , that are able to explain the current accelerated expansion of the universe. That is, a non-standard dark energy model could be defined on a framework of general relativity or modified gravity.

where we will argue about the tension and the estimator adopted in order to computed it. Additionally, we will introduce the cosmic variance and its error budget through linear perturbation theory. The basis of Bayesian statistical methods here used will be discussed in Chapter 4, where we also show the cosmological data sets used in order to obtain the cosmological constraints. Results of the data analysis, provided by Bayesian inference, will be showed and discussed in Chapter 5. Finally, we will conclude in Chapter 6.

Also, it is worth to stress that this dissertation has three Appendixes, which were included in order to provide a better understanding of some topics. For example, Appendix A shows a qualitative derivation of the Friedmann-Lemaître-Robertson-Walker metric through the theory of maximal symmetric spaces. On the other hand, Appendix B shows a brief discussion about cosmological distances, which are essential to the understanding of cosmological observations presented in the Chapter 4. Last but not least, the Appendix C shows the discussion and results of cosmological constraints when the full likelihood does not include the local Hubble constant H_0^{R16} and RSD data is not marginalized. We have to mention that most of the results and discussions here showed are presented in [38].

Finally, a few clarifications regarding notation. We adopt the signature $(-, +, +, +)$ and after the beginning of Subsection 1.1.1 we put the speed of light to $c = 1$. Also, hereafter the subscript “0” will be used to denote the present value of the corresponding quantity.

1 Standard cosmology and the concordance model

Cosmology is a field of physics that studies the universe as a whole, as a unique system, concentrating mainly on aspects such as its dynamics and content. The cosmological approximation of the universe as a homogeneous whole is meaningful if we look, and therefore study, the universe at large scales or, as we usually say, cosmological scales.¹ The uniqueness of the universe puts cosmology in a special place with respect to other fields of physics and leads to philosophical particularities as, for instance, the anthropic principle [39]. Though these philosophical issues can play an important role in cosmology, we should distinguish between problems caused by the uniqueness of universe and those that arise by its own physical features. The status of cosmology as an empirical science has strikingly changed owing to the increase of observational data during the last decades, to the point that it is now playing an important role on other fields of physics. For example, the best constraints on neutrinos masses are obtained from cosmological observations [40]. At large scales non-gravitational forces are negligible and therefore the dynamics of the universe is dictated by the theory of gravity. It could be difficult to explain our current understanding of gravitational phenomena without first mention at least some facts about the history behind gravitation. For a deep discussion about this topic see [41, 42].

Before Einstein's proposal, Newton's mechanics and laws of universal gravitation, introduced in 1687 [43], were widely used in physics and in the study of gravitational phenomena. For instance, movement of the planets, or celestial bodies, were predicted with great success by Newtonian gravity. Part of Newton's works is built on definition of inertial frames and the idea of an absolute space. On the other hand, all Newton's laws are only valid in inertial frames and therefore invariant under Galilean transformations, which are transformations performed by the set of ten parameters of Galilean group. This fact leads to think that all physical laws would have to be invariant under transformations of the Galilean group, but the electrodynamics would contradict this idea. The laws of electrodynamics are sum up in the Maxwell equations, which are not invariant under Galilean transformations and also establish that the speed of light in the vacuum is a universal constant. This latter result suggested that electromagnetic waves were carried by a medium, denominated ether, hypothesis that were ruled out by experiments, such as performed in 1887 by Michelson and Morley [44]. Besides the lack of concordance between Newtonian laws and electrodynamics, Newtonian gravity showed not to be able to explain Mercury's perihelion precession.

¹ A accurate definition of cosmological scales will be stated in the subsection 1.2.1.

It is not clear if Einstein knew about the results obtained in [44] or whether he was motivated by Mercury's perihelia problem to construct his theories, but is clear that Einstein looked for a set of transformations, that had already been derived by Lorentz [45], that could leave Maxwell equations invariant. The new set of transformations used by Einstein, that would substitute the Galilean group, belongs to the Lorentz group. The use of the Lorentz transformations led Einstein to modify the laws of Newtonian mechanics that later would yield the theory of special relativity [46]. After he presented the theory of special relativity, and showed that both laws of Newtonian mechanics and Maxwell equations are not invariant under the same group of transformations, Einstein starts to work on the idea of a relativistic gravitational theory. Thus, finally in 1916 Einstein introduced the theory of general relativity [47].

As we already pointed out, the theory of gravitation is at the heart of cosmology. We use Einstein's field equations to describe the dynamics of the universe. Though a variety of matter contents and geometries are possible, only a small subset of the latter is capable of explaining the wealth of present-day observations. For example, a model such as the standard cold dark matter (sCDM) model [48, 49] is not a suitable cosmological model as it cannot explain the acceleration of the universe. Nowadays, the model that presents the highest level of concordance with data is the Λ CDM model.² Its material content is composed of three physical species: non-relativistic matter (baryons and cold dark matter), radiation (photons and massless neutrinos) and dark energy (represent by the cosmological constant Λ), being the last component responsible by the current accelerated expansion of the universe.

In this first chapter, we show a brief review of the theory of gravity used in standard cosmology, the theory of general relativity. We will then discuss the basis of the Λ CDM model, discussing its relationship with observations and some problems that it suffers.

1.1 GENERAL RELATIVITY

General relativity can be thought of as a geometrical theory of gravity. It uses concepts such as: manifolds, tensors and curvature. Thus, before studying standard cosmology from the point of view of the theory of general relativity, it is important to state some fundamental concepts about Einstein's theory.

1.1.1 Geometry of spacetime

At the beginning of this chapter, we said that it is necessary to introduce a new set of transformations, that replaces the Galilean transformations, and modifies the Newtonian

² We will refer to Λ CDM model as the model of concordance or standard cosmological model, indistinguishably.

mechanics in order to find agreement among the laws of mechanics and electrodynamics. However, we did not indicate how this changes the structure of spacetime. In non-relativistic physics, spacetime is understood like a continuous composition of events, that can be represented by four numbers, three for space and one to time, where time has an absolute definition. That definition of spacetime is partially kept in relativistic physics. Maybe, the most important difference is the conception of time as absolute, which is dropped as the latter becomes a coordinate with the same status of the spatial coordinates. For instance, consider two events $A = (t_a, x_a, y_a, z_a)$ and $B = (t_b, x_b, y_b, z_b)$. In non-relativistic physics all inertial observers will agree on value of the quantities $\Delta t = t_a - t_b$ and $d^2 = \Delta x^2 + \Delta y^2 + \Delta z^2$, independently among them. While in special relativity, observers only agree on the measure of

$$\Delta s^2 = -c^2 \Delta t^2 + \Delta x^2 + \Delta y^2 + \Delta z^2 , \quad (1.1)$$

where c is the velocity of light. For the sake of simplicity, henceforth, we shall adopt $c = 1$. So, introducing time as a new coordinate alters the geometrical structure of spacetime. Formally, both for special relativity and general relativity, the distance in the spacetime is defined according to

$$ds^2 = g_{\mu\nu} dx^\mu dx^\nu , \quad (1.2)$$

where $g_{\mu\nu}$ is the metric tensor. It is a symmetric tensor of second rank and has, at most, ten independent components. In the particular case of special relativity, the metric tensor is the Minkowski tensor:

$$\eta_{\mu\nu} = \begin{pmatrix} -1 & 0 & 0 & 0 \\ 0 & 1 & 0 & 0 \\ 0 & 0 & 1 & 0 \\ 0 & 0 & 0 & 1 \end{pmatrix} . \quad (1.3)$$

The spacetime of special relativity is a flat spacetime known as the Minkowski spacetime. The theory of special relativity establish a metric, $\eta_{\mu\nu}$, that remains fixed in the presence of matter. This will not be true for general relativity, where the geometry of spacetime is influenced by the presence of matter and the properties of the spacetime are described by the metric, which is not necessarily flat. It is worth mentioning that Einstein was motivated by Mach's principle when he included a metric that should be affected by the presence of matter [50]. The connection between spacetime geometry, gravity and the distribution of matter will be qualitatively more clear after stating the principle of equivalence and quantitatively more clear with Einstein equations.

The spacetimes required by general relativity are represented by pseudo-Riemannian manifolds endowed with a metric $g_{\mu\nu}$. The mathematical structure of the semi-Riemannian manifolds is studied in the framework of differential geometry and has a non-trivial structure. Perhaps, the first thing that one has to point out is the importance of $g_{\mu\nu}$. The metric tensor shall come on the scene in almost all quantities defined in space time, such

as distances, curvature and others and it shall carry out information about the geometry of spacetime. In general relativity one requires the compatibility of the metric $\nabla_\alpha g_{\mu\nu} = 0$, which leads us to define a unique differential operator, characterized by the connection:

$$\Gamma^\alpha_{\mu\nu} = \frac{1}{2}g^{\alpha\beta}(\partial_\mu g_{\nu\beta} + \partial_\nu g_{\beta\mu} + \partial_\beta g_{\mu\nu}) , \quad (1.4)$$

known as the Christoffel symbol, where ∇_α is the covariant derivative defined as

$$\begin{aligned} \nabla_\gamma T^{\mu_1 \dots \mu_m}_{\nu_1 \dots \nu_n} &= \partial_\gamma T^{\mu_1 \dots \mu_m}_{\nu_1 \dots \nu_n} - \Gamma^\alpha_{\gamma\nu_1} T^{\mu_1 \dots \mu_m}_{\alpha \dots \nu_n} - \dots - \Gamma^\alpha_{\gamma\nu_n} T^{\mu_1 \dots \mu_m}_{\nu_n \dots \alpha} \\ &\quad + \Gamma^{\mu_1}_{\gamma\alpha} T^{\alpha \dots \mu_m}_{\nu_1 \dots \nu_n} + \dots + \Gamma^{\mu_n}_{\gamma\alpha} T^{\mu_1 \dots \alpha}_{\nu_1 \dots \nu_n} , \end{aligned} \quad (1.5)$$

and $T^{\mu_1 \dots \mu_m}_{\nu_1 \dots \nu_n}$ is a tensor of rank $m+n$.

Note that ∇_μ differs from ∂_μ : the first have a more complex definition because the tensorial structure has to be kept after applying it to any tensor. It means that equation (1.5) ensures that $\nabla_\gamma T^{\mu_1 \dots \mu_m}_{\nu_1 \dots \nu_n}$ is a tensor, and, hence, obeys the law of transformation of tensors. Derivative operators are often read as a rate of change. For instance, if we have a differentiable function $\mathcal{T} = \mathcal{T}(x, y)$ that represents the temperature field of a 2d-surface, the partial derivative $\partial_y \mathcal{T}(x, y)|_{x=x_0}$ will represent how fast the temperature changes along the y direction at $x = x_0$. Because that tensors are not simple functions, but rather maps that take vectors and duals vectors towards the space of real numbers, the interpretation of ∇_μ as a rate of change is neither immediately nor easily intuitive. If we wish to approach this kind of interpretation, it is necessarily to call upon the definition of parallel transport.

In a flat spacetime, either Euclidean or pseudo-Euclidean, parallel transport of a vector is trivial. That is different in non-flat spacetime. A classic example of that is the case of a vector parallel transported on a 2-sphere to the same point along two different paths. As shown in [51], the vector that results from the parallel transport depends on the path followed. Given a path $x^\mu(\lambda)$ it is useful to define the directional derivative

$$\frac{D}{d\lambda} = \frac{dx^\mu}{d\lambda} \nabla_\mu . \quad (1.6)$$

Bearing this in mind, we shall say that a tensor is parallel transported along a path $x^\mu(\lambda)$ if the application of the directional derivative on the tensor gives zero. Then, instead of relating the covariant derivative to a rate of change, we use the directional derivative (1.6) to represent the variation that would suffer the tensor T if it would be parallel transported along a path.

After having defined the directional derivative we are able to discuss geodesics. A geodesic is defined as a curve along which its own tangential vector is parallel transported. Thereby, a curve $x^\mu(\lambda)$ with the tangent vector $dx^\mu/d\lambda$, will be a geodesic if:

$$\frac{D}{d\lambda} \frac{dx^\mu}{d\lambda} = 0 ,$$

or in a more explicit way

$$\frac{d^2x^\mu}{d\lambda^2} + \Gamma_{\alpha\beta}^\mu \frac{dx^\alpha}{d\lambda} \frac{dx^\beta}{d\lambda} = 0 . \quad (1.7)$$

Equation (1.7) is dubbed the geodesic equation and is particularly important as non-accelerated test particles follow geodesic paths, i.e. observers in free fall follow geodesics. Using the four-velocity of a test particle $U^\mu = dx^\mu/d\lambda$, we can cast (1.7) as

$$U^\alpha \nabla_\alpha U^\mu = 0 , \quad (1.8)$$

which could be trivially repeated using the four-momentum $p^\mu = mU^\mu$. Also, it is possible to obtain the geodesic equation by means of the variational principle applied to the functional form of the proper time with respect to the metric.

The path that one follows when parallel transported matters, this leads to think that the order in which the covariant derivatives act on a vector matters as well, i.e. the commutator $[\nabla_\mu, \nabla_\nu]V^\gamma$ is not trivial. Formally, and in absence of torsion, this commutator is defined by

$$[\nabla_\mu, \nabla_\nu]V^\gamma = R^\gamma_{\alpha\mu\nu}V^\alpha , \quad (1.9)$$

where $R^\gamma_{\alpha\mu\nu}$ is the Riemann tensor. Thus, it is not a surprise that the mathematical entity that quantifies the curvature of the spacetime, $R^\gamma_{\alpha\mu\nu}$, comes from definitions such as parallel transport or covariant derivative. Once the covariant derivative is uniquely defined, i.e. the connexion is strictly the Christoffel symbols, the Riemann tensor is [51]

$$R^\rho_{\sigma\mu\nu} = \partial_\mu \Gamma^\rho_{\nu\sigma} - \partial_\nu \Gamma^\rho_{\mu\sigma} + \Gamma^\rho_{\mu\lambda} \Gamma^\lambda_{\nu\sigma} - \Gamma^\rho_{\nu\lambda} \Gamma^\lambda_{\mu\sigma} . \quad (1.10)$$

Besides the Riemann tensor, there are others quantities used to describe the curvature of spacetime. Two of most used are the Ricci tensor $R_{\mu\nu} = R^\lambda_{\mu\lambda\nu}$ and the Ricci scalar $R = R^\alpha_\alpha$. Here, it is important to mention some properties of Riemann tensor.

The Riemann tensor is antisymmetric both in its first two indices as in its last two indices,

$$\begin{aligned} R_{\rho\sigma\mu\nu} &= -R_{\sigma\rho\mu\nu} , \\ R_{\rho\sigma\mu\nu} &= -R_{\rho\sigma\nu\mu} , \end{aligned}$$

also it obeys

$$R_{\rho\sigma\mu\nu} = R_{\mu\nu\rho\sigma} ,$$

which takes to

$$R_{\rho\sigma\mu\nu} + R_{\rho\mu\nu\sigma} + R_{\rho\nu\mu\sigma} = 0 .$$

However, the most important property of the curvature tensor is the Bianchi identity, which states

$$\nabla_\lambda R_{\rho\sigma\mu\nu} + \nabla_\rho R_{\sigma\lambda\mu\nu} + \nabla_\sigma R_{\lambda\rho\mu\nu} = 0 . \quad (1.11)$$

Using the definition of the Ricci tensor, the Ricci scalar and some of the properties above, we can recast the Bianchi identity (1.11) [51] as

$$\nabla^\mu R_{\alpha\mu} = \frac{1}{2} \nabla_\alpha R . \quad (1.12)$$

This form of the Bianchi identity will be important later.

The previous review is far from being a rigorous and complete description of spacetime geometry, but we consider it a sufficient discussion for the purposes of this work. Softicated, rigorous and complete descriptions of this physical-mathematical formalism can be found in the literature, for instance [41, 50, 51].

1.1.2 Equivalence principle

The weak equivalence principle is a cornerstone of Newton laws. It states that, for any object independently of its composition, the inertial mass – that quantifies the resistance of a body against changes of its current state of motion – is equivalent to the gravitational mass – which is proportional to gravitational force according to the laws of universal gravitation. Then, the behavior of trajectories that bodies in free fall follow is universal and independent of the bodies' composition. There is no such thing as a gravitationally neutral body and all bodies interact in the same way with gravity. Thus, in tiny regions of space-time, the movement of particles in free fall is the same both in a gravitational field and in a uniformly accelerated frame.

Einstein proposed an extension of the weak equivalence principle, known as Einstein's equivalence principle. It establishes that it is not possible to detect the existence of a gravitational field by local experiments in small regions of space-time, where laws of physics reduce to laws of special relativity [51]. Roughly speaking, space-time is always locally Minkowski space-time. Einstein's equivalence principle shows a similarity with Gauss' axiom, that states that at any point in a curved space one can build a coordinate system which is locally Cartesian and it is governed by Pythagora's laws [41]. This connection among family of paths and gravity suggests an intrinsic relationship between the geometry of the space-time and gravity. Consequently, to incorporate these ideas it is necessary a mathematical structure consistent with them. Such mathematical structure, as we discussed before, is associated with differential manifolds.

Both the weak and Einstein's equivalence principles have been largely tested by experiments. Perhaps the most famous was the one performed by Loránd Eötvös. The original experiment of the austro-hungarian physicist consisted in a torsion balance with two weights of wood and platinum. He obtained that the difference between inertial and gravitational mass was less than 10^{-9} [52]. After Eötvös's measurements more experiments were performed, including more sophisticated and accurate methods, see [53] and references therein. For instance, Baeßler et al.[54] use data from lunar-ranging to constraint the

deviation to 1.3×10^{-13} and [Schlamminger et al.](#)[55] use a torsion balance with test bodies of beryllium and titanium to found a deviation about 10^{-15} .

1.1.3 Einstein equations

Einstein equations are the main result of the theory of general relativity and they can be obtained in different ways. One of the most elegant way is through the Lagrangian formalism with Hilbert-Einstein action

$$S_H[g] = \frac{1}{2\kappa^2} \int R\sqrt{-g} d^4x , \quad (1.13)$$

where $\kappa^2 = 8\pi G$, G is the universal gravitational constant, $g = \det[g_{\mu\nu}]$ and R the Ricci scalar. Thus, using the principle of least action

$$\delta S_H = 0 , \\ \int \sqrt{-g} g^{\mu\nu} \delta R_{\mu\nu} d^4x + \int \sqrt{-g} \delta g^{\mu\nu} R_{\mu\nu} d^4x + \int \delta \sqrt{-g} g^{\mu\nu} R_{\mu\nu} d^4x = 0 . \quad (1.14)$$

The first term on the left-hand side of the previous equation, related to $\delta R_{\mu\nu}$, will become a boundary contribution at infinity which will be set to zero, due to Stokes's theorem and the compatibility of metric [51]. In contrast, the last term shall give an important contribution to the Einstein equations. Using the property of the determinant of a matrix $\ln g = \text{Tr}(\ln g_{\mu\nu})$, we have

$$\delta \sqrt{-g} = -\frac{1}{2} \sqrt{-g} g_{\mu\nu} \delta g^{\mu\nu} . \quad (1.15)$$

Thus, replacing (1.15) in equation (1.14) we arrived to Einstein equations

$$R_{\mu\nu} - \frac{1}{2} R g_{\mu\nu} = 0 . \quad (1.16)$$

Note that an important step in the derivation of (1.16) was the assumption of a compatible metric; this allows to avoid the first term. The application of the principle of least action under the assumption of $\nabla_\alpha g_{\mu\nu} = 0$ is dubbed metric formalism. However, it is possible to drop the compatibility of the metric and perform the Palatini formalism. Differently from the metric formalism, in Palatini formalism the connection is not assumed to be the Christoffel symbols (1.4) and hence the Ricci tensor does not depend on the second derivatives of metric. Surprisingly, variation of S_H using the Palatini formalism also leads to Einstein equations, leading more naturally to the compatibility of metric.³ Variation of (1.13), both by metric and Palatini formalism, takes us to Einstein equations in vacuum (1.16), given that only the gravity action was considered. Einstein equations in presence of matter fields will be obtain from the general action

$$S[g, \Psi] = S_H[g] + S_M[g, \Psi] , \quad (1.17)$$

³ This could be not true in modified gravity models, for instance, in $f(R)$ models [56, 57].

where Ψ represents the matter fields. Thus, we shall have

$$G_{\mu\nu} \equiv R_{\mu\nu} - \frac{1}{2}Rg_{\mu\nu} = \frac{8\pi G}{c^4}T_{\mu\nu}, \quad (1.18)$$

where $G_{\mu\nu}$ is called Einstein tensor and the energy-momentum tensor is defined by

$$T_{\mu\nu} = -2\frac{1}{\sqrt{-g}}\frac{\delta S_M}{\delta g^{\mu\nu}}. \quad (1.19)$$

Equation (1.18) shows explicitly the relation between matter and geometry. The left hand-side depends on the curvature tensor, metric and curvature scalar, therefore it is identified as the geometry of space-time. On the other hand, the right-hand side has the energy-momentum tensor that is built from S_M and represents the matter distribution on space-time. Then, space-time geometry is disturbed by the presence of matter and this will have a dynamics governed by space-time geometry.

In addition to Einstein equations we have another set of equations, the equations of conservation of matter and momentum. The laws of conservation in general relativity becomes $\nabla_\mu T_{\mu\nu}$. From equation (1.12) it is obvious that

$$\nabla^\alpha G_{\alpha\nu} = \nabla^\alpha R_{\alpha\nu} - \frac{1}{2}g^{\alpha\nu}\nabla_\alpha R = 0, \quad (1.20)$$

so that, due to Einstein equations, we get the law of conservation of matter and momentum, $\nabla_\mu T^{\mu\nu} = 0$.

1.1.4 Cosmological constant

The history of the cosmological constant is comparable to the ugly duckling story. It appeared for the first time in 1917, when Einstein introduced the first cosmological model in the framework of general relativity [58]. The cosmological constant was included by Einstein in order to obtain a static and finite universe, which could not otherwise be found using the field equations. Although this model failed in the attempt to represent our universe [59], the cosmological constant Λ plays a important role in the current standard cosmological model.

The cosmological constant can be introduced in the fields equations through the action:

$$S_H = \frac{1}{2\kappa^2} \int (R - 2\Lambda) \sqrt{-g} d^4x, \quad (1.21)$$

which leads to reshape Einstein's equations according to

$$R_{\mu\nu} - \frac{1}{2}Rg_{\mu\nu} + 2\Lambda g_{\mu\nu} = 8\pi GT_{\mu\nu}. \quad (1.22)$$

The cosmological constant can be interpreted as an intrinsic constant of the gravitational theory or as vacuum energy. This last because it has a parameter of equation of state equal to -1 (see Section ??), which coincides with the parameter of vacuum according quantum field theory. Some aspects of Λ deserve a deeper discussion, for an extensive discussion about cosmological constant see [60, 61].

1.2 STANDARD COSMOLOGY

The basis of standard cosmology lies on general relativity and so the dynamics of universe is governed by Einstein equations. Nevertheless, dynamics is not completely fixed by the theory of general relativity, so we need to take other considerations. In the present section we will discuss which are the considerations that have to be taken into account to fully define the cosmological context.

1.2.1 Cosmological principle and the FLRW metric

The cosmological principle says that at large scales the universe is spatially homogeneous and isotropic (or isotropic at all points), pragmatically: we do not occupy a privileged place in the universe. This means, space-time has a maximally symmetric subspace, or said in a more attractive way for physicists, hypersurfaces of space-time at a given time $t = t_0$ are maximally symmetric. According to the theory of maximally symmetric spaces, summarized in the Appendix A, the metric that satisfies the cosmological principle is given by (A.7). Considering the coordinates t, r, θ e ϕ , we are able to write

$$ds^2 = -dt^2 + a^2(t) \left[\frac{dr^2}{1 - kr^2} + r^2 d\theta^2 + r^2 \sin^2 \theta d\phi^2 \right], \quad (1.23)$$

where we defined $a^2(t) = f(t)$ (see Appendix A) and k takes values according to the curvature of the maximally symmetric sub-space

$$k = \begin{cases} +1 & \text{spherical sub-space } K > 0, \\ 0 & \text{Euclidean sub-space } K = 0, \\ -1 & \text{hyperbolic sub-space } K < 0. \end{cases} \quad (1.24)$$

This metric is known as the Friedmann-Lemaître-Roberson-Walker metric or simply FLRW metric. It is worth to point out that if two metrics have the same symmetries, the same value to K and the same numbers of positive and negative eigenvalues is always possible to find a coordinate transformation that leads from one to the other [41]. This guarantees that the FLRW metric is the unique metric that describes a universe in which the cosmological principle is valid.

Homogeneity and isotropy of the universe can be tested to find at which scale can be applied the cosmological principle. For instance, Beisbart[62] show that data coming from the CMB, the X-ray background, radio sources and the Lyman- α support very well the cosmological principle at scales of $\sim 100 - 1000 h^{-1}$, where h is the Hubble constant normalized to $100 \text{ km s}^{-1} \text{ Mpc}^{-1}$. Gonçalves et al.[63] besides showing that BAO data are in good agreement with the cosmological principle, he proclaims that scale of homogeneity is about $70 - 150 h^{-1} \text{ Mpc}$. Despite the several data supporting the cosmological principle, it has been questioned if it is justified to assume its validity [62] and it has been discussed the

philosophical problems related to its status [39]. Here, we consider that the cosmological principle is valid at scales larger than $\gtrsim 100$ Mpc.

1.2.2 Friedmann equations

Once the cosmological principle is assumed, quantities corresponding to geometry are fixed and, hence, the left-hand side of the Einstein equation is completely determined. However, to obtain the differential equations related to cosmological dynamics we should specify the right-hand side of (1.18), i.e. the energy-momentum tensor $T_{\mu\nu}$. In the present case, the energy-momentum tensor for a homogeneous and isotropic universe is the energy-momentum tensor for a perfect fluid, which is:

$$T_{\mu\nu} = (\rho + p) U_\mu U_\nu + p g_{\mu\nu}, \quad (1.25)$$

where U_μ is the four-velocity of fluid, p is the pressure and ρ the energy density. For a perfect fluid it is often used a barotropic equation of state (hereafter, EoS) with the functional form $p = w\rho$, where w is named the EoS parameter, or simply the EoS. Conservation of energy and momentum lead to the continuity equation:

$$\dot{\rho} + 3H(\rho + p) = 0, \quad (1.26)$$

$$\dot{\rho} + 3H(1 + w)\rho = 0. \quad (1.27)$$

Using (1.18), (1.23) and (1.25) we have

$$H^2 = \frac{8\pi G}{3}\rho - \frac{k}{a^2}, \quad (1.28)$$

$$\frac{\ddot{a}}{a} = -\frac{4\pi G}{3}(\rho + 3p), \quad (1.29)$$

where $H(a)$ is the Hubble parameter, defined as $H = \frac{\dot{a}}{a}$. Also it is possible to obtain the Friedmann equations with the cosmological constant. For that, we will have to use (1.22) instead to (1.18):

$$H^2 = \frac{8\pi G}{3}\rho + \frac{\Lambda}{3} - \frac{k}{a^2}, \quad (1.30)$$

$$\frac{\ddot{a}}{a} = -\frac{4\pi G}{3}(\rho + 3p) + \frac{\Lambda}{3}. \quad (1.31)$$

As we have mentioned earlier, the cosmological constant can be interpreted as an intrinsic constant of gravity or a vacuum energy—a component of the perfect fluid. So, consider equation (1.22), if the term related to Λ is put on the right-hand side we could define

$$T_{\mu\nu}^\Lambda = -\frac{\Lambda}{8\pi G} g_{\mu\nu}, \quad (1.32)$$

and taking into account the definition of the energy-momentum tensor for a perfect fluid, one has

$$\rho_\Lambda = \frac{\Lambda}{8\pi G} , \quad (1.33)$$

$$p_\Lambda = -\frac{\Lambda}{8\pi G} . \quad (1.34)$$

From these equations it is easily to note that $w_\Lambda = -1$. The EoS to the cosmological constant matches the EoS of the vacuum, according to quantum field theory. Thus, the cosmological constant is often dubbed vacuum energy. It is worth noting that (1.28) is named the Friedmann equation, while (1.29) is known as the acceleration equation, this due to the fact that the sign on the right-hand side of equation (1.29) will define whether the universe has an accelerated or decelerated expansion. Specifically, just a component with $w < -1/3$ is able to accelerate the expansion of the universe, this will be important for dark energy models. We will not distinguish between Friedmann equations with and without cosmological constant because they are equivalent under the definition of ρ_Λ and p_Λ .

We define the critical density as the energy density that is necessary to obtain an euclidean sub-space $k = 0$:

$$\rho_{cri} \equiv \frac{3H^2}{8\pi G} .$$

From this definition we can define the density parameter, which is

$$\Omega \equiv \frac{\rho}{\rho_{cri}} = \frac{8\pi G}{3H^2} \rho , \quad (1.35)$$

and recast equation (1.28) as

$$1 = \Omega - \frac{k}{a^2 H^2} . \quad (1.36)$$

Note that in the case of a flat universe, i.e. $k = 0$, the total parameter energy density is constrained to be 1.

1.2.3 The expanding universe and the Hubble law

The idea of an expanding universe is very well supported by data. Also, it is compatible with the cosmological principle and its FLRW metric, which features the effect of expansion through the scale factor $a(t)$. The expansion of the universe implies that not only the scale factor is a function of time, but also that it increases with time, i.e. at early times $a < a_0$. Thus, because the scale factor plays an important role in the FLRW metric, distances are obviously affected by the expansion. Distances in the context of an expanding universe are not trivial and deserve a special discussion, which is showed in Appendix B.

Observations unveil that we are living in an expanding universe and hence we can see galaxies receding from us. The rate of expansion is quantified by the Hubble parameter

$H(a)$, which determines how fast the scale factor increases. To determine how the Hubble parameter (or the scale factor) evolves with time we have to know the energy density of the universe and use the Friedmann equations. Particular is the case of the current value of $H(a)$, named Hubble constant H_0 , whose value can be determined in a model independent way.

The universe is composed of different large structures, such as galaxies, clusters and others, which are very far from us. Because we live on the Earth, we are only able to observe cosmological structures from our position, i.e. we are limited to study them by their emitted radiation. Before the detection of gravitational waves, we observed the universe mainly through electromagnetic radiation.⁴ However, the first direct detection of gravitational waves, performed by LIGO/Virgo collaborations (GW150914 [64], GW151226 [65], GW170104 [66], GW170814 [67] and GW170817 [68]) changed the paradigm and opened a new window on cosmology (and physics in general). Despite of that, most of the information continues to be provided by photons.

Light emitted, for instance, by a galaxy is stretched out due to the expansion of the universe, and is observed at a wavelength λ_o larger than the emitted one λ_e . This leads us to define a parameter that quantifies this stretching [69],

$$z \equiv \frac{\lambda_o}{\lambda_e} - 1 , \quad (1.37)$$

which is named redshift. The geodesic equations allow us to show that photon energy is inversely proportional to the scale factor. As photon energy is also inversely proportional to its wave length, it is easily to show:

$$z = \frac{a_0}{a} - 1 ,$$

where a corresponds to the scale factor of λ_{emit} and a_0 to λ_{obs} . The current value of the scale factor, a_0 , is often normalized to 1, we will follow this choice.⁵

Hubble law provided the first observational and most direct evidence of the expansion of the universe. Although there is a discussion about whether it is correct to attribute the discovery to Edwin Hubble, there is nothing we can do to remove its name from the *Hubble law*. Instead, we can say that the discovery of the Hubble law resulted from the efforts of several physicists, such as: Lemaître[70], Slipher[71], Lundmark[72] and, finally, Hubble[3] himself. For a thorough discussion of the discovery of the Hubble law see [73, 74, 75] and references therein. The Hubble law states that the radial velocity v of an object, for instance a galaxy, away from us is directly proportional to the distance d , where the slope is given by H_0 :

$$v = H_0 d . \quad (1.38)$$

⁴ Cosmic rays coming from galactic and extra-galactic sources are also observed.

⁵ There is not a problem in setting $a_0 = 1$, because we do not measure it directly, rather, we measure, for instance, H_0 which is invariant under the scale transformation of a .

Note that d is the physical distance and, at $z \ll 1$, the recessional velocity $v \approx cz$. Hubble used the 100-inch Hooker telescope to measure the distances to 24 galaxies, belonging to the Local Group and the Virgo cluster, and employed published radial velocities to determinate $H_0 = 500 \text{ km s}^{-1}\text{Mpc}^{-1}$ [3], which can be inferred by Figure 1. Units of Hubble constant are given in $\text{km s}^{-1}\text{Mpc}^{-1}$, it means a galaxy at 1 Mpc away from us has a velocity $v = 100h \text{ km s}^{-1}$, while a galaxy at 20 Mpc away from us has velocity $v = 2000h \text{ km s}^{-1}$.⁶

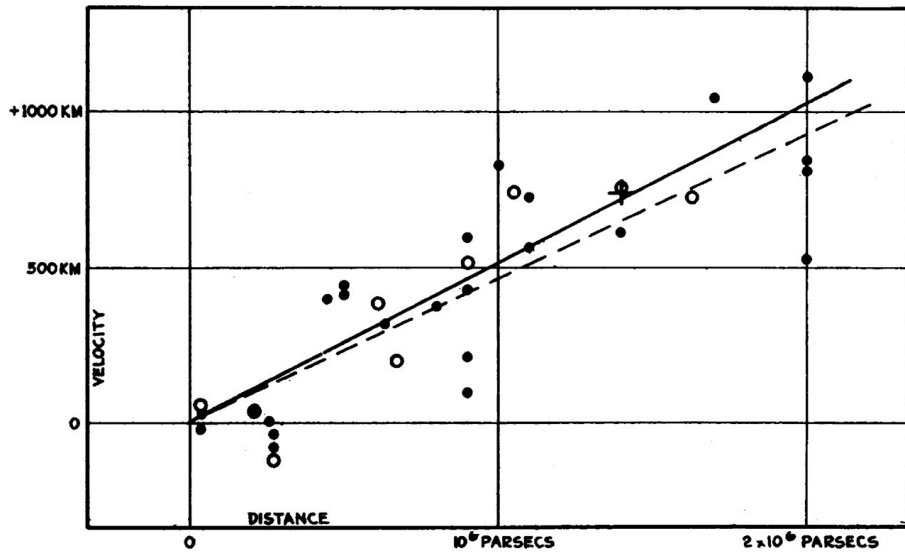


Figure 1 – Hubble diagram from [3].

The use of the Hubble law to determinate H_0 consists, basically, in measuring distances and velocities. The latter, at $z \ll 1$, can be easily determined from redshift $v \approx cz$, where we have assumed the effect of peculiar velocities as negligible; the real problem lies in determining distances. Thus, the challenge to get an accurate value of H_0 is actually the challenge to get an accurate d . Nowadays, we are using several methods to measure distances, among them we can mention: Cepheid distance scale, tip of the Red Giant Branch method, Faber-Jackson relation, Tully-Fisher relation and type Ia Supernovae.⁷ The most accurate and current measurement of the Hubble constant is provided by Riess et al.[1]:

$$H_0 = 73.24 \pm 1.74 \text{ km s}^{-1} \text{ Mpc}^{-1}. \quad (1.39)$$

Besides the Hubble law, there are other ways to constraint H_0 . Due to the Friedmann equation (1.28), cosmological quantities such as distances depend on H_0 . Thus, cosmological observations, such as the CMB [6], gravitational time delays [14], BAO [15] and recently

⁶ Remember that is often used the dimensionless h instead H_0 , considering the relationship $H_0 = 100h \text{ km s}^{-1}\text{Mpc}^{-1}$.

⁷ See [76, 9], and references therein, for detailed descriptions of some of these methods.

gravitational waves [16], also are able to measure H_0 . Perhaps, the most important is the most recent estimation from Planck [2]

$$H_0 = 66.93 \pm 0.62 \text{ km s}^{-1} \text{ Mpc}^{-1}. \quad (1.40)$$

1.3 THE Λ CDM MODEL

The Λ CDM model is often dubbed the concordance model, due to the large level of agreement with the observations, see for instance Figure 2. It is composed of three kinds of material components: non-relativistic matter (baryons and cold dark matter), radiation (photons and massless neutrinos) and dark energy, represented by Λ . Each of these components contributes in a particular way to the dynamics of the universe. Despite that Λ CDM can show a well agreement with the data, the physics behind it is not fully understood. Perhaps, the most mysterious components are the dark energy and the dark matter, altogether called the dark sector of the universe. The standard cosmological model has six free parameters that are not fixed by theory but rather by observations, these parameters are showed in Table 1.

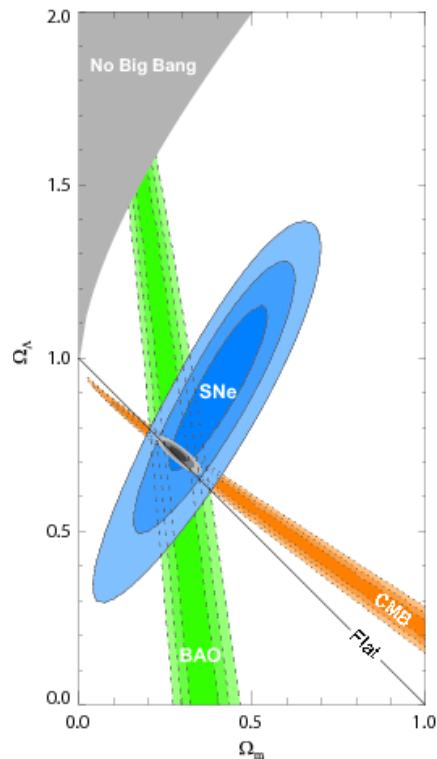


Figure 2 – Λ CDM show a good agreement with cosmological data, in this cases data corresponding to SNe Ia, BAO and CMB. One can see that inference about cosmological parameters, $\Omega_\Lambda - \Omega_m$, are in concordance to experiments of different nature. Although this figure does not correspond to recently analysis, it is useful to illustrated concordance in Λ CDM. This figure is from [4].

In the present section, we review the cosmological concordance model. First, we show the properties of its components and the background dynamics. Then, we will discuss briefly the Λ CDM model at level of perturbations focusing on results that will be important for the scope of this work. It is worth mentioning that data constrain $\Omega_{k0} \equiv \frac{k}{a_0^2 H_0^2} \approx 0$ [6]. Therefore, hereafter, we will consider a flat universe.

Parameter	Value constraints [6]
$\Omega_b h^2$	0.0223 ± 0.00014
$\Omega_c h^2$	0.1188 ± 0.0010
100θ	1.04093 ± 0.00030
τ	0.066 ± 0.012
$\ln(10^{10} A_s)$	3.064 ± 0.023
n_s	0.9667 ± 0.0040

Table 1 – The 6 free parameters of Λ CDM: baryon energy density $\Omega_b h^2$, cold dark matter energy density $\Omega_m h^2$, angular diameter distance to sound horizon at last scattering θ , reionization optical depth τ , amplitude A_s and tilt n_s of primordial scalar fluctuations. We also show the latest constraints by the Planck satellite [6].

1.3.1 Radiation

Radiation, or relativistic matter, consists of photons and massless neutrinos.⁸ Radiation has a parameter EoS $w_r = 1/3$, which according to the conservation of energy and momentum gives:

$$\dot{\rho}_r + 4\frac{\dot{a}}{a}\rho_r = 0 , \\ \rho_r(a) = \rho_{r0}a^{-4} ; \quad (1.41)$$

or using the density parameter:

$$\rho_r(a) = \frac{3H_0^2}{8\pi G}\Omega_{r0}a^{-4} , \\ \Omega_r(a) = \left(\frac{H_0}{H}\right)^2 \Omega_{r0}a^{-4} , \quad (1.42)$$

where the subscript r refers to radiation. Roughly speaking, the energy density is the total energy in a unit of volume. Thus, if the energy is constant, energy density should obey $\rho \propto a^{-3}$, as the volume is proportional to a^3 . However, as one can see from (1.42), this is not true for radiation. The extra a^{-1} , in the behavior of ρ_r , comes from the fact that the energy of a photon decreases with the scale factor a due to the expansion of the universe (as we have already pointed, this can be demonstrated by geodesic equations).

⁸ Although neutrino flavour oscillations suggest the existence of massive neutrinos, we follow the Standard model of particles, which consider massless neutrinos species. For a thorough discussion of neutrinos see [77, 78].

Now, consider a flat universe ($k = 0$) dominated by radiation $\rho = \rho_{r0}a^{-4}$. Thus, from the Friedmann equation (1.28)

$$\begin{aligned} \left(\frac{\dot{a}}{a}\right)^2 &= \frac{8\pi G}{3}\rho_{r0}a^{-4}, \\ \Rightarrow a &\propto t^{1/2}. \end{aligned} \quad (1.43)$$

1.3.2 Matter

In the Λ CDM model, the matter sector is composed by baryons and cold dark matter. The baryons are very well known and described by Standard Model of particles, while cold dark matter has still an unknown nature.⁹ Matter, or non-relativistic matter, is expected to have a negligible pressure, and so $w_m = 0$. Note that a negligible pressure does not guarantee an EoS equal to zero, but rather it sets $w_m \ll 1$. However, it is useful to pragmatically approximate it to zero. Thus, due to conservation of energy and momentum

$$\begin{aligned} \dot{\rho_m} + 3\frac{\dot{a}}{a}\rho_m &= 0, \\ \rho_r(a) &= \rho_{r0}a^{-3}, \end{aligned} \quad (1.44)$$

or using the density parameter:

$$\begin{aligned} \rho_m(a) &= \frac{3H_0^2}{8\pi G}\Omega_{m0}a^{-3}, \\ \Omega_m(a) &= \left(\frac{H_0}{H}\right)^2\Omega_{m0}a^{-3}, \end{aligned} \quad (1.45)$$

where the subscript m refers to matter. In this case, as expected, matter follows $\rho \propto a^{-3}$. Note that $\Omega_m = \Omega_b + \Omega_c$, where subscripts b and c represent baryons and cold dark matter, respectively.

In analogy to the radiation case, we consider a flat universe dominated by matter. So, the Friedmann equation (1.28) gives:

$$\begin{aligned} \left(\frac{\dot{a}}{a}\right)^2 &= \frac{8\pi G}{3}\rho_{r0}a^{-3}, \\ \Rightarrow a &\propto t^{2/3}. \end{aligned} \quad (1.46)$$

1.3.3 Dark Energy

The last, but not less important, component of our universe is the dark energy. Contrary to its already mentioned birth [58], Λ is not used to address a static universe but rather an accelerated expanding universe. As already discussed, the parameter of the

⁹ It has also been considered the existence of warm and hot dark matter [79]. For extensive reviews concerning dark matter see [80, 81].

EoS of the cosmological constant is $w_\Lambda = -1$. Also, the energy density ρ_Λ and pressure p_Λ were already defined by (1.33) and (1.34), respectively.

Unlike radiation and matter, the energy density of dark energy, in the Λ CDM context, does not depend on scalar factor and hence it remains constant in time. As we see later, this will be problematic for Λ CDM. Considering $k = 0$ and a universe dominated by Λ , we obtain:

$$\begin{aligned} \left(\frac{\dot{a}}{a}\right)^2 &= \frac{\Lambda c^2}{3}, \\ \Rightarrow a &= \exp \sqrt{\frac{\Lambda}{3}} ct. \end{aligned} \quad (1.47)$$

1.3.4 Background dynamics

As the universe is expanding ($\dot{a} > 0$), at early times $a < a_0 = 1$. Equations (1.44), (1.41) and (1.33) say which density energy decreases faster, slower or remains constant. Consequently, the background dynamics of universe will consist basically of three stages: a radiation dominated era, a matter dominated era and a dark energy dominated era.¹⁰

To understand background evolution, we should use the Friedmann (1.28) and acceleration (1.29) equations, with the total energy density $\rho_T = \rho_r + \rho_m + \rho_\Lambda$. Therefore, according to (1.44), (1.41) and (1.33), we have:

$$E^2(a) = \Omega_{m0}a^{-3} + \Omega_{r0}a^{-4} + \Omega_{\Lambda0}, \quad (1.48)$$

$$q(z) = \frac{1}{2} [\Omega_m(z) + 2\Omega_r(z) - 2\Omega_\Lambda(z)], \quad (1.49)$$

where we have defined the normalized Hubble rate $E(a) \equiv H(a)/H_0$ and the deceleration parameter $q \equiv -\ddot{a}/\dot{a}^2$. The parameter q is particularly important because it determines if the universe is accelerating, $q < 0$, or decelerating, $q > 0$. Note that, though ρ_Λ is constant, Ω_Λ is not, due to the Hubble parameter. Thus, $\Omega_\Lambda \neq \Omega_{\Lambda0}$.

To solve (1.48) and (1.49) we need to know the initial conditions, which will be given, in this case, at the present time by Ω_{m0} , Ω_{r0} and $\Omega_{\Lambda0}$. For instance, observations of SNe Ia give $\Omega_{m0} = 0.295$ [83], for a flat Λ CDM universe. While observations of the CMB, obtained by the Planck collaboration, yield $\Omega_{m0} = 0.3089$, $\Omega_{r0} = 5.38916 \times 10^{-5}$ and $\Omega_{\Lambda0} = 0.691046$ [6]. We adopted these Planck results as initial conditions.

Figure 3 shows the background evolution of each component as a function of redshift. It is easy to note the three stages of the universe. At high redshift, the dynamics of the universe is dominated by radiation. Later, the contribution of matter becomes important

¹⁰ A rigorous discussion requires the inclusion of another stage of accelerated expansion, which occurs at very early times and is dubbed inflation. Inflation is out of the scope of this work; for an extensive review see [82].

and at z_{eq} we have $\Omega_m(z_{eq}) = \Omega_r(z_{eq})$, the epoch of matter-radiation equality. The redshift of equality is formally defined as $z_{eq} = (\Omega_{m0}/\Omega_{r0}) - 1$. Thus, the universe enters the era dominated by matter, during which the cosmological structures that we see form. Finally, we arrive at the current state of the universe, the accelerated expansion. Dark energy will drive the accelerated expansion at later times.

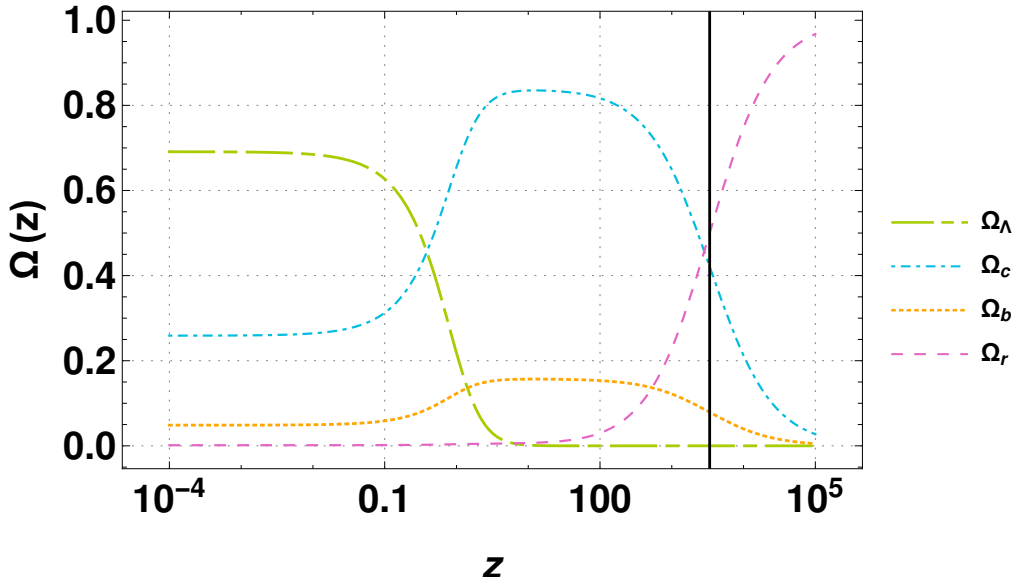


Figure 3 – Background evolution of dark energy Ω_Λ , cold dark matter Ω_c , baryons Ω_b and radiation Ω_r in a Λ CDM universe. Vertical line point out the equivalence redshift, here $z_{eq} \sim 3370$.

On the other hand, we have computed the Hubble rate and the deceleration parameter according to (1.48) and (1.49), respectively, see Figure 4. At $z > 1$, the universe is decelerating. This because the dark energy does not yet contribute and the EoS of both matter and radiation are not able to cause an accelerated expansion. Later, at $z < 1$ the cosmological constant starts to play an important role, as we see from Figure 3. Note that the change of sign on the deceleration parameter, occurs at $z \sim 0.643$.

1.3.5 Evolution of perturbations

In this section we will use conformal time, $\eta = \int dt/a$, instead of cosmic time t . Derivatives respect η will be denoted by ' and we define the Hubble parameter in conformal time as $\mathcal{H} \equiv \frac{a'}{a} = aH$. Thus, it is easily to show that the Friedmann (1.28) and acceleration (1.29) equations, in conformal time, are

$$\mathcal{H}^2 = \frac{8\pi G}{3}\rho a^2 , \quad (1.50)$$

$$\mathcal{H}' = -\frac{4\pi G}{3}(1+3w)\rho a^2 . \quad (1.51)$$

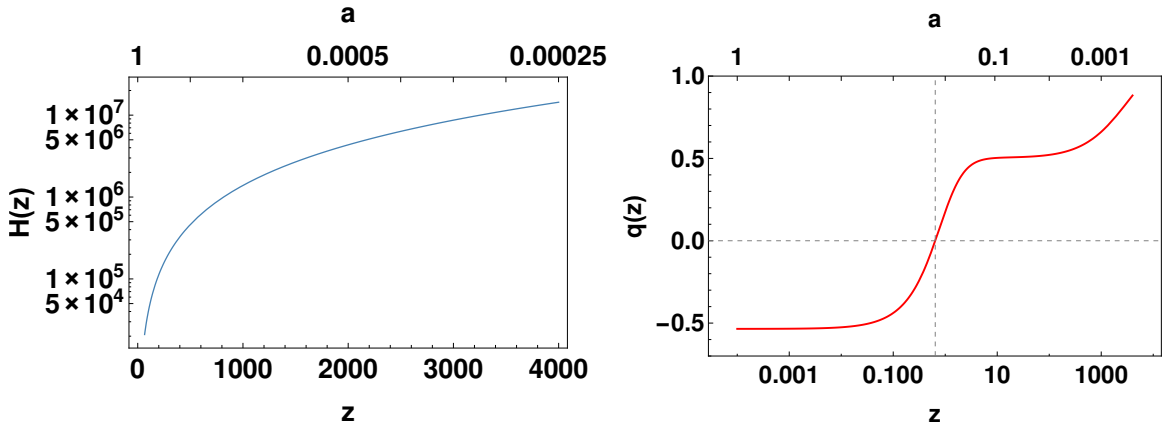


Figure 4 – **Left panel:** Hubble rate as function of redshift (or scale factor) to Λ CDM model. **Right panel:** Deceleration parameter on function of z (or a). The vertical and horizontal dashed line indicate when the deceleration becomes negative, in this case is estimated $z \sim 0.643$.

The universe seems homogeneous and isotropic at large scales. Despite of that, we cannot avoid to note that, at non-cosmological scales, this homogeneity and isotropy is broken. That is, the universe is full of structures such as galaxies, galaxy clusters, voids and filaments, and if we study them at scales of a few Mpc we will not be able to infer that we live in a homogeneous and isotropic universe. Although we embraced the cosmological principle, we must be aware that it is necessary to describe deviations from a homogeneous and isotropic background. This can be done through a very useful mathematical structure, perturbation theory. General relativity allows us to use the theory of perturbation not only to study cosmological perturbations but also, for instance, to study gravitational waves and black holes.

Cosmological perturbation theory is built under the assumption that the general metric is composed by the FLRW metric plus a small deviation. That is:

$$g_{\mu\nu} = \bar{g}_{\mu\nu} + \delta g_{\mu\nu}, \quad (1.52)$$

where $\bar{g}_{\mu\nu}$ is the background metric, in this case FLRW metric, and $\delta g_{\mu\nu}$ is the small deviation. We will use the over line of a quantity to label that as a background quantity. Also, $\delta g_{\mu\nu}$ is small in sense that it is much smaller than $\bar{g}_{\mu\nu}$. Here, we aim at obtaining the perturbed Einstein equations, which are:

$$\begin{aligned} \delta G_{\mu\nu} &= 8\pi G \delta T_{\mu\nu}, \\ \delta R_{\mu\nu} - \frac{1}{2}\delta g_{\mu\nu}R - \frac{1}{2}g_{\mu\nu}\delta R &= 8\pi G \delta T_{\mu\nu}. \end{aligned} \quad (1.53)$$

First, we shall concentrate on the geometric part, $\delta G_{\mu\nu}$. Subsequently, we will address the matter side, $\delta T_{\mu\nu}$.

Although the basic statement of cosmological perturbation theory, equation (1.52), seems very simple and trivial, there is something about it that has to be discussed. The

metrics $\bar{g}_{\mu\nu}$ and $\delta g_{\mu\nu}$ are not defined on the same manifold. Then, in order to be possible to write (1.52), it is necessary to define a map between both manifolds. However, a problem arises, this map is not uniquely defined, and, therefore, perturbations will be dependent on the map that one chooses. This is problem is known as the gauge problem. A pragmatical solution to the gauge problem is to define gauge invariant quantities. Before arguing about gauge invariant perturbations it is useful to define the perturbed metric.

The background metric, $\bar{g}_{\mu\nu}$, will be the FLRW metric. Thus, the most general perturbed metric of FLRW is

$$\delta g_{\mu\nu} = a^2 \begin{pmatrix} -2\psi(\eta, \vec{x}) & w_i(\eta, \vec{x}) \\ w_i(\eta, \vec{x}) & 2\phi(\eta, \vec{x})\delta_{ij} + h_{ij}(\eta, \vec{x}) \end{pmatrix}, \quad (1.54)$$

where ψ and ϕ are scalars, w_i is a 3-vector and h_{ij} is traceless a 3-tensor [84]. For the sake of simplicity, we will write only ζ instead of $\zeta(\eta, \vec{x})$, where ζ represents a perturbation quantity, such as ψ , ϕ , w_i or h_{ij} . Although $\delta g_{\mu\nu}$ is the most general perturbed metric to a homogeneous and isotropic universe, it can be decomposed in a more useful form using the scalar-vector decomposition (hereafter, SVT decomposition).

Lifshitz was the first to performe SVT decomposition [85]. He used Helmholtz's theorem to recast (1.54), considering that it can be separated in scalar, vector and tensor perturbations. For instance, we can decompose w_i as:

$$w_i = w_i^\parallel + w_i^\perp,$$

where it is imposed $\epsilon^{ijk}\partial_j w_k^\parallel = \partial^i w_i^\perp = 0$. Also, by Stokes theorem one has $w_i^\parallel = \partial_i E$. Therefore, the vector w_i can be rewritten as

$$w_i = \partial_i E + S_i, \quad (1.55)$$

where $S_i \equiv w_i^\perp$. One can apply the same procedure to h_{ij} so that:

$$h_{ij} = \left(\partial_i \partial_j - \frac{1}{3} \delta_{ij} \nabla^2 \right) B + \partial_i A_j + \partial_j A_i + h_{ij}^T, \quad (1.56)$$

where E and B are scalar perturbations, S_i and A_i are vector perturbations and h_{ij} is a tensor perturbation. Here, vector perturbations are solenoidal, i.e. $\partial^k S_k = \partial^k A_k = 0$, and tensor perturbations are traceless $h^k_k = 0$. The importance of the SVT decomposition lies in the fact that, if one considers perturbations at first order, the different kinds of perturbations will not be coupled and we shall able to track their evolutions, one by one independently.

Both tensor and vector perturbations are important in cosmology, for instance, to study gravitational waves or topological defects. However, we shall only focus on the scalar perturbations.¹¹ Considering only scalar cosmological perturbations $S_i = A_i = h_{ij}^T = 0$,

¹¹ See [86] for a discussion about the three kinds of perturbations.

then one has

$$\delta g_{\mu\nu} = a^2 \begin{pmatrix} -2\psi & \partial_i E \\ \partial_i E & 2\phi\delta_{ij} + (\partial_i\partial_j - \frac{1}{3}\delta_{ij}\nabla^2)B \end{pmatrix}. \quad (1.57)$$

Now, in order to fix completely the gauge, we choose $E = B = 0$. Thereby, we will have the perturbed metric in the Newtonian (or longitudinal or shear-free) gauge [84]:

$$ds^2 = a^2(\eta) [- (1 + 2\psi) d\eta^2 + (1 + 2\phi) \delta_{ij} dx^i dx^j]. \quad (1.58)$$

Gauges invariant quantities are built in order to tackle the gauge problem. For the case of geometry one usually uses the Bardeen's potentials [87], which are:

$$\begin{aligned} \Psi &= \psi + \frac{1}{a} \left[\left(E + \frac{B'}{2} \right) a \right]', \\ \Phi &= \phi + \mathcal{H} \left(E - \frac{B'}{2} \right) - \frac{1}{6} \nabla^2 B. \end{aligned}$$

It is easy to note that in the Newtonian gauge the Bardeen's potentials are the potentials of the metric, i.e. $\Psi = \psi$ and $\Phi = \phi$. We will assemble the Einstein equation using Bardeen's potentials. So far, we have used “ ϕ ” to represent the gravitational potential. Henceforth, we will use only the Bardeen's potentials Φ and Ψ . Later on we will use “ ϕ ” to represent the scalar field of coupled quintessence models.

Given (1.58), we are able to compute $\delta G_{\mu\nu}$. For that, we have to use the perturbed version of (1.4) and (1.10), which are:

$$\begin{aligned} \delta \Gamma_{\nu\lambda}^\mu &= \frac{1}{2} \delta g^{\mu\alpha} (\partial_\lambda g_{\alpha\nu} + \partial_\nu g_{\alpha\lambda} - \partial_\alpha g_{\nu\lambda}) + \frac{1}{2} g^{\mu\alpha} (\partial_\lambda \delta g_{\alpha\nu} + \partial_\nu \delta g_{\alpha\lambda} - \partial_\alpha \delta g_{\nu\lambda}), \\ \delta R_{\mu\nu} &= \partial_\alpha \delta \Gamma_{\mu\nu}^\alpha - \partial_\nu \delta \Gamma_{\mu\alpha}^\alpha + \delta \Gamma_{\mu\nu}^\alpha \Gamma_{\alpha\beta}^\beta + \Gamma_{\mu\nu}^\alpha \delta \Gamma_{\alpha\beta}^\beta - \delta \Gamma_{\mu\beta}^\alpha \Gamma_{\alpha\nu}^\beta - \Gamma_{\mu\beta}^\alpha \delta \Gamma_{\alpha\nu}^\beta. \end{aligned}$$

Thus, the components of Einstein tensor are:

$$\delta G_0^0 = 2a^{-2} [3\mathcal{H}(\mathcal{H}\Psi - \Phi') + \nabla^2 \Phi], \quad (1.59)$$

$$\delta G_i^0 = 2a^{-2} \partial_i (\Phi' - \mathcal{H}\Psi), \quad (1.60)$$

$$\begin{aligned} \delta G_j^i &= 2a^{-2} [(\mathcal{H}^2 + 2\mathcal{H}')\Psi + \mathcal{H}\Psi' - \Phi'' - 2\mathcal{H}\Phi'] \delta_j^i \\ &\quad + a^{-2} [\nabla^2 (\Psi + \Phi) \delta_j^i - \partial^i \partial_j (\Psi + \Phi)]. \end{aligned} \quad (1.61)$$

Now, we shall focus on $\delta T_{\mu\nu}$.

Before showing the perturbed energy-momentum tensor it is useful to define the density contrast ρ and the velocity divergence θ . They are defined as:

$$\delta \equiv \frac{\delta\rho}{\rho}, \quad (1.62)$$

$$\theta \equiv \partial_i v^i, \quad (1.63)$$

where $v^i = \frac{dx^i}{d\eta}$ is the peculiar velocity, which comes from the definition of the four-velocity

$$U^\mu = \left[\frac{1}{a} (1 - \Psi), \frac{v^i}{a} \right] . \quad (1.64)$$

Also, the sound speed is defined according to:

$$c_s^2 \equiv \frac{\delta p}{\delta \rho} . \quad (1.65)$$

Thus, the perturbed energy-momentum tensor for a perfect fluid (1.25), is

$$\delta T_\nu^\mu = [(1 + c_s^2) U^\mu U_\nu + c_s^2 \delta_\nu^\mu] \delta \rho + (1 + w) (\delta U^\mu U_\nu + U^\mu \delta U_\nu) \rho . \quad (1.66)$$

From (1.66) we determine its components

$$\delta T_0^0 = -\delta \rho , \quad (1.67)$$

$$\delta T_i^0 = (1 + w) \rho v^i , \quad (1.68)$$

$$\delta T_j^i = c_s^2 \delta_j^i \delta \rho . \quad (1.69)$$

We have derived both sides of (1.53). Then, using (1.59)-(1.61) and (1.67)-(1.69), we arrive to

$$3\mathcal{H}(\mathcal{H}\Psi - \Phi') + \nabla^2 \Phi = 4\pi G a^2 \rho \delta , \quad (1.70)$$

$$\nabla^2 (\Phi' - \mathcal{H}\Psi) = -4\pi G a^2 (1 + w) \rho \theta , \quad (1.71)$$

$$\Psi = -\Phi , \quad (1.72)$$

$$\Phi'' + 2\mathcal{H}\Phi' - \mathcal{H}\Psi' - (\mathcal{H}^2 + 2\mathcal{H}')\Psi = -4\pi G a^2 c_s^2 \rho \delta . \quad (1.73)$$

This set of equations is the perturbed Einstein equation and each of them has a particular role in the physics of cosmological perturbations. For instance, (1.70) is called the relativistic Poisson equation, as in the limit $a = 1$ and $\mathcal{H} = 0$ it becomes to the Newtonian Poisson equation. It relates directly the matter distribution to the gravitational potentials. On the other hand, equation (1.72) comes from the anisotropic stress of $T_{\mu\nu}$, which is often represented by $\pi_{\mu\nu}$. We have approached the Einstein equations using a perturbed perfect fluid and so $\pi_{\mu\nu} = 0$. This is completely valid for the aim of this work, but we have to be careful. At early times, neutrinos and photons cause anisotropic stress due their quadrupole moments [69]. Also, finding any deviation from $\Psi = -\Phi$ have become an important test for physics beyond Λ CDM [88, 8]. Finally, (1.73) is related to pressure perturbations.

Besides the perturbed Einstein equation, we can derive the perturbed conservation equation (1.27) by calculating $\delta(\nabla_\mu T_\nu^\mu) = 0$:

$$\delta(\nabla_\mu T_\nu^\mu) = \partial_u \delta T_\nu^\mu - \delta \Gamma_{\nu\beta}^\alpha T_\alpha^\beta - \Gamma_{\nu\beta}^\alpha \delta T_\alpha^\beta + \delta \Gamma_{\beta\alpha}^\alpha T_\nu^\beta + \Gamma_{\beta\alpha}^\alpha \delta T_\nu^\beta . \quad (1.74)$$

For $\nu = 0$ (1.74) becomes:

$$\delta' + 3\mathcal{H}(c_s^2 - w)\delta = -(1 + w)(\theta + 3\Phi') , \quad (1.75)$$

which is called the perturbed continuity equation. On the other hand, if $\nu = i$, we get

$$\theta' + \left[\mathcal{H}(1 - 3w) + \frac{w'}{1+w} \right] \theta = -\nabla^2 \left(\frac{c_s^2}{1+w} \delta + \Psi \right), \quad (1.76)$$

which is the perturbed Euler equation. We can see that most of equations (1.59)-(1.76) have both spatial and temporal derivatives. So, in order to simplify the treatment we use the Fourier transformation.

Given a function $g(\vec{x})$, we define its Fourier transform by

$$\tilde{g}(\vec{k}) = \int g(\vec{x}) e^{-i\vec{k}\cdot\vec{x}} d^3x, \quad (1.77)$$

and, consequently, its inverse as

$$g(\vec{x}) = \frac{1}{(2\pi)^3} \int \tilde{g}(\vec{k}) e^{i\vec{k}\cdot\vec{x}} d^3k. \quad (1.78)$$

Thus, to practical effects, performing Fourier transforms means:

$$\begin{aligned} g(\vec{x}) &\rightarrow e^{i\vec{k}\cdot\vec{x}} \tilde{g}(\vec{k}), \\ \partial_i g(\vec{x}) &\rightarrow ik_i e^{i\vec{k}\cdot\vec{x}} \tilde{g}(\vec{k}), \\ \nabla^2 g(\vec{x}) &\rightarrow -k^2 e^{i\vec{k}\cdot\vec{x}} \tilde{g}(\vec{k}). \end{aligned}$$

In order to simplify notation, in this chapter, we drop the \sim of quantities defined in Fourier space. Tilde will only be used if we need to distinguish between quantities in the real or Fourier space.

In Fourier space, equations (1.59)-(1.76) are (note that we have used $\Phi = -\Psi$):

$$k^2 \Phi + 3\mathcal{H}(\Phi' + \mathcal{H}\Phi) = 4\pi G a^2 \rho \delta, \quad (1.79)$$

$$k^2 (\Phi' + \mathcal{H}\Phi) = -4\pi G a^2 (1+w) \rho \theta, \quad (1.80)$$

$$\Phi'' + 3\mathcal{H}\Phi' + (\mathcal{H}^2 + 2\mathcal{H}')\Phi = -4\pi G a^2 c_s^2 \rho \delta, \quad (1.81)$$

$$\delta' + 3\mathcal{H}(c_s^2 - w)\delta = -(1+w)(\theta + 3\Phi'), \quad (1.82)$$

$$\theta' + \left[\mathcal{H}(1 - 3w) + \frac{w'}{1+w} \right] \theta = k^2 \left(\frac{c_s^2}{1+w} \delta - \Phi \right). \quad (1.83)$$

To track the evolution of perturbations, we should solve this set of equations. As we have already pointed out, considering (1.66) was an important step to obtain (1.79)-(1.83). However, we have not specified $\delta T_{\mu\nu}$. As it happens in the background, we address the cosmos as a perfect fluid composed of radiation, matter and dark energy. Then, energy density, density contrast, velocity divergence and the EoS parameter in the perturbed

Einstein equations (1.79)-(1.81) that represent the total material contributions are

$$\begin{aligned}\rho_T &= \rho_m + \rho_r + \rho_\Lambda , \\ \delta_T &= \Omega_m \delta_m + \Omega_r \delta_r , \\ \theta_T &= \frac{(1+w_m)\Omega_m\theta_m + (1+w_r)\Omega_r\theta_r}{1+w_{ef}} , \\ w_{ef} &= \Omega_m w_m + \Omega_r w_r + \Omega_\Lambda w_\Lambda .\end{aligned}$$

Instead, due to the absence of interactions between species the relationship $\delta\nabla^\mu T_{\mu\nu} = 0$ is always true, at least in general relativity, and equations (1.82) and (1.83) are valid for all material components. It means that the quantities δ , θ , w and c_s^2 are related to just one material component. Thus, we have for matter and radiation

$$\delta'_m = -(\theta_m + 3\Phi') , \quad (1.84)$$

$$\theta'_m = -(\mathcal{H}\theta_m + k^2\Phi) , \quad (1.85)$$

$$\delta'_r = -\frac{4}{3}(\theta_r + 3\Phi') , \quad (1.86)$$

$$\theta'_r = k^2 \left(\frac{\delta_r}{4} - \Phi \right) , \quad (1.87)$$

where we have been used, $c_s^2 = w$, which is valid both for matter and radiation.

We can put together the equations previously shown. For example, using (1.79) and (1.80), one can demonstrate that

$$k^2\Phi = 4\pi G\rho_T \left[\delta_T + \frac{3\mathcal{H}}{k^2}(1+w_{ef})\theta_T \right] . \quad (1.88)$$

Also, using (1.79) and (1.81), we have

$$\Phi'' + 3\mathcal{H}(1+c_s^2)\Phi' + [c_s^2k^2 + (1+3c_s^2)\mathcal{H}^2 + 2\mathcal{H}']\Phi = 0 . \quad (1.89)$$

Now, using (1.82) and (1.83), we get

$$\delta''_i + \mathcal{H}(1-3w_i)\delta'_i + k^2c_s^2\delta_i = (1+w_i)\{-3[\Phi'' + \mathcal{H}(1-3w_i)\Phi'] + k^2\Phi\} , \quad (1.90)$$

whenever the subscript is $i = \{r, m\}$. Obtaining solutions of these equations is only possible for particular cases. It means that we have to restrict our study to particularly scales, such as super-horizon ($k \ll \mathcal{H}$) or sub-horizon scales ($k \gg \mathcal{H}$), and for specific epochs of the universe, for instance, matter-dominated or radiation-dominated epochs. Despite in this work we have interest in the evolution of perturbations at scales inside the Hubble radius in the matter-dominated epoch, let us show a brief discussion about the evolution on super-horizon scales.

By (1.50) and (1.51), we obtain the useful relation $2\mathcal{H}' = -(1+3w_{ef})\mathcal{H}^2$. Thus,

$$\Phi'' + 3\mathcal{H}(1+c_s^2)\Phi' + [c_s^2k^2 + \mathcal{H}^2(c_s^2 - w_{ef})]\Phi = 0 ,$$

under assumption that $c_s^2 = w_{ef}$, and for scales outside of Hubble radius ($k \ll \mathcal{H}$), we have

$$\Phi'' + 3\mathcal{H}(1 + c_s^2)\Phi' = 0 ,$$

which leads to the solution $\Phi' = 0$. The hypothesis $c_s^2 = w_{ef}$ is only satisfied during the radiation- or matter-dominated epochs. In order to clarify this fact, we use the definition of c_s^2 and w_{ef} which is valid for a radiation-matter fluid, given by

$$c_s^2 = \frac{1}{3(1 + 3\Omega_m/4\Omega_r)} , \quad (1.91)$$

$$w_{ef} = w_r\Omega_r + w_m\Omega_m . \quad (1.92)$$

Asymptotically, one can note that $c_s^2 = w_{ef}$. For instance, deep into the radiation-dominated epoch, $\Omega_r \rightarrow 1$, we have $c_s^2 = w_{ef} = 1/3$. Analogously, when $\Omega_m \rightarrow 1$ it is $c_s^2 = w_{ef} = 0$. However, during the equality epoch, where $\Omega_r \sim \Omega_m$, the situation looks different. We illustrate c_s^2 and w_{ef} as a function of redshift in Figure 5. In conclusion, for scales $k \ll \mathcal{H}$, the gravitational potential remains constant both for the radiation-dominated and matter-dominated epochs, being this not true for the transition epoch.¹² Using the Poisson equation (1.79), we can also find that $\delta = \text{const}$. Therefore, perturbations at scales outside the Hubble radius, $1/\mathcal{H}$, do not evolve during matter-dominated and radiation-dominated epochs.

We now particularize (1.90) to the matter case ($w_i = 0$). Taking into account (1.88), we have

$$\delta_m'' + \mathcal{H}\delta_m' + k^2c_s^2\delta_m = -3[\Phi'' + \mathcal{H}\Phi'] + 4\pi G\rho_T \left[\delta_T + \frac{3\mathcal{H}}{k^2}(1 + w_{ef})\theta_T \right] .$$

As we have said before, at $k \ll \mathcal{H}$ scales, both Φ and δ remain constant. Here, we investigate the case of sub-horizon scales, defined by $k \gg \mathcal{H}$. A limit at sub-horizon scales neglects the term related to velocity fields θ_T coming from the Poisson equation. However, it is not the only term that shall be neglected. The first term on the right-hand side of the last equation will also be negligible. Using (1.80) and the Friedmann equation (1.50) one has, under $k \gg \mathcal{H}$, $\Phi'' + \mathcal{H}\Phi' \approx 0$. Therefore:

$$\delta_m'' + \mathcal{H}\delta_m' + c_s^2k^2\delta_m - \frac{3}{2}\mathcal{H}^2\delta_T = 0 , \quad (1.93)$$

where we have used again the Friedmann equation (1.50). This is the fundamental equation in the study of gravitational instability [89]. For example, considering $\delta_T = \delta_m$, one has

$$\delta_m'' + \mathcal{H}\delta_m' + \left(c_s^2k^2 - \frac{3}{2}\mathcal{H}^2 \right) \delta_m = 0 ,$$

in which the behavior of δ_m will be defined by the sign of $(c_s^2k^2 - \frac{3}{2}\mathcal{H}^2)$. Matter shall cluster, $\delta_m' > 0$, if the effect of pressure is negligible and so $(c_s^2k^2 - \frac{3}{2}\mathcal{H}^2) < 0$. Instead

¹² Actually, it is possible to demonstrate that during the transition the potential loses 1/10 of its value [69].

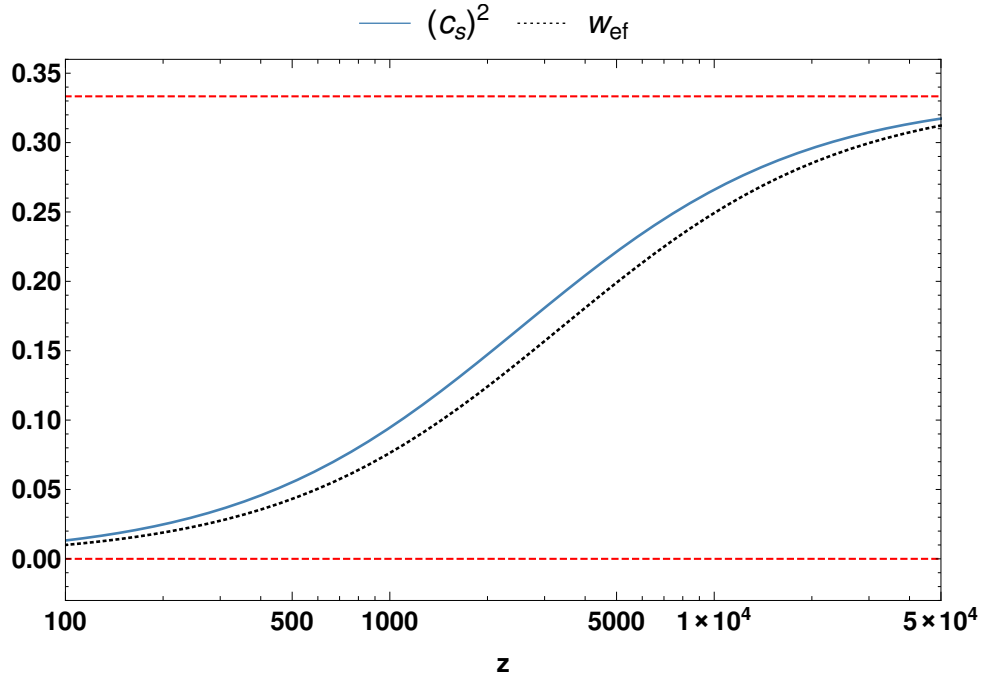


Figure 5 – Sound velocity c_s^2 and w_{ef} for a matter-radiation fluid. Red dotted lines are the values $w_r = 1/3$ and $w_m = 0$. It is easy to note that during the transition between radiation-dominated and matter-dominated epoch $c_s^2 \neq w$.

clustering will be stopped when the pressure is strong enough to be comparable to the force of gravity. Pressure of non-relativistic matter is negligible and then we expect that δ_m always grows. How fast δ_m grows will be determined by $\mathcal{H}^2\delta_m$ (or $\mathcal{H}^2\delta_T$, in general).

We are interested in the phase of the universe during which radiation can be neglected in the δ_T shown in (1.93). Consequently, we have $\delta_T = \Omega_m\delta_m$. Obviously, $\delta_\Lambda = 0$, because ρ_Λ is constant. It is useful to define the growth rate $f(z)$, given by

$$f(z) \equiv \frac{d \ln \delta_m}{d \ln a} , \quad (1.94)$$

which quantifies how fast matter clusters with respect to the scale factor. Also, we use de e-fold numbers $N \equiv \ln a$. From $dN = \mathcal{H}d\eta$, and using (1.94), we can recast (1.93) as:

$$\frac{df}{dN} + f^2 + \frac{1}{2} [1 - 3w_{ef}] f - \frac{3}{2}\Omega_m = 0 ,$$

where we have used $2d\mathcal{H}/dN = -(1 + w_{ef})\mathcal{H}$. Finally, we have neglected radiation, i.e. $w_{ef} = w_\Lambda\Omega_\Lambda = w_\Lambda(1 - \Omega_m)$, and hence

$$\frac{df}{dN} + f^2 + \frac{1}{2} [1 - 3w_\Lambda(1 - \Omega_m)] f - \frac{3}{2}\Omega_m = 0 . \quad (1.95)$$

This equation does not have an analytic solution. Instead one can obtain an approximate solution using the template $f(z) = \Omega_m^\gamma$. For ΛCDM one has $\gamma \approx 0.55$. We reserve a more extensive discussion of this equation and its solution for the next chapter.

So far, we have dealt with the density contrast δ . Now, we discuss the velocity fields θ . Equation (1.79) for scales inside the Hubble horizon, $k \gg \mathcal{H}$, is

$$k^2\Phi = 4\pi G a^2 \rho_T \delta_T = \frac{3}{2} \mathcal{H}^2 \delta_T ,$$

substituting that in (1.84), we have

$$\delta'_m = -\theta_m - \frac{9}{2} \frac{\mathcal{H}^2}{k^2} [\delta'_T - (1 + 3w_{ef}) \delta_T \mathcal{H}] .$$

At sub-horizon scales, $k \gg \mathcal{H}$, the last term is negligible and hence

$$\delta'_m = -\theta_m .$$

We have introduced the velocity gradient in (1.63) in order to simply the computation, but here it is convenient to return to the peculiar velocity v_i . Equation (1.63) in Fourier space becomes $\theta = ik_l v^l$ so that we have

$$\delta'_m = -ik_j v^j \tag{1.96}$$

or, using the growth rate $f \equiv d \ln \delta_m / d \ln a = \delta'_m / \mathcal{H} \delta_m$:

$$v^j = i \mathcal{H} f \delta_m \frac{k^j}{k^2} . \tag{1.97}$$

While equation (1.96) relates the distribution of matter to the peculiar velocity field, equation (1.97) shows how the field of peculiar velocity can be computed using the growth rate $f(z)$. The peculiar velocity is the deviation from the recession velocity due to Hubble expansion. Likewise to δ_m , the field of velocities v^i becomes important at local scales. Later, we shall investigate how peculiar velocities could bias the local measurements of H_0 .

The target of this subsection was to arrive at equations (1.95) and (1.97), which will be fundamental in the study of the cosmic variance. We have not discussed other important topics about cosmological perturbations. For instance, using the perturbed Einstein equations (corrected to π_{ij}) together with the Boltzmann equations allow us to study the spectrum of CMB and thermal history of the universe, see for example [69, 76]. Here, we have based our examination of cosmological perturbations mostly on [84].

1.4 PROBLEMS IN THE STANDARD PARADIGM

Despite the incredible success of the Λ CDM model, some problems, both theoretical and observational, do affect this cosmological model. For instance: the fine-tuning problem [90], the coincidence problem [91], the small scales problems [92], the Lithium problem [93], the CMB anomalies [94] and tensions on the values of parameters such as H_0 and

σ_8 ¹³. Although all of them are largely discussed in the literature, we shall focus the ones that relate to dark energy, that is, the fine-tuning problem and the coincidence problem.

Cosmological observations allow us to constraint the energy density of Λ to the very small value $\rho_\Lambda^{\text{obs}} \approx 10^{-47} \text{GeV}^4$ [6]. The value of vacuum energy should be predicted by quantum field theory. A problem arises when one compares $\rho_\Lambda^{\text{obs}}$ with the value predicted by quantum field theory, which is $\rho_\Lambda^{\text{QTF}} \approx 10^{76} \text{GeV}^4$. The ratio between these is about 10^{123} (or $\sim 10^{30}$ if one considers energy scales). This mismatch between $\rho_\Lambda^{\text{obs}}$ and $\rho_\Lambda^{\text{QTF}}$ is dubbed the fine-tuning problem and it would indicate that vacuum energy is not well represented by ρ_Λ . Another problem related to dark energy is the so-called coincide problem. In essence, the coincidence problem questions why the universe is currently dominated by the dark energy, that is why $\Omega_{\Lambda 0}/\Omega_{c0} \sim \mathcal{O}(1)$.

Both the coincidence and fine-tuning problems are often used to attack the Λ CDM model. In fact, both problems are interconnected: solving the fine-tuning problem could help explaining why $\Omega_{\Lambda 0}/\Omega_{c0} \sim \mathcal{O}(1)$, see for example [95]. Although the fine-tuning problem could be the biggest problem of Λ CDM, some authors point out that there is not nothing relevant behind the ratio $\rho_\Lambda^{\text{QTF}}/\rho_\Lambda^{\text{obs}} \sim 10^{123}$, and that this problem concerns quantum field theory rather than cosmology [96].

¹³ Strictly speaking, tensions are not yet problems of Λ CDM. We will discuss this later.

2 Beyond the cosmological constant

As we have already pointed out before, the cosmological constant is the first (and perhaps the simplest) attempt to explain the accelerated expansion of the universe. We can put Λ on the right-hand side or left-hand side of Einstein equations, consider it as a material component or a geometrical feature. In fact, this ambiguity is inherent to most of the dark energy models; modifying $T_{\mu\nu}$ or $G_{\mu\nu}$ can lead to equivalent models. Summarizing, to tackle the accelerated expansion of the universe we can either modify gravity or add a new material component.

The number of dark energy models that have been proposed could be found scary. They do not only quantify our scientific enthusiasm, but they also reflect the level of our ignorance. Among them, we can mention: quintessence model, k -essence model, Chaplygin gas model, dark sector interactions, $f(R)$ theories, braneworld models and scalar tensor theories.¹ For the scope of this work, we study interacting quintessence models, which have been considered in order to cure tensions in Λ CDM [18, 19]. Here, we show the background dynamics and some aspects of perturbations that characterize this model. Also, we consider some useful extensions of Λ CDM in order to better understand the nature of dark energy and cure the tension on H_0 (which will be discussed in Chapter 3).

2.1 COUPLED QUINTESSENCE

The presumable existence of a dark sector and the fact that $\Omega_{\Lambda 0}/\Omega_{c0} \sim \mathcal{O}(1)$ seems to suggest that there is a “communication” between components of the dark sector. Coupled quintessence corresponds to an extension of classical quintessence [101, 102] in which the canonical scalar field, ϕ , interacts with the non-relativistic matter. This model was proposed by Amendola[103] and has been largely studied in the literature [18, 19, 104, 105, 106, 107, 108, 109, 110, 111, 112, 113, 114, 115]. The action is:,

$$S = \int \left(\frac{R}{2\kappa^2} + \mathcal{L}_{CQ} \right) \sqrt{-g} d^4x + S_M, \quad (2.1)$$

$$\mathcal{L}_{CQ} = -\frac{1}{2}\partial_\mu\phi\partial_\nu\phi - V(\phi) - m(\phi)\bar{\psi}\psi + \mathcal{L}_{\text{kin}}[\psi], \quad (2.2)$$

where $V(\phi)$ is the self-interaction potential, $m(\phi)$ is the mass of a matter particle, ψ represent the matter fields and $\mathcal{L}_{\text{kin}}[\psi]$ is the kinetic term of the matter Lagrangian.

¹ See [56, 84, 97, 98, 99, 100], and references therein, for a review of the most important models of dark energy.

2.1.1 Background dynamics

Evidently, Friedmann equations will govern background dynamics, but unlike the Λ CDM case the equations coming from $\nabla_\nu T_\mu^\nu = 0$ will be modified by the presence of the interaction between ϕ -DM. For a multi-component system, the total energy-momentum tensor is conserved, but this is not necessarily true for the energy-momentum tensor of each component [116]. Consider that $T_\nu^\mu = \sum_i T_{(i)\nu}^\mu$, where i represents each component, that is, radiation, matter and dark energy (scalar field ϕ). Energy-momentum conservation states

$$\nabla_\mu \sum_i T_{(i)\nu}^\mu = 0 ,$$

but for each component one has:

$$\nabla_\mu T_{(i)\nu}^\mu = Q_{(i)\nu} ,$$

where, in order to satisfy the total conservation, it is necessary that $\sum_i Q_{(i)\nu} = 0$. In order not to affect the dynamics of baryons, we consider only interactions between dark energy ϕ and dark matter. So,

$$\begin{aligned} \ddot{\phi} + 3H\dot{\phi}^2 + \dot{\phi} \frac{dV}{d\phi} &= Q_{(\phi)0} , \\ \dot{\rho}_c + 3H\rho_c &= -Q_{(\phi)0} . \end{aligned}$$

The coupling term, $Q_{(\phi)\mu}$, is defined by the Lagrangian (2.2), from which one obtains

$$Q_{(\phi)\mu} = \frac{\partial \ln m(\phi)}{\partial \phi} \rho_c \partial_\mu \phi .$$

We shall limit our study to $m(\phi) = m_0 e^{\sqrt{2/3}\kappa\beta}$,² then:

$$\ddot{\phi} + 3H\dot{\phi} + \frac{dV}{d\phi} = \sqrt{\frac{2}{3}}\kappa\beta\rho_c , \quad (2.3)$$

$$\dot{\rho}_c + 3H\rho_c = -\sqrt{\frac{2}{3}}\kappa\beta\rho_c\dot{\phi} . \quad (2.4)$$

Now, before discussing background dynamics, we have to clarify some things about the interaction.

The interaction between DE-DM transfers energy from one component to the other, through the coupling $Q \equiv Q_{(\phi)0} = \sqrt{\frac{2}{3}}\kappa\beta\rho_c\dot{\phi}$. The sign of Q defines the direction of energy transfer. That is, if $Q > 0$ the energy of DM will be transferred to DE, while if $Q < 0$ the opposite happens. On the other hand, the strength of the coupling is determined by β . It can be shown that background dynamics is insensitive to the sign of β [117, 103], then, following the convention adopted in the literature [104, 105, 106], we consider $\beta > 0$. Also, it is useful to define $\mathcal{Q} \equiv \sqrt{\frac{2}{3}}\kappa\beta$. Current constraints on β are $\beta \lesssim 0.06$ [118].

² The numerical factor $\sqrt{2/3}$ arises in order to simplify computations, as we will see shortly.

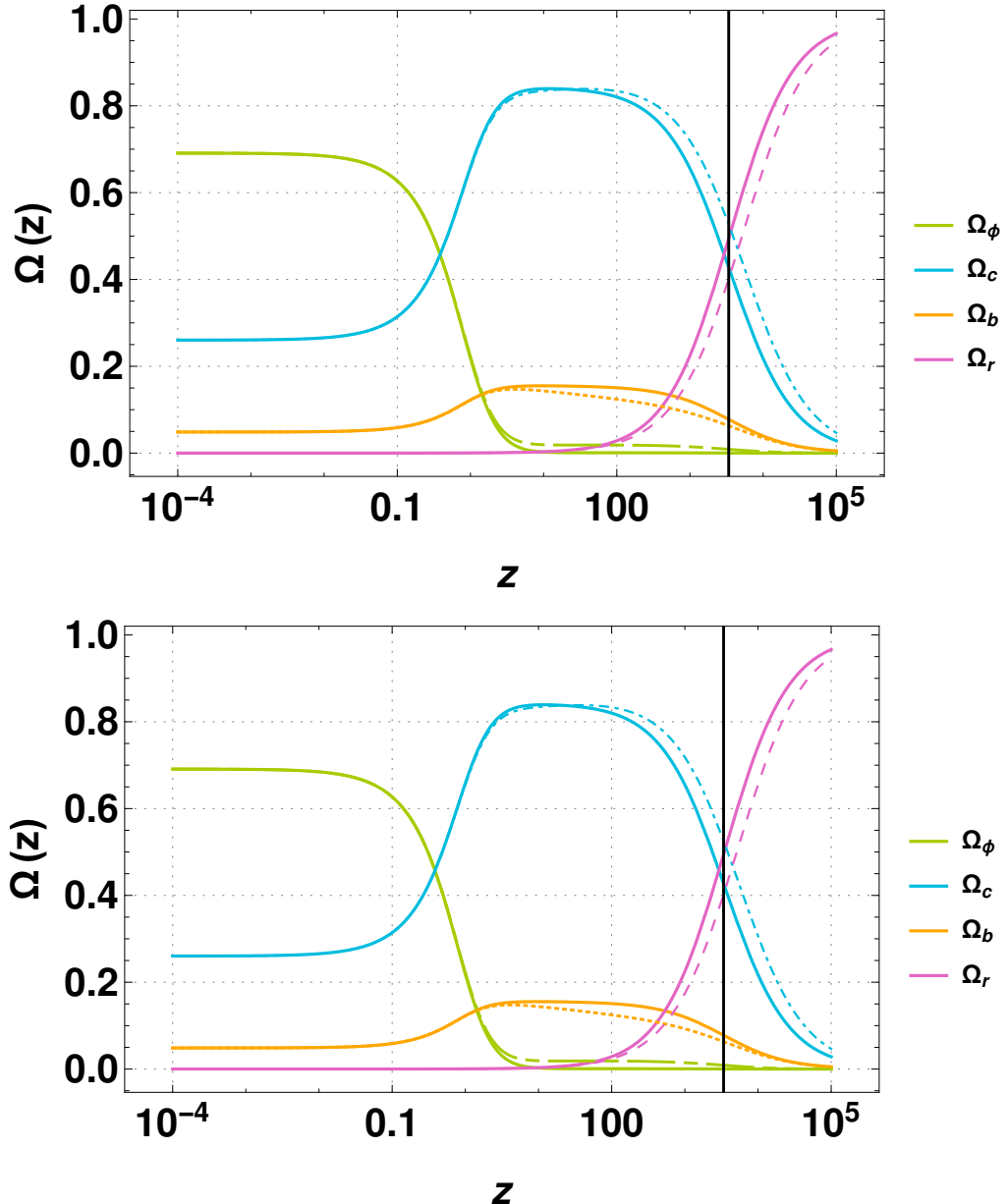


Figure 6 – **Top panel:** Background dynamics for $\alpha = 0.1$. Solid lines represent the case with weak coupling $\beta = 0.05$, while dashed lines the case with strong coupling $\beta = 0.25$. **Bottom panel:** Background dynamics for $\alpha = 0.08$. Solid lines represent the case with weak coupling $\beta = 0.05$, while dashed lines the one with strong coupling $\beta = 0.25$. In both cases a vertical line is placed at z_{eq} . See the text for more details.

As the coupling is only between DE-DM, the others components are conserved and they evolve as showed in equations (1.41) and (1.44). Now, we can write the Friedmann equation:

$$H^2 = \frac{8\pi G}{3} (\rho_r + \rho_b + \rho_c + \rho_\phi) , \quad (2.5)$$

where, as usual, we have defined $\rho_\phi = \dot{\phi}/2 + V$ (the pressure is defined as $p_\phi = \dot{\phi}/2 - V$). As it is not possible to get an analytical solution of (2.3), we have to solve it numerically.

For that, we use the dimensionless variables

$$x_1 \equiv \frac{\kappa \dot{\phi}}{\sqrt{6}H}, \quad x_2 \equiv \frac{\kappa \sqrt{V}}{\sqrt{3}H}, \quad x_r \equiv \frac{\kappa \sqrt{\rho_r}}{\sqrt{3}H}, \quad x_b \equiv \frac{\kappa \sqrt{\rho_b}}{\sqrt{3}H}, \quad (2.6)$$

where $\Omega_\phi = x_1^2 + x_2^2$, $\Omega_{\{r,b\}} = x_{\{r,b\}}^2$ and due to the assumed flatness of the universe $\Omega_c = 1 - x_1^2 - x_2^2 - x_r^2 - x_b^2$. These definitions stem from the study of dynamical systems applied to cosmology [103, 119, 120]. Thus, the complete set of equations for the background dynamics is

$$\begin{aligned} \frac{dx_1}{dN} &= \frac{x_1}{2} (3x_1^2 - 3x_2^2 + x_r^2 - 3) - \sqrt{\frac{3}{2}} \frac{1}{\kappa V} \frac{dV}{d\phi} x_2^2 + \sqrt{\frac{3}{2}} \frac{Q}{\kappa} (1 - x_1^2 - x_2^2 - x_r^2 - x_b^2), \\ \frac{dx_2}{dN} &= \frac{x_2}{2} (3x_1^2 - 3x_2^2 + x_r^2 + 3) + \sqrt{\frac{3}{2}} \frac{1}{\kappa V} \frac{dV}{d\phi} x_1 x_2, \\ \frac{dx_b}{dN} &= \frac{x_b}{2} (3x_1^2 - 3x_2^2 + x_r^2), \\ \frac{dx_r}{dN} &= \frac{x_r}{2} (3x_1^2 - 3x_2^2 + x_r^2 - 1), \\ \frac{dH}{dN} &= -\frac{H}{2} (3x_1^2 - 3x_2^2 + x_r^2 + 3), \end{aligned}$$

where we have put explicitly the term $\sqrt{3Q^2/2\kappa^2}$ in order to justify the factor $\sqrt{2/3}$ in Q . One can note that in order to solve the background dynamics it is necessary to set the potential $V(\phi)$. We choose the potential $V(\phi) = V_0 e^{-\sqrt{2/3}\kappa\alpha\phi}$, where the numerical factor $\sqrt{2/3}$ arises for the same reason as in Q . Therefore, we have

$$\frac{dx_1}{dN} = \frac{x_1}{2} (3x_1^2 - 3x_2^2 + x_r^2 - 3) + \alpha x_2^2 + \beta (1 - x_1^2 - x_2^2 - x_r^2 - x_b^2), \quad (2.7)$$

$$\frac{dx_2}{dN} = \frac{x_2}{2} (3x_1^2 - 3x_2^2 + x_r^2 + 3) - \alpha x_1 x_2, \quad (2.8)$$

$$\frac{dx_b}{dN} = \frac{x_b}{2} (3x_1^2 - 3x_2^2 + x_r^2), \quad (2.9)$$

$$\frac{dx_r}{dN} = \frac{x_r}{2} (3x_1^2 - 3x_2^2 + x_r^2 - 1), \quad (2.10)$$

$$\frac{dH}{dN} = -\frac{H}{2} (3x_1^2 - 3x_2^2 + x_r^2 + 3). \quad (2.11)$$

These equations are presented for instance in [107].

In order to illustrate the effect of coupling, we solve the background dynamics for four cases, given by $(\alpha, \beta) = \{(0.1, 0.05), (0.1, 0.25), (0.08, 0.05), (0.08, 0.25)\}$; see Figure 6. Note that the coupling mainly changes the evolution at redshifts $z > 10$ and always leads to an accelerated expansion. On the other hand, Figure 7 shows how the Hubble rate and deceleration parameter in the CQ model with $\alpha = 0.08$ evolve. We have to highlight that the accelerated expansion of the universe occurs later in CQ models ($z \sim 0.652$ to $\beta = 0.05$) as compared with the Λ CDM model ($z \sim 0.643$). Initial conditions are given at $z = 0$ by $\{x_1(0), x_2(0), x_b(0), x_r(0), H(0)\} = \{0, \sqrt{\Omega_{A0}}, \sqrt{\Omega_{b0}}, \sqrt{\Omega_{r0}}, H_0\}$, where

$\Omega_{\Lambda 0} = 0.691$, $\Omega_{b0} = 0.0486$, $\Omega_{b0} = 5.389 \times 10^{-5}$ and $H_0 = 69.278 \text{ km s}^{-1} \text{Mpc}^{-1}$, according to Planck 2015 [6]. The study of the critical points is useful in order to understand the landscape of possible solutions, see [103, 119, 120].

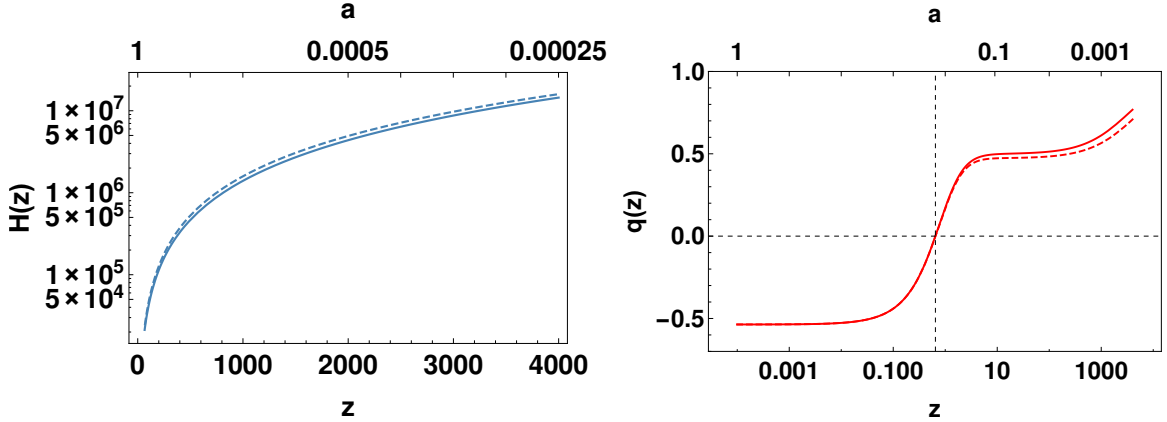


Figure 7 – **Left panel:** Hubble rate as function of redshift for the CQ model, with $\alpha = 0.08$. **Right panel:** Deceleration parameter as a function of z for the same CQ model. The vertical and horizontal dashed lines indicate when the deceleration becomes negative, in this case at $z \sim 0.652$ for $\beta = 0.25$ and $z \sim 0.652$ for $\beta = 0.05$. In both cases solid lines correspond to weak coupling $\beta = 0.05$ and dashed lines to strong coupling $\beta = 0.25$.

2.1.2 Evolution of perturbations

To track the evolution of perturbations we should compute the same equations that were obtained in Section 1.3.5. That is, we should recalculate the set of equations (1.79)-(1.83) for the CQ model. To this end, we must use (1.53), where $\delta G_{\mu\nu}$ does not change with respect to the standard case. However, $\delta T_{\mu\nu}$ will be different. Both the introduction of the coupling and the dynamical nature of dark energy (in general $\delta\phi \neq 0$) shall change the perturbed equations.

The set of equations that will describe the evolution of perturbation, at sub-horizon scales, are:

$$k^2\Phi = \frac{3}{2}\mathcal{H}^2(\delta_c\Omega_c + \delta_b\Omega_b) , \quad (2.12)$$

$$k^2\varphi = \mathcal{H}^2\beta\Omega_c\delta_c , \quad (2.13)$$

$$\delta'_b = -\theta_b , \quad (2.14)$$

$$\theta'_b = -(\mathcal{H}\theta_b + k^2\Phi) , \quad (2.15)$$

$$\delta'_c = -\theta_c , \quad (2.16)$$

$$\theta'_c = -[(1 - 2\beta x)\mathcal{H}\theta_c + k^2\Phi + 2k^2\beta\varphi] , \quad (2.17)$$

where we have defined $\varphi = \kappa\delta\phi/\sqrt{6}$. Detailed computations of these equations can be found in [103, 107, 108, 121]. The effects of the coupling and of the scalar field are easy to

distinguish. First, equations related to δ'_i are unchanged by Q and ϕ and hence coincide with Λ CDM case. This will allow us to use (1.97) even for coupling models. Similar is the case of θ'_b : if we compare it to θ'_m in equation (1.85), derived in the Λ CDM context, we shall note that they are similar. Here, one can wonder why $k^2\Phi$ does not have a direct contribution from φ , i.e. why the Poisson equation (2.12) does not have a term that depends on $\delta\varphi$ (which is different from zero). The answer is given by the equation (2.13). First, we can define $\lambda \equiv \mathcal{H}/k$ and note that $\varphi \sim \lambda$. When it is inserted in the Poisson equation, which states that $\Phi \sim \lambda$, the scalar field contributes as $\mathcal{O}(\lambda^2)$. Then, at sub-horizon scales, i.e. $\lambda \ll 1$, its contribution is totally negligible.³ Finally, (2.17) shows explicitly the contribution of Q .

By combining (2.12)-(2.17) we obtain:

$$\delta''_b + \mathcal{H}\delta'_b - \frac{3}{2}\mathcal{H}^2(\delta_c\Omega_c + \delta_b\Omega_b) = 0 , \quad (2.18)$$

$$\delta''_c + (1 - 2\beta x)\mathcal{H}\delta'_c - \frac{3}{2}\mathcal{H}^2\left[\left(1 + \frac{4}{3}\beta^2\right)\delta_c\Omega_c + \delta_b\Omega_b\right] = 0 , \quad (2.19)$$

which reduces to (1.3.5) (with $c_s^2 = 0$) if $\beta = 0$. We assumed a bias b between baryons and dark matter, $\delta_b = b\delta_c$, so that the growth rate of both is the same, i.e. (1.94) is still valid for both δ_c and δ_b . Note that if $\Omega_b \ll \Omega_c$, baryons will follow asymptotically the evolution of DM, as the latter dominates. Similar to the Λ CDM case, there is not an analytic solution for $f(z)$. Furthermore, one cannot use the simple parametrization $\Omega_m(z)^\gamma$. A suitable parametrization is the one provided by [106]:

$$f(z) \approx \Omega_m^{\tilde{\gamma}} \left(1 + 2.4\tilde{\gamma}\beta \frac{\Omega_c}{\Omega_m}\right) , \quad (2.20)$$

where $\tilde{\gamma} = 0.56$, and we have used a tilde in order to distinguish $\tilde{\gamma}$ from the value in the Λ CDM context, $\gamma \approx 0.55$.

2.2 Λ CDM EXTENSIONS

The tension in H_0 (to be discussed in Chapter 3) could be a hint for physics beyond the Λ CDM model. Then, considering CQ cosmologies could help to understand this problem. However, picking up just a model from a wide variety of dark energy models, offered in the literature, could be fruitless. Therefore, we will also investigate parametric Λ CDM extensions. To assess the usefulness of a non-standard dark energy we use two parameters w_{de} and γ . Thus, we will discuss in the next sections the three parametrizations: γ CDM, γw CDM and γ_a CDM.

³ Although, at sub-horizon scales, $\delta\varphi$ does not contribute to δ_T in the Poisson equation, the scalar field is always present in the background dynamics, that is, in general $\mathcal{H}_{\Lambda\text{CDM}} \neq \mathcal{H}_{\text{CQ}}$.

2.2.1 γ CDM parametrization

A dark energy that is different from Λ does not only change the background evolution but also alters the evolution of perturbations and, consequently, structure formation. As we pointed out before, a useful way to characterize the growth of perturbations, at least for matter, is the use of the growth rate $f(z)$. For some dark energy models it is possible to use $f(z) \approx \Omega(z)^\gamma_m$, but with $\gamma \neq 0.55$. For instance, in Dvali-Gabadadze-Porrati braneworld theory the cosmic growth index is $\gamma_{\text{DGP}} \approx 0.68$ [122].⁴

The γ CDM parametrization will be used to investigate models for which perturbations are different but the background evolves as in the standard Λ CDM model. More specifically, we will add γ to the set of 6 standard parameters of Λ CDM.

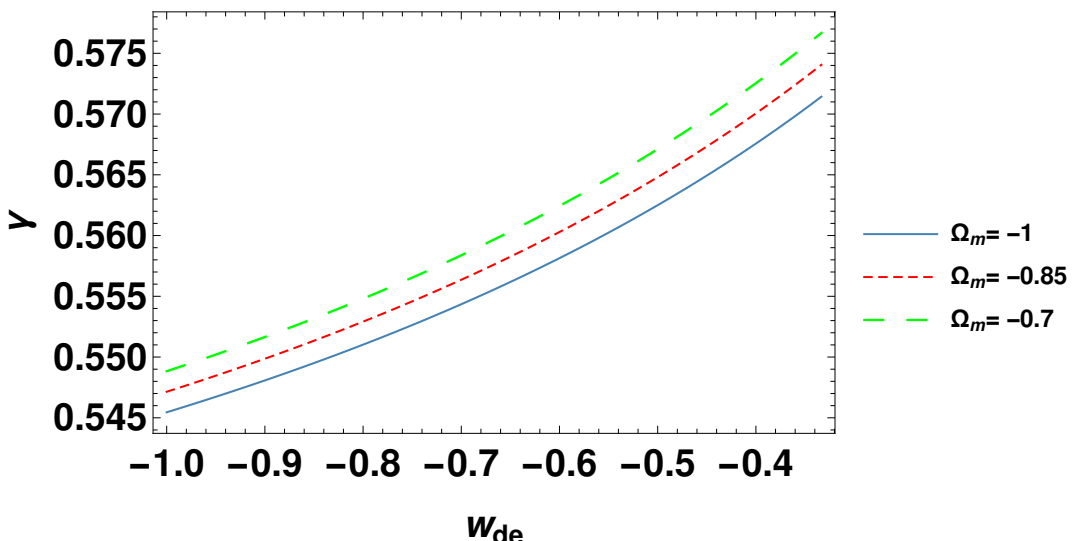


Figure 8 – Cosmic growth index γ as a function of w_{de} , see equation (2.24), for different values of Ω_m .

2.2.2 γw CDM parametrization

Now, we turn back to equation (1.95). Considering the case in which baryons and dark matter are not interacting, we can cast (2.9) as:

$$\begin{aligned} \frac{dx_m}{dN} &= \frac{3}{2}x_m(x_1^2 - x_2^2) , \\ \frac{d\Omega_m}{dN} &= 3\Omega_m(x_1^2 - x_2^2) , \\ \frac{d\Omega_m}{dN} &= 3w_{de}\Omega_m(1 - \Omega_m) , \end{aligned} \quad (2.21)$$

⁴ Strictly speaking, DGP model is not a model of dark energy but rather a gravity model beyond to General Relativity [123, 124].

where we have used the fact that $\Omega_m = x_m^2$ and $x_1^2 - x_2^2 = w_{de}\Omega_{de}$. Equation (2.21) allows us to recast equation (1.95) as [125]:

$$3w_{de}\Omega_m(1-\Omega_m)\frac{df}{d\Omega_m} + f^2 + \frac{1}{2}[1-3w_{de}(1-\Omega_m)]f - \frac{3}{2}\Omega_m = 0. \quad (2.22)$$

Finally, using the ansatz $f = \Omega_m^\gamma$ we obtain

$$3w_{de}\Omega_m(1-\Omega_m)\ln\Omega_m\frac{d\gamma}{d\Omega_m} - 3w_{de}\left(\gamma - \frac{1}{2}\right)\Omega_m + \Omega_m^\gamma - \frac{3}{2}\Omega_m^{1-\gamma} + 3w_{de}\gamma - \frac{3}{2}w_{de} + \frac{1}{2} = 0. \quad (2.23)$$

Under the condition $|d\gamma/d\Omega_m| \ll 1/(1-\Omega_m)$, the cosmic growth index will be

$$\gamma = \frac{3(1-w_{de})}{5-6w_{de}} + \frac{3(1-w_{de})(2-3w_{de})}{2(5-6w_{de})^3}(1-\Omega_m) + \mathcal{O}((1-\Omega_m)^2), \quad (2.24)$$

as was showed for the first time in [125]. If one considers a matter-dominated epoch $\Omega_m \approx 1$, and states that $w_{de} = w_\Lambda = -1$, we shall get $\gamma \approx 0.55$ —the cosmic growth index of Λ CDM case. Even if the conditions to get $\gamma \approx 0.55$ seem strict, the parametrization $\Omega_m(z)^{0.55}$ works well for the Λ CDM model for a wide range of redshifts. Figure 8 shows the cosmic growth index as a function of w_{de} when different values of Ω_m are considered. The three cases illustrated in Figure 8 are very similar. Figure 9 shows the relative error between the cases $\Omega_m = 1$ and $\Omega_m = 0.7$. It is easy to note that the error is always less than 1%.⁵

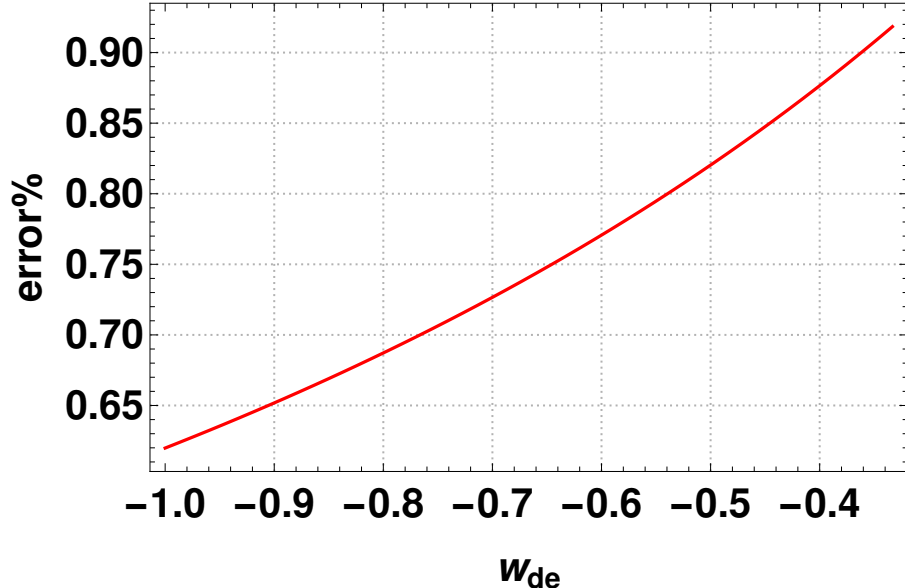


Figure 9 – Relative difference in γ when using (2.24) with $\Omega_m = 1$ and $\Omega_m = 0.7$.

Despite that (2.24) offers a relation $\gamma - w_{de}$, this could not be valid for dark energy models different from Λ , see [126] for some examples. For the same reason Figure 8 cannot

⁵ To generate these plots, we have used (2.24) neglecting terms of order $\mathcal{O}((1-\Omega_m)^2)$.

be extrapolated to phantom dark energy, i.e. when $w_{de} < -1$. However, this relationship suggests that a non-standard dark energy model could have both a $\gamma \neq 0.55$ and $w_{de} \neq -1$. Then, we shall use the γw CDM parametrization, adding w_{de} to the set of free parameters.

2.2.3 γ_a CDM parametrization

The previous discussion also suggests that γ could evolve with time, due its dependence on w_{de} . Thus, a useful extension to the previous parameterizations is to consider a dynamical cosmic growth index $\gamma = \gamma(a)$. One can find in the literature a wealth of dark energy models that can be parametrized by a growth index that evolves with time, for instance see [127, 128, 129, 130]. We will use the following simple parametrization [128] in order to study the effect of a dynamical γ

$$\gamma(a) = \gamma_0 + \gamma_1(1-a) . \quad (2.25)$$

3 The tension on H_0 and the effect of cosmic variance

Observations have been crucial for the evolution of modern cosmology. The fact that by observing the sky we can infer constraints on cosmological parameters, such as vacuum energy or the number of neutrino species, is impressive and, at some level, unexpected. At the heart of modern cosmology there are observations, such as CMB, BAO and RSD, and a large effort to obtain more accurate data is undertaken by several international collaborations such as Euclid [88], J-PAS [131] or DES [132]. However, a great amount of data does not only mean a huge opportunity to improve our knowledge about the universe, or physics in general, but also a wealth of information that has to be processed and studied. Thus, in an era where cosmological measurements are characterized by their great precision, it is fundamental to understand where errors come from and how could they affect a measurement. In the particular case of this work, it is necessary to understand what causes the tension on H_0 .

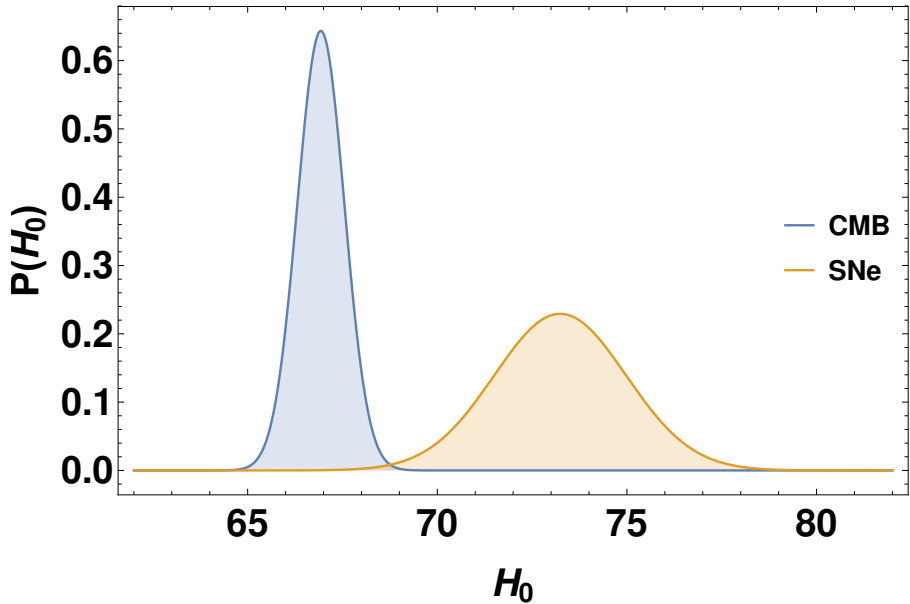


Figure 10 – Gaussian distributions for both measurements of the Hubble constant, H_0^{Pl} (CMB) and H_0^{R16} (SNe Ia). The discordance between them is evident.

The values provided by [2] and [1] are the most important current measurements of H_0 . While observations of SNe Ia at local scales provided $H_0 = 73.24 \pm 1.74 \text{ km s}^{-1} \text{ Mpc}^{-1}$ (H_0^{R16}), the analysis of fluctuations of the temperature of photons released at the last scattering constrains the Hubble constant to $H_0 = 66.93 \pm 0.62 \text{ km s}^{-1} \text{ Mpc}^{-1}$ (H_0^{Pl}). It is easy to note that there is a large discordance among these values, see Figure 10.

Nevertheless, claiming that there is a tension using only a graphical method could be non-objective and so it is better to have a quantitative description of this discordance or tension. Before discussing the problem quantitatively, we will argue why it is qualitatively important to understand what generates this discordance or tension. It is important to mention that the tension between global and local values of H_0 has been unveiled by the increasing precision on measurements of H_0 , as showed in Figure 11.

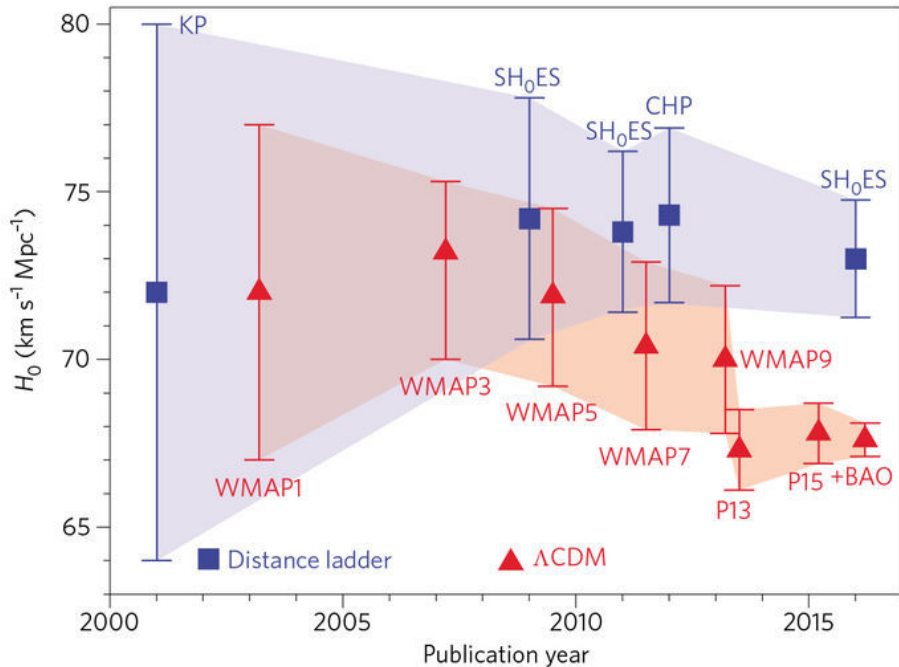


Figure 11 – A historical review of H_0 values and their error bars for different experiments. Note that the large increase in precession has unveiled the tension between local and global measurements. This figure is from [5].

The CMB allows us to constrain cosmological parameters with large precision. However, to that end, it is necessary to use a fiducial model, in this case Λ CDM. Then, when we proclaim that the CMB provided a Hubble constant equal to H_0^{Pl} , we actually mean that the analysis of fluctuations of the temperature of primordial photons, under the assumption that we live in a Λ CDM universe, gives H_0^{Pl} . In other words, the CMB results are model dependent and a re-analysis of CMB data for a model beyond Λ CDM could lead to a value different from H_0^{Pl} . Opposite is the case of $H_0^{\text{R}16}$. It is obtained in a model-independent way, through the use of standard candles, SNe Ia and Cepheids, and geometric distances at $z \ll 1$. However, despite the fact that the value of $H_0^{\text{R}16}$ is model-independent it could be biased by unknown systematics on the cosmic distance ladder. Thus, the tension between global (coming from CMB) and local (coming from SNe Ia) determinations could be tackled from both sides, that is, considering physics beyond Λ CDM, which could provide a Hubble constant higher than H_0^{Pl} [18, 19, 20, 21, 22, 23, 24, 25], and biases on the cosmic ladder distances used to determinate $H_0^{\text{R}16}$ [26, 27, 28, 29, 30, 31, 32, 33, 34].

As we have pointed out in the previous paragraph, considering a model different from Λ CDM could give us a higher Hubble constant in agreement with H_0^{R16} and hence alleviate the tension. However, this way to alleviate the tension could lead to a poor description of the universe at early time, which is well constrained by the CMB [133]. Here, we will tackle the tension problem in a safer way by considering also the presence of a systematic error on the determination of the local expansion rate. Specifically, we shall study the effect of the cosmic variance in the measurements of the local Hubble constant, considering a non-standard dark energy component instead of the common Λ . This non-standard dark energy shall be represented by the CQ model and the γ CDM and γw CDM and γ_a CDM parameterizations. We have to mention that the cosmic variance has already been considered in order to alleviate the tension in the Λ CDM context. The effect produced by cosmic variance, due to local structures, has been showed to be insufficient to explain the whole tension [33, 34].

It is worth to point out that the Λ CDM model suffers from tensions on other cosmological parameters. For example, the value of the amplitude of the power spectrum at 8 Mpc, σ_8 , provided by the South Pole Telescope is 2.6σ lower than the value predicted by Planck [134, 135].¹

In this chapter, first, we shall discuss how local cosmic flows generate a deviation of H_0^{loc} regarding the global value H_0 . Then, we will obtain its cosmic variance and so quantify the impact on local measurements. Finally, we will study the contribution of CQ model, γ CDM and γw CDM parameterizations to cosmic variance. For that, we will compute the error budget due to cosmic variance by fixing the background cosmology to the Λ CDM fiducial, see Table 1 (we also fix $H_0 = H_0^{\text{Pl}}$). Obviously, fixing the background to the Λ CDM fiducial could bias our results. However this first study will be important in order to understand the results provided by the statistic inference of Chapter 5.

3.1 TENSIONS, DISCORDANCES OR INCONSISTENCIES

Before arguing about cosmic variance and its effect on H_0^{loc} , we have to quantify the tension. There is neither a standard process nor estimator to determine the tension among two or more experiments. However, tension or inconsistencies can be identified, for instance, by graphics such as Figure 10. Using only a graphic method to quantity an inconsistency could be a non-objective method, and so, it is fundamental to adopt an estimator that quantifies the tension in order to avoid non-objective results. At this point, it seems intuitive that an estimator of tension, discordance or inconsistency should take into account the mode the value that maximizes the PDF, and a measure of the dispersion

¹ It has also been reported a 2.1σ discordance between Kilo Degree Survey and Planck determinations of the cosmological parameter $S_8 \equiv \sigma_8 (\Omega_m/0.3)^{1/2}$ [35]. Note that discordances in σ_8 and S_8 are often addressed as the same problem.

of the PDF, such as the variance. Several estimators have been proposed in the literature, such as the tension [17] or the index of inconsistency [136].² Here, we will use the simple estimator

$$T_{H_0} = \frac{|H_0 - H_0^{\text{R16}}|}{\sqrt{\sigma_{H_0}^2 + \sigma_{\text{loc}}^2}}, \quad (3.1)$$

employed in [35] to calculate the σ_8 tension. Note that in (3.1), H_0 and σ_{H_0} are the mean and the variance of the H_0 probability distribution function, respectively. We will return later to the quantity σ_{loc} .

The current tension between H_0^{Pl} and H_0^{R16} can be computed using this estimator. If we assume that the local error is only given by [1], that is $\sigma_{\text{loc}} = \sigma_{\text{R16}}$, we obtain a tension of about 3.4σ in concordance with [1, 17]. In order to know how serious is the mismatch between the global and local determinations of H_0 one can use Jeffrey's scale. Here, as (3.1) is a particular case of the index of inconsistency defined in [136], we use the interpretation showed in Table III of [136]. According that, there is a moderate tension (or inconsistency) between H_0^{Pl} and H_0^{R16} .

3.2 LINEAR PERTURBATION THEORY AND PECULIAR VELOCITIES

3.2.1 Cosmic variance

At local scales there are important spatial fluctuations of the expansion rate, which are produced by the density fluctuations. In other words, peculiar velocities are generated by the local distribution of matter and its gravitational potential. This field of velocities generates a deviation with respect to the global H_0 . To illustrate that, consider an observer at \vec{r}_i that measures the expansion rate H_0^{loc} using N objects, each one located at \vec{r}_j , where $j = 1, 2, 3, \dots, N$. The observer will notice, on average, $H_0^{\text{loc}}(\vec{r}_i) = H_0 + H_0\delta H$, where the fluctuation is:

$$\delta H(\vec{r}_i) = \frac{H_0^{\text{loc}}(\vec{r}_i) - H_0}{H_0},$$

where H_0 is the global value of the Hubble constant. The measurement obtained by the observer at \vec{r}_i depends on the position $H_0^{\text{loc}} = H_0^{\text{loc}}(\vec{r}_i)$, as the distribution of matter $\delta = \delta(\vec{r}_i)$. Deviations of the Hubble constant, as we have already mentioned, are known as peculiar velocities, which are produced by local structures. We will consider that each object has a peculiar velocity \vec{v}_j , then, the observer will only be able to measure the radial component of \vec{v}_j , as velocities are measured by redshift (Doppler effect). That is, the contribution from \vec{v}_j to $H_0(\vec{r}_i)$ shall be parallel to the line of sight $(\vec{r}_j - \vec{r}_i)$, see Figure 12.

² Although throughout this work we have used “tension” to call the difference between H_0^{R16} and H_0^{Pl} , it is important to say that we do not refer to the estimator proposed in [17] but rather to an inconsistency or discordance, in general.

Thus, the deviation is given by:

$$\delta H(\vec{r}_i) = \frac{1}{N} \sum_{j \neq i} \vec{v}_j \cdot \frac{(\vec{r}_j - \vec{r}_i)}{|\vec{r}_j - \vec{r}_i|^2} . \quad (3.2)$$

Now, we consider the continuous case. The deviation δH for a sphere of radius R , centered around x , is given by

$$\delta H_R(\vec{x}) = \int d^3y \frac{\vec{v}(y)}{H_0} \cdot \frac{(\vec{y} - \vec{x})}{|\vec{y} - \vec{x}|^2} W(\vec{y} - \vec{x}) , \quad (3.3)$$

where $W(\vec{y} - \vec{x})$ is the top-hat window function with radius R :

$$W(\vec{y} - \vec{x}) = \begin{cases} (4\pi R^3/3)^{-1}, & |\vec{y} - \vec{x}| \leq R \\ 0, & |\vec{y} - \vec{x}| > R . \end{cases} \quad (3.4)$$

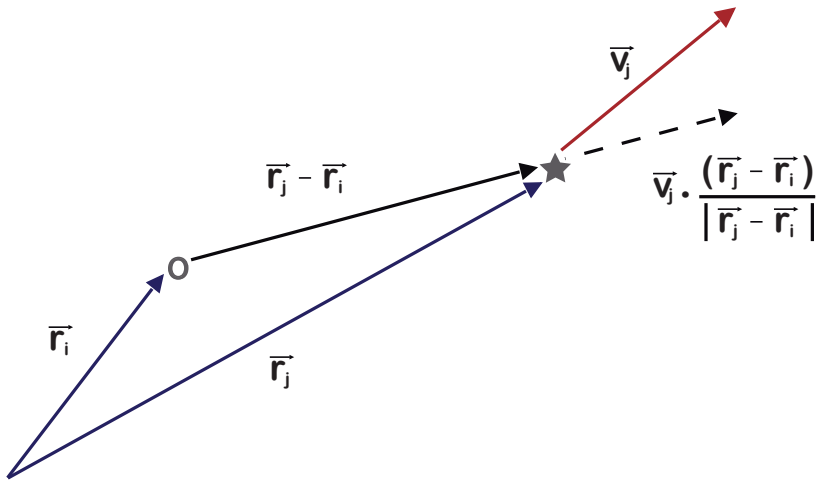


Figure 12 – The observer is located at \vec{r}_i . (S)he measures the velocity of a star at \vec{r}_j , which has the peculiar velocity \vec{v}_j . The velocity measured by the observer is always parallel to the line of sight $\vec{r}_j - \vec{r}_i$ and it will be composed by both the recession velocity $H_0 |\vec{r}_j - \vec{r}_i|$ and the contribution of the peculiar velocity $\vec{v}_j \cdot (\vec{r}_j - \vec{r}_i) / |\vec{r}_j - \vec{r}_i|$.

Using linear theory, we have derived an expression for the peculiar velocity (1.97) in Fourier space. Evaluating it today $\mathcal{H}_0 = H_0$, we have

$$\tilde{v} = iH_0 f \tilde{\delta}_m \frac{\vec{k}}{k^2} ,$$

and, going back to real space, we have

$$\vec{v}(y) = \frac{iH_0 f}{(2\pi)^3} \int d^3k e^{i\vec{k} \cdot \vec{y}} \tilde{\delta} \frac{\vec{k}}{k^2} . \quad (3.5)$$

Replacing (3.5) in (3.3), we get

$$\delta H_R(\vec{x}) = \frac{if}{(2\pi)^3} \int d^3y \int d^3k \tilde{\delta}_m \frac{\vec{k}}{k^2} \cdot \frac{(\vec{y} - \vec{x})}{|\vec{y} - \vec{x}|^2} W(\vec{y} - \vec{x}) e^{i\vec{k}\cdot\vec{y}},$$

defining $\vec{\xi} = \vec{y} - \vec{x}$, then

$$\delta H_R(\vec{x}) = \frac{if}{(2\pi)^3} \int \frac{d^3k}{V} \tilde{\delta}_m e^{i\vec{k}\cdot\vec{x}} I_\xi, \quad (3.6)$$

where $V \equiv 4\pi R^3/3$. Also, we have defined

$$I_\xi \equiv \int d^3\xi \frac{\vec{k}}{k^2} \frac{\vec{\xi}}{\xi^2} e^{i\vec{k}\cdot\vec{\xi}}.$$

Computing the integral we get

$$\begin{aligned} I_\xi &= \frac{1}{k^2} \int_0^{2\pi} d\phi \int_0^\pi d\theta \sin \theta \int_0^R d\xi k \xi \cos \theta e^{ik\xi \cos \theta}, \\ I_\xi &= \frac{2\pi}{ik^3} \int_0^\pi d\theta \sin \theta \left(k \xi e^{ikR \cos \theta} + \frac{ie^{ikR \cos \theta}}{\cos \theta} \right)_0^R, \\ I_\xi &= \frac{2\pi}{ik^3} \int_0^\pi d\theta k R \sin \theta \left(e^{ikR \cos \theta} + \frac{ie^{ikR \cos \theta}}{kr \cos \theta} \right). \end{aligned}$$

Then, doing the change of variable $\zeta = kR \cos \theta$, we can rewrite the last integral as

$$\begin{aligned} I_\xi &= \frac{2\pi}{ik^3} \left(\int_{-kR}^{+kR} d\zeta e^{i\zeta} + \int_{-kR}^{+kR} d\zeta \frac{e^{i\zeta}}{\zeta} \right), \\ I_\xi &= \frac{4\pi}{ik^3} \left[\sin(kR) - \int_0^{kR} d\zeta \frac{\sin \zeta}{\zeta} \right]. \end{aligned} \quad (3.7)$$

We can put (3.7) in (3.6) to get the deviation of the local Hubble constant [137, 138]

$$\delta H_R(\vec{x}) = \frac{f(z)}{(2\pi)^3} \int d^3k \tilde{\delta}_m \mathcal{L}(kR) e^{i\vec{k}\cdot\vec{x}}, \quad (3.8)$$

where we have defined

$$\mathcal{L}(x) \equiv \frac{3}{x^3} \left(\sin x - \int_0^x dy \frac{\sin y}{y} \right). \quad (3.9)$$

The deviation (3.8) is caused by peculiar velocities, and, consequently by the local matter distribution. It is easy to note that the Hubble constant is overestimated if the observer lives in an overdensity ($\delta_m > 0$), and underestimated if the observer lives in a underdensity ($\delta_m < 0$).

We can average this deviation over positions, we will find $\langle \delta H_R \rangle = 0$, this is due to the fact that $\langle \tilde{\delta}_m \rangle = 0$, where $\langle \rangle$ represents the average over the position \vec{x} . It means, contributions to peculiar velocities are, on average, null. However, this result is not true if

we calculate the variance, which is defined as $\sigma^2(\delta H) = \langle \delta H_R^2 \rangle - \langle \delta H_R \rangle^2$, where, of course, the last term is zero. Thus,

$$\langle \delta H_R^2 \rangle = \frac{f^2(z)}{(2\pi)^6} \int d^3 \vec{k} \tilde{\delta}_m \mathcal{L}(kR) \int d^3 \vec{k}' \tilde{\delta}_m^* \mathcal{L}(k'R) \int d^3 \vec{x} e^{(\vec{k}' - \vec{k}) \cdot \vec{x}} ,$$

and by definition of Dirac delta $\delta(\vec{k}' - \vec{k}) \equiv (2\pi)^{-3} \int d^3 \vec{x} e^{(\vec{k}' - \vec{k}) \cdot \vec{x}}$, it is

$$\langle \delta H_R^2 \rangle = \frac{f^2(z)}{2\pi^2 R^2} \int_0^\infty dk P(k) [(kR) \mathcal{L}(kR)]^2 , \quad (3.10)$$

where $P(k) = |\tilde{\delta}_m|^2$ is the power spectrum. The cosmic variance $\langle \delta H_R^2 \rangle$, unlike the average, is different from zero. In order to illustrate the cosmic variance we plot the deviation of H_0^{loc}/H_0 at 1, 2 and 3 standard deviations $\sigma(\delta H)$, see Figure 13. Note that at $z = 0.01$ the deviation is about 1% as stated in [1]. Although one could say that this deviation is negligible, the error caused by $\langle \delta H_R^2 \rangle$ could be non-negligible as we will see in the next section. The approach above is not the only way to compute the variance of local H_0 , see, for example, the non-linear velocity power spectra derived from N-body simulations [32].

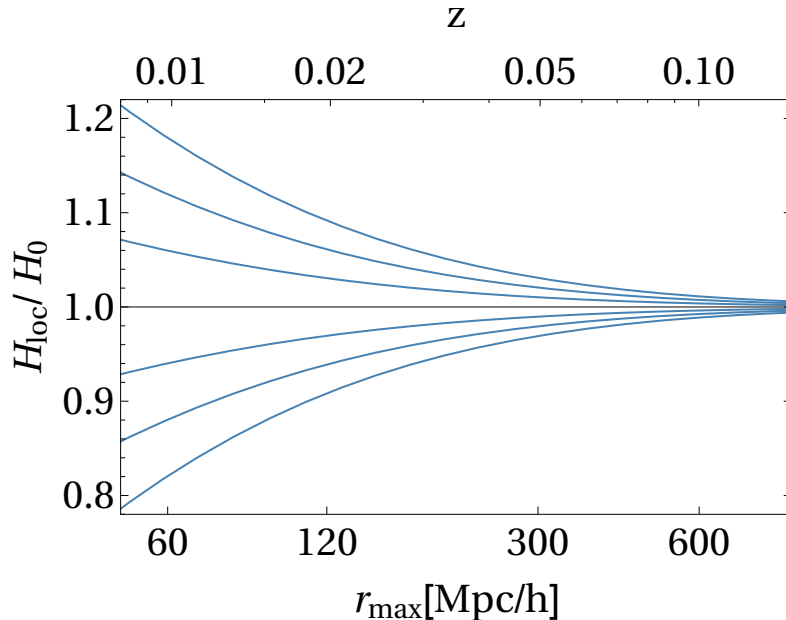


Figure 13 – Deviation of H_0^{loc}/H_0 as a function of scales (or redshift). One can note that, as expected, the variance decreases at higher redshifts, at which the contribution of peculiar velocities become less important.

We defined the power spectrum as:

$$P(k) = \frac{2\pi^2}{k^3} A_s \left(\frac{ck}{H_0} \right)^{3+n_s} T^2(k, z) \frac{D^2(z)}{D^2(0)} , \quad (3.11)$$

where A_s is the amplitude of the power spectrum, $T(k, z)$ the transfer function and $D(z)$ the growth function. The shape of the power spectrum is determined by the transfer

function. An analytic expression for the transfer function is only available for special cases – for example, when neglecting baryons and neutrino anisotropic stress. In the more general case, one can use numerical codes, such as CLASS [139], to solve the equations of perturbations and obtain $T(k, z)$. For the sake of simplicity, we adopt the transfer function obtained in [140]. It is worth to mention that we have also used the nonlinear HaloFit power spectrum [141] in order to compute (3.10). However, we have found that the linear and nonlinear power spectra give indistinguishable results. Therefore, in order to reduce computation time, we have used the simpler linear power spectrum.

3.2.2 Relative systematic error $\sigma_{\delta H}$

The cosmic variance $\langle \delta H_R^2 \rangle$ was computed under the assumption that sources are distributed uniformly in $W(\vec{y} - \vec{x})$. In order to obtain the real variance relative to a particular survey we should use the actual distribution in (3.3). However, in general, the distribution of sources is more complicated than a simple top-hat window function and then we would not be able to get an analytical expression for the cosmic variance. Instead, we would have to get it numerically, which could be computationally expensive. In order to avoid that, we follow the method adopted in [33]. Neglecting anisotropies in the supernova distribution, the error generated by cosmic variance in local measurements can be estimated using:

$$\sigma_{\delta H} = \left[\int_{z_{min}}^{z_{max}} dz W_{SN}(z) \langle \delta H^2 \rangle \right]^{\frac{1}{2}} \quad (3.12)$$

where $W_{SN}(z)$ is the redshift distribution of the SNe Ia used in [1]. It means that we average the cosmic variance according to the distributions of sources. We have to mention that (3.12) is a relative error and, in order to obtain an absolute error, it has to be multiplied by H_0 . Now, we return to the discussion of σ_{loc}^2 , which was included at the beginning of this chapter. We use σ_{loc}^2 to represent the error at local scales. Then, it will be composed by both σ_{R16}^2 and $\sigma_{\delta H}^2$, unless stated otherwise. Thereby, we define

$$\sigma_{loc}^2 \equiv \sigma_{R16}^2 + H_0^2 \sigma_{\delta H}^2 . \quad (3.13)$$

The tension defined in (3.1) uses this definition. We can calculate the relative error generated by cosmic variance in the Λ CDM fiducial, it is $\sigma_{\delta H} = 0.0298$, and the absolute error, $H_0 \sigma_{\delta H} = 1.99 \text{ km s}^{-1} \text{ Mpc}^{-1}$. Note that if $H_0 \sigma_{\delta H}$ and σ_{R16} are of the same order, then the total local error is $\sigma_{loc} \approx 1.41 \sigma_{R16}$. When this σ_{loc} is used to recompute the tension between H_0^{R16} and H_0^{Pl} one finds that the tension reduces to $T = 2.4\sigma$.

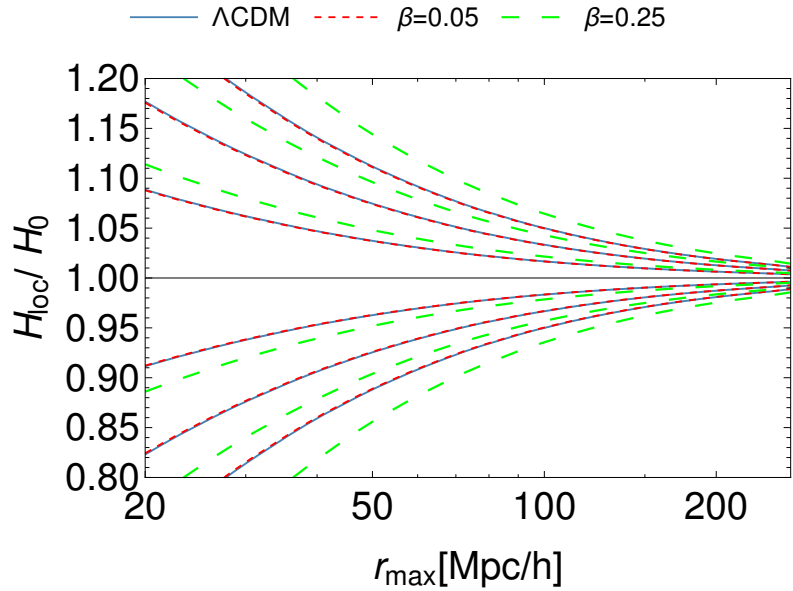


Figure 14 – Deviation of H_0^{loc}/H_0 as a function of scales in the CQ model, with $\alpha = 0.08$, for weak ($\beta = 0.05$) and strong ($\beta = 0.25$) coupling.

3.3 THE LOCAL DETERMINATION OF H_0 AND A NON-STANDARD DARK ENERGY

3.3.1 Cosmic variance in Coupled Quintessence

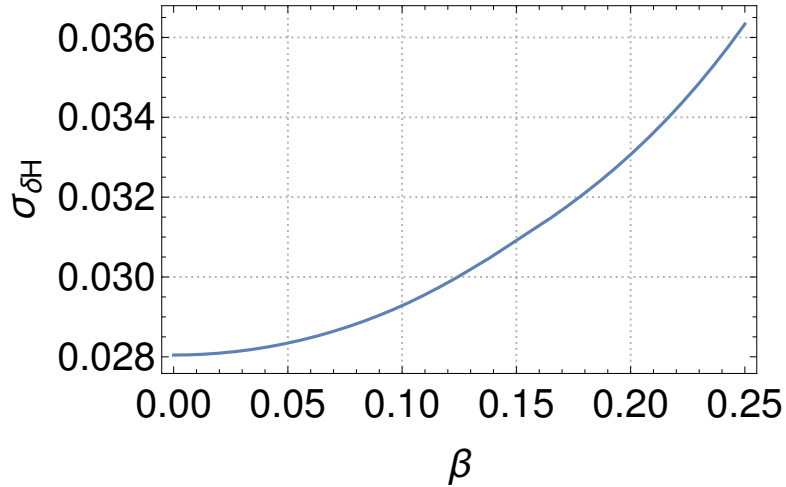


Figure 15 – Systematic error produced by cosmic variance in the CQ context, with $\alpha = 0.08$, as function of β .

We have discussed how coupling changes the perturbed Einstein equations and therefore the evolution of perturbations. In this case, we need to use (2.20) instead of Ω_m^γ . Taking this into account, we computed the deviation of H_0^{loc} with respect to the global H_0 for the CQ model with $\alpha = 0.08$ in the presence of a weak and strong coupling, see

Figure 16. Weak coupling and Λ CDM are indistinguishable, instead a strong coupling provides a higher deviation of the local Hubble constant. Besides, Figure 15 shows how the systematic error due to cosmic variance evolves according to the coupling strength β . One can see that stronger couplings provide higher errors. This first analysis of CQ model shows that β has a non-negligible effect on cosmic variance and its systematic error is comparable to σ_{R16} . However, current constraints on β are $\beta \lesssim 0.06$ [118] so that the strong coupling case seems to be disfavored by observations.

3.3.2 Cosmic variance in γ CDM

Now, we investigate the effect of γ on cosmic variance $\langle \delta H^2 \rangle$ and, consequently, the error $\sigma_{\delta H}$. From Figure 16 we can see how different values of the cosmic growth index change the deviation of H_0^{loc}/H_0 . For instance, $\gamma = 0.35$ provided a higher deviation than the standard $\gamma = 0.55$. According to $f(z) = \Omega_m^\gamma$, we expect that $\gamma < 0.55$ produces a universe in which δ_m grows faster than in Λ CDM, and so, there are more large structures. Consequently, the effects of peculiar velocities in the local measure of the Hubble constant are boosted. Once cosmic variance is computed we are able to calculate the systematic error. Figure 18 shows the corresponding $\sigma_{\delta H}$ as function of γ . As expected, lower values of γ predict a higher error than Λ CDM. Thus, this analysis shows that a dark energy model that predicts a $\gamma < 0.55$ could help to face the tension.

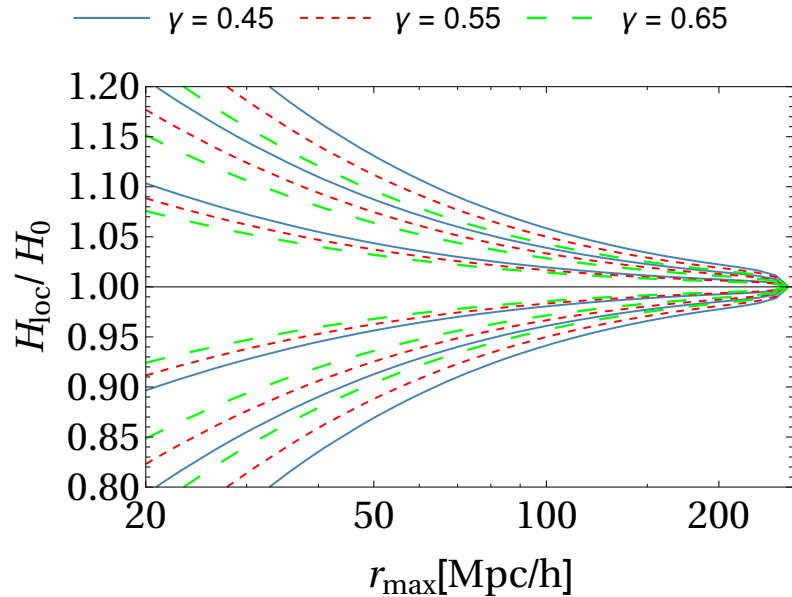


Figure 16 – Deviation of H_0^{loc}/H_0 as a function of scales for different values of γ .

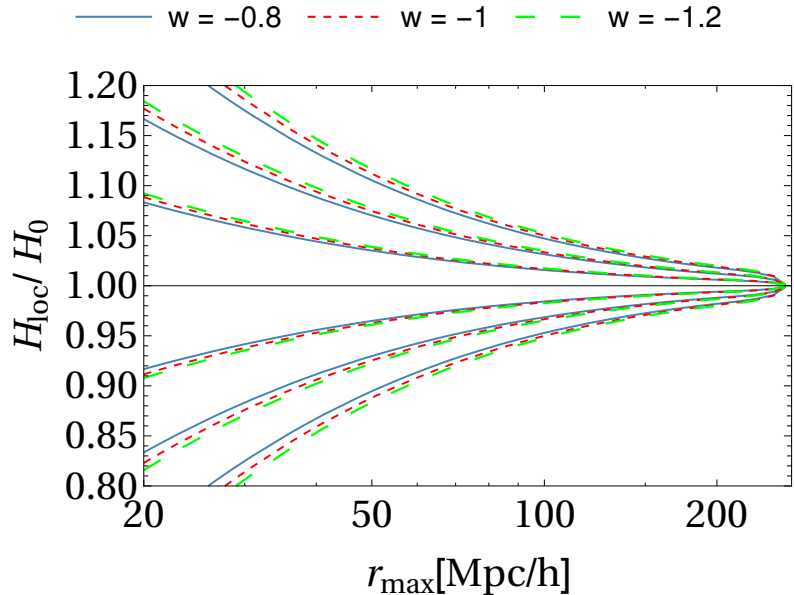


Figure 17 – Deviation of H_0^{loc}/H_0 as a function of scales for different values of w_{de} .

3.3.3 Cosmic variance in γw CDM

Here, we explore how w_{de} contributes to cosmic variance. For that, we computed (3.8) and (3.12) for three cases: $w_{de} = \{-0.8, -1, -1.2\}$. The corresponding deviations at 1, 2 and 3 standard deviations are showed in Figure 17. Lower values of w_{de} lead to a higher variance, however, this increase seems virtually negligible with respect to the standard case $w_{de} = -1$. It means that w_{de} is less important for $\sigma_{\delta H}$ as compared with γ and β . That is due to the fact that, unlike CQ and γ CDM, the parameter of EoS does not change directly $f(z)$ but rather it changes, principally, the background evolution. Nevertheless, as we have discussed before, although the deviation seems negligible, the systematic error could be not. We show the relative error $\sigma_{\delta H}$ for the three cases here considered. Note from Figure 18 that a $\Delta w_{de} = 0.2$ represents a change $\sim 5\%$ in the relative error $\sigma_{\delta H}$ for any value of γ .

Although the EoS parameter seems to have a negligible contribution to cosmic variance, it is important to mention that the tension not only can be alleviated by a huge $\sigma_{\delta H}$ but also by a higher H_0 . In this sense, it is worth pointing out that w_{de} is strongly correlated to H_0 [134] and any change in w_{de} implies a change in global H_0 . In conclusion, we must not underestimate the γw CDM parametrization.

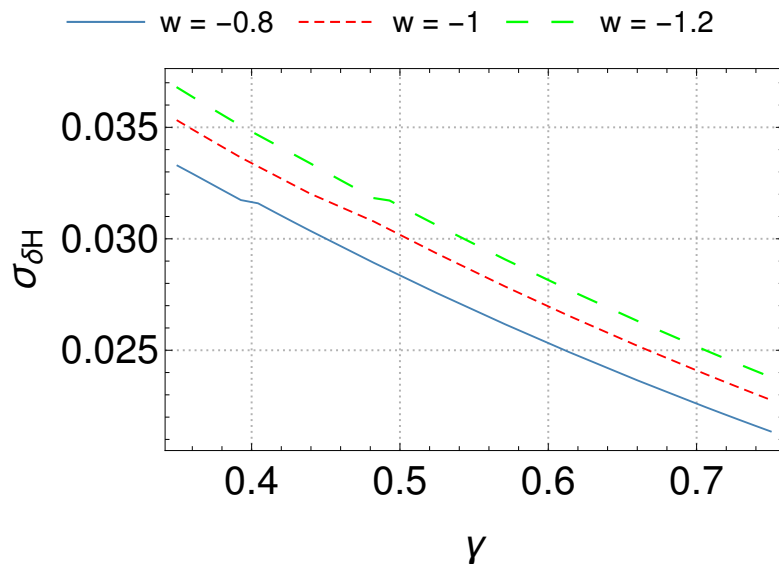


Figure 18 – Systematic error produced by cosmic variance as a function of γ and for different values of w_{de} . Note, that here we have used the common parametrization for the growth rate $f(z)$.

4 Bayesian statistics and observational cosmology

4.1 BAYESIAN STATISTICS

The current status of cosmology has been reached thanks to observations. We are able to test our cosmological models through astrophysical or cosmological observations. Nevertheless, cosmology is distinguished from other areas of physics when we talk about observations or experiments—the universe is unique and we are not able to “produce” a universe in the lab, much less control the conditions under which it is created. This fact puts cosmology in a special place regarding other fields of physics, for instance, consider the case of high energy physics where it is possible to reproduce experiments at certain conditions (as in the case of the Higgs boson [142]). Then, data analysis in cosmology has to be performed using a framework that helps to overcome this issue. Such framework is Bayesian statistics.

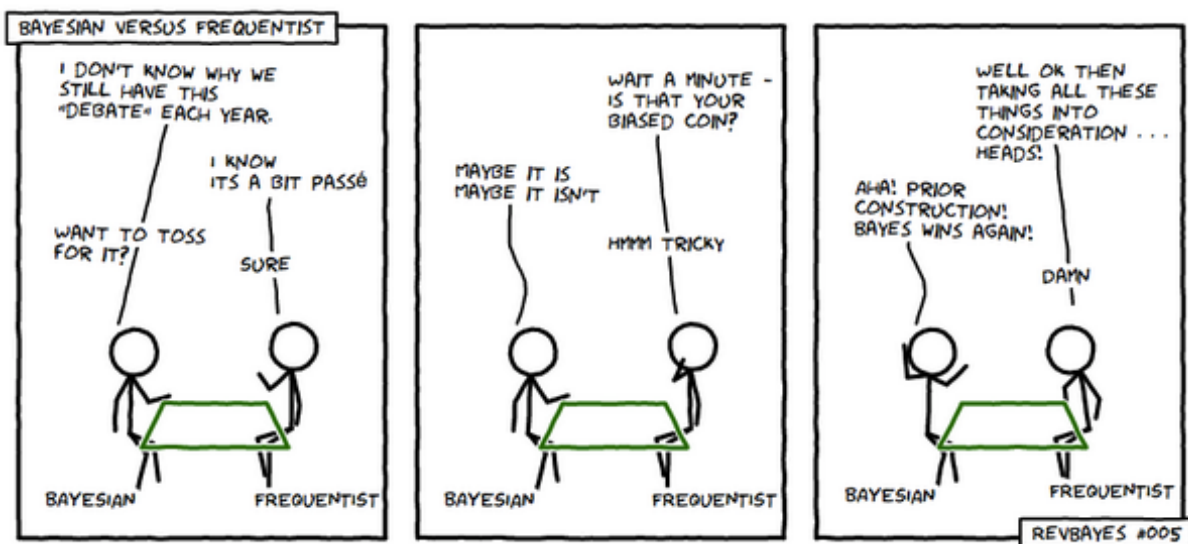


Figure 19 – Cartoon illustrating one of the differences between Bayesian and frequentist inference: inclusion of prior. This cartoon is from <<https://twitter.com/RevBayes>>.

Bayesian inference is largely used in cosmology.¹ It is based on Bayes’ theorem, which states

$$p(A|B) = \frac{p(A)p(B|A)}{p(B)}, \quad (4.1)$$

¹ See [143, 144] for a review of Bayesian statistics in cosmology.

where $p(A)$ is the probability of a preposition A and $|$ represents conditional probability. Despite that (4.1) is a cornerstone in the formulation of Bayes statistics, it is also used – with a different interpretation – in the frequentists framework. Frequentists use Bayes' theorem only to compute conditional probabilities, for instance, which is the probability that the total of two dice will be less than ten given that the first die is a four. Bayesian will use it in a more sophisticated form, to perform statistical inference. Considering $A = \theta$ and $B = D$, one has

$$p(\theta|D) = \frac{p(\theta)p(D|\theta)}{p(D)},$$

where θ represents the parameters of a theory and D the data sets. Note that it was implicitly assumed that the parameters θ are random variables and so follow the same mathematical rules of D . This assumption is only valid within the Bayesian framework, so that, it can be considered as the first difference with respect to the framework adopted by frequentists. The status of θ as a random variable explains why in cosmology results of inference are probability distribution functions, see for example Figure 10. Another feature of Bayesian statistics regards the function $p(D|\theta)$, which we will consider as a function of parameters θ instead of data D . Then, finally, we shall arrive to

$$\mathcal{P}(\theta|D) = \frac{p(\theta)\mathcal{L}(\theta)}{p(D)}, \quad (4.2)$$

where $\mathcal{P}(\theta|D)$, $p(\theta)$ and $\mathcal{L}(\theta)$ are named posterior, prior and likelihood, respectively. To finalize this very brief discussion of Bayesian statistics, we will describe each term in (4.2).

- Prior $p(\theta)$: it is our *a priori* information of a parameter, provided either by theoretical definitions or observations. The prior is often pointed out as the main difference between Bayesian and frequentist inferences and one can demonstrate that the inclusion of a prior can have a large impact on inference [143, 144]. A cartoon about prior is showed in Figure 19.
- Likelihood $\mathcal{L}(\theta)$: it represents the probability of having data given the parameters θ . The likelihood becomes a function of θ once the data is fixed. The construction of $\mathcal{L}(\theta)$ within the frequentist framework is more complicated than within the Bayesian approach, due to the fact that a frequentist cannot see θ as a random variable.
- Posterior $\mathcal{P}(\theta|D)$: it is a probability distribution function, the final outcome of Bayesian inference. In particular cases the posterior may coincide with the (unnormalized) likelihood.

It is worth to stress that Bayes' theorem (4.2) will also set forth something that we could call the “Bayesian cycle”. The prior represents our current state of knowledge and the posterior will be the improvement of this knowledge thanks to the new data, represented

by the likelihood. As we improve our knowledge, we will “recycle” our results and renew the Bayesian cycle, that is, today’s posterior will be tomorrow’s prior.

4.1.1 The χ^2 function and likelihood

In this work, we adopt flat priors over to cosmological parameters. Then, we will only have to deal with the likelihood. To perform Bayesian inference we will use the minimum χ^2 method. First, we will assume a Gaussian likelihood (unnormalized) distribution given by:

$$\mathcal{L}(\theta) \equiv e^{-\chi^2/2}, \quad (4.3)$$

where also $\chi = \chi(\theta)$. According to the discussion about $\mathcal{L}(\theta)$, its definition should include data. Consequently, χ should include data as well. Thus, we shall define χ^2 variable as

$$\chi^2(\theta) = \sum_{i=1}^N \left(\frac{y_i - y(x_i|\theta)}{\sigma_i} \right)^2, \quad (4.4)$$

where y_i is a data point, σ_i its error, $y(x_i|\theta)$ the theoretical prediction for the parameters θ of our theory.² The χ^2 function quantifies, roughly speaking, about how many standard deviations our theory deviates from the observations. Therefore, the minimum χ^2 method finds which values of parameters θ minimize the numbers of standard deviations between theory and observation. Suppose that $\theta = \hat{\theta}$ gives the minimum χ^2_{min} , in technical jargon the values $\hat{\theta}$ are dubbed best fit values. As $\chi^2(\hat{\theta}) = \chi^2_{min}$ we shall have

$$\mathcal{L}(\hat{\theta}) = e^{-\chi^2_{min}/2} = \mathcal{L}_{max}.$$

Note that θ corresponds, in general, to a set of parameters, that is $\theta = \{\theta_1, \theta_2, \theta_3, \dots, \theta_K\}$ and the minimum chi square method will provide a set of best-fit values $\hat{\theta} = \{\hat{\theta}_1, \hat{\theta}_2, \hat{\theta}_3, \dots, \hat{\theta}_K\}$. The number K of parameters θ_i will be defined both by our interest and the nature of data. An issue arises when our interest is only in a few parameters, suppose $\{\theta_1, \theta_2\}$, and theoretical predictions request more parameters, for instance $\{\theta_1, \theta_2, \theta_3, \theta_4\}$. Obviously, we might perform the inference for whole set $\{\theta_1, \theta_2, \theta_3, \theta_4\}$ and only pay attention to the parameters of interest. However, a multidimensional space is difficult to grasp, and it would be useful to focus just on the parameters of interest. One could fix θ_3, θ_4 . However, choose a particular value for θ_3 or θ_4 could be arbitrary and could remove the effect of possible degeneracies. The way out to this issue is to “marginalize” the posterior. It means, if we are only interested on θ_1, θ_2 , we shall consider the marginal distribution:

$$\mathcal{L}'(\theta_1, \theta_2) \equiv \int d\theta_3 \int d\theta_4 \mathcal{L}(\theta),$$

² This is the most simple definition of the χ^2 function, in which correlations between parameters have been neglected. When there are correlations, we will replace the errors σ_i by the covariance matrix. See, for further information, [143, 144].

where $\mathcal{L}'(\theta_1, \theta_2)$ is the marginalized likelihood. The definition of marginalization is a consequence of the product rule. Once again, frequentists are not able to perform a marginalization over the parameters of a theory.

4.1.2 Model selection criteria

Bayesian inference produces the posterior for each model that will be analyzed. In particular one will obtain the best fit parameters $\hat{\theta}$ and the corresponding χ^2_{min} . Most of the time, we need to conclude which model can be proclaimed as the most successful according to the data, i.e. we need to have a model selection criteria. Intuitively, one might think that the model with the smallest χ^2_{min} is the best, but this approach is not competently right.

If we compare models with the same quantity of free parameters θ , using χ^2_{min} could be enough to perform model selection. However, the case is quite different for models with a different number of free parameters. Furthermore, χ^2_{min} only probes a small region of the posterior distribution and more information is, in principle, available. A formal way to carry out model selection is through the use of Bayes' factor. Roughly speaking, Bayes' factor is the ratio between $\mathcal{P}(M_i|D)$ and $\mathcal{P}(M_j|D)$, where M_i represents a model in particular.³ Despite that Bayes' factor might be the most natural way to do model selection, it is computationally expensive and highly dependent on the choice of the prior.

To escape from the limitations of χ^2_{min} and from the excessive complications of Bayes' factor, we shall use methods that approximate Bayes' factor. First of them, the Akaike information criterion (AIC) [36]

$$\text{AIC} \equiv -2 \ln \mathcal{L}_{\max} + 2k ,$$

and also the Bayesian information criterion (BIC) [37]

$$\text{BIC} \equiv -2 \ln \mathcal{L}_{\max} + k \ln N .$$

Because of the gaussianity of the likelihood, we shall get:

$$\text{AIC} = \chi^2_{min} + 2k , \quad (4.5)$$

$$\text{BIC} = \chi^2_{min} + k \ln N , \quad (4.6)$$

where N is the total number of data points and K the number of free parameters.

Both AIC and BIC are extension of χ^2_{min} , which approximate Bayes' factor. Unlike the simple χ^2_{min} , AIC and BIC shall penalize models with more free parameters.

³ Note that here the parameter θ is understood as describing the set of available models.

4.2 COSMOLOGICAL DATA

Here we show the cosmological sets used to constrain the cosmological parameters and test the power of the cosmic variance. In order to reach accurate results and eliminate degeneracies between cosmological parameters, we include data sets coming from experiments of different nature, such as CMB, BAO, SNe Ia, RSD and local H_0 .

4.2.1 Cosmic microwave background

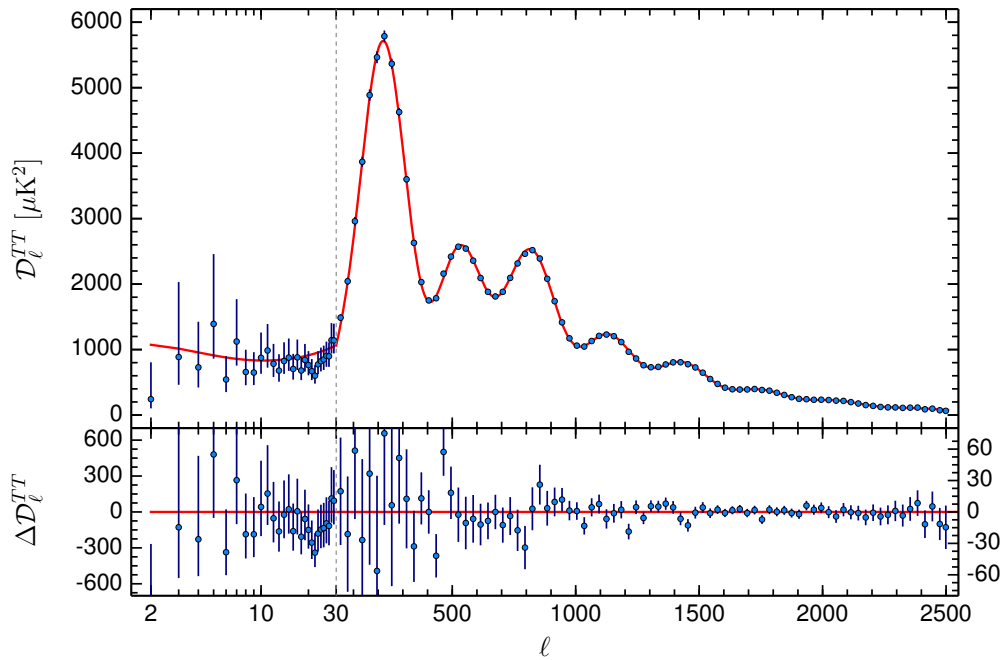


Figure 20 – The temperature power spectrum of the CMB. Blue dots are data while the red line is a theoretical prediction according to the ΛCDM model. This figure is from [6].

The study of the cosmic microwave background provides, perhaps, one of the most important observations in cosmology. CMB data have a great precision and are largely sensitive to cosmology. The main result of CMB observations is the temperature power spectrum of Figure 20. Theoretical predictions of the temperature power spectrum are obtained through solutions of the relativistic Boltzmann and perturbed Einstein equations [69]. As these equations do not have analytic solutions, one has to use numerical methods in order to obtain the theoretical temperature power spectrum. There are some codes that provide these solutions, for instance, CMBFAST [145], CAMB [146], CLASS [139] and others. These codes are usually valid for the ΛCDM model and extending them to models beyond ΛCDM , such as coupling models, is complicated. Then, for the sake of

simplicity, instead of considering the whole temperature power spectrum, we shall focus on the position of the first peak.

Then parameters that characterize the position of first peak of CMB power spectrum are the shift parameter \mathcal{R} and the angular scales of the sound horizon at last scattering l_A . One can show that these parameters contain a great part of information provided by the whole CMB power spectrum, see for instance [147, 148]. They are defined as [149]

$$l_A = \frac{\pi r(z_*)}{r_s(z_*)} , \quad (4.7)$$

$$\mathcal{R} = \frac{\sqrt{\Omega_{m0} H_0^2}}{c} r(z_*) , \quad (4.8)$$

where $r(z) = (1+z)d_A(z)$ is the comoving distance and z_* is the redshift decoupling. Note that the sound horizon $r_s(z)$ can be approximated to [150]:

$$r_s(z) = \frac{2}{3k_{eq}} \sqrt{\frac{6}{R_{eq}}} \ln \left(\frac{\sqrt{1+R} + \sqrt{R+R_{eq}}}{1 + \sqrt{R_{eq}}} \right) , \quad (4.9)$$

with $R = 3\Omega_b/4\Omega_\gamma$ and $R_{eq} = R(z_{eq})$. Also, for z_* we adopted the best fit showed in [150].

We will use CMB data coming from Planck [151], which provided $\mathcal{R} = 1.7488 \pm 0.0074$ and $l_A = 301.76 \pm 0.14$. This data is correlated, the inverse of the covariance matrix is

$$\text{Cov}_{\text{CMB}}^{-1} = 10^3 \begin{pmatrix} 25.779 & -0.7358 \\ & 0.072 \end{pmatrix} .$$

We have only showed the upper diagonal part because the matrix is symmetric. In order to improve our analysis, we will also include the amplitude of the power spectrum $\ln[10^{10}A_s] = 3.089 \pm 0.036$, coming from [6]. Once the CMB data is fixed, we are able to defined the χ^2_{CMB} function:

$$\chi^2_{\text{CMB}} = (d_{\text{CMB}} - \mu_{\text{CMB}}) \cdot \text{Cov}_{\text{CMB}}^{-1} \cdot (d_{\text{CMB}} - \mu_{\text{CMB}})^T + \left(\frac{3.089 - \ln[10^{10}A_s]}{0.036} \right)^2 , \quad (4.10)$$

where the vector $d_{\text{CMB}} = \{1.7488, 301.76\}$ corresponds to the data and $\mu_{\text{CMB}} = \{\mathcal{R}, l_A\}$ to the theoretical predictions defined before.

4.2.2 Baryonic acoustic oscillations

The expansion of the universe tells us that at very early times the universe was filled by a hot plasma. Before recombination and decoupling, this plasma was mostly composed of baryons and photons, which were tight coupled by Thomson scattering. They were in equilibrium and oscillating, as sound modes, due to the competition between the pressure of the photons and the gravity force of baryons. These oscillations are dubbed as baryon acoustic oscillations and are characterized by the speed of sound $c_s^2 = 1/3(1+R)$.

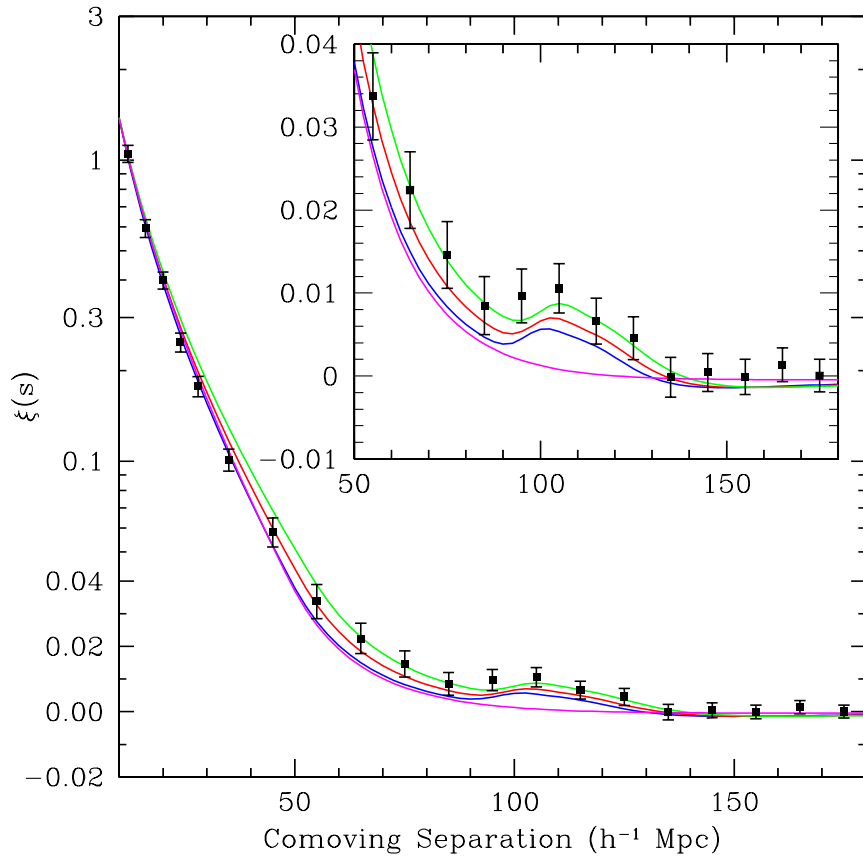


Figure 21 – Correlation function of baryons measured from a sample of 46,748 luminous red galaxies from Sloan Digital Sky Survey. BAO show up as a peak in the correlation function, here it is located at $100h^{-1}$ Mpc. The different lines represent different cosmology. This figure corresponds to first observation of the BAO peak and it is from [7].

Once Thomson scattering falls below the Hubble rate, photons decouple from baryons and free stream. These photons, that were released during the last scattering, form the very well known CMB, while BAO signatures are impressed on the power spectrum and correlation function of baryons.

The BAO scale size is similar to the sound horizon, $r_s(z_d)$, that is, (4.9) is evaluated at the redshift of drag epoch z_d [152]. These BAO scales can be determined from the correlation function or power spectrum of matter see, for instance, Figure 21. As $r_s(z_d)$ is the same at different redshifts, BAO oscillations are effectively standard rulers. BAO measurements determinate $d_A(z)$ and $H(z)$ with large precision. Indeed, one can obtain characteristic scales both along, $r_{s\parallel}$, and transverse, $r_{s\perp}$, to the line-of-sight which shall be related to $d_A(z)$ and $H(z)$ [153]:

$$r_{s\parallel} = \frac{\Delta z}{H(z)} , \quad (4.11)$$

$$r_{s\perp} = \Delta\theta(1+z)d_A(z) . \quad (4.12)$$

An advantage of the use of BAO as standard rulers is that BAO is based on the theory of linear perturbation, which is very well known and understood. It means, BAO do not need taking into account assumptions on astrophysical processes that could be not well understood. Using equations (4.11) and (4.12), one can get $D_v(z)$ (see Appendix B), which represents an isotropic measurement of the BAO signature.

We shall use data sets from six different surveys: 6dFGS, SDSS-LRG, BOSS-MGS, BOSS-LOWZ, WiggleZ, BOSS-CMASS, BOSS-DR12. For the sake of simplicity, we separate the data sets in two groups, organized in Table 2 and Table 3. There is a difference in format between these data sets.

Survey	z	$d_z(z)$	σ
6dFGS [154]	0.106	0.336	0.015
SDSS-LRG [155]	0.35	0.1126	0.0022

Table 2 – BAO data sets in old format.

Survey	z	$\alpha^*(z)$ (Mpc)	σ	r_s^{fid} (Mpc)
BOSS-MGS [156]	0.15	664	25	148.69
BOSS-LOWZ [157]	0.32	1264	25	149.28
WiggleZ [158]	0.44	1716	83	148.6
	0.6	2221	101	148.6
	0.73	2516	86	148.6
BOSS-CMASS [157]	0.57	2056	20	149.28
BOSS-DR12 [152]	0.38	1477	16	147.78
	0.51	1877	19	147.78
	0.61	2140	22	147.78

Table 3 – BAO data sets in new format.

Parameters showed in the tables are defined as:

$$d_z(z) = \frac{r_s(z_d)}{D_v(z)}, \quad (4.13)$$

$$\alpha^*(z) = \frac{D_v(z)}{r_s(z_d)} r_s^{fid}. \quad (4.14)$$

We build two χ^2 functions considering that there are two formats for BAO data sets. Thus, we shall get

$$\chi_{\text{BAO}1}^2 = \frac{(d_z^i - d_z(z_i))^2}{\sigma_i^2}, \quad (4.15)$$

$$\chi_{\text{BAO}2}^2 = (\alpha_i^* - \alpha^*(z_i)) \cdot \text{Cov}_{\text{BAO}}^{-1} \cdot (\alpha_i^* - \alpha^*(z_i))^T, \quad (4.16)$$

where d_z^i , σ_i and z_i to $\chi_{\text{BAO}1}^2$ are showed in the Table 2, while α_i^* and z_i belonging to $\chi_{\text{BAO}2}^2$ are showed in Table 3. The covariance matrix $\text{Cov}_{\text{BAO}}^{-1}$ is built using the errors σ_i showed

in Table 3 and considering that the WiggleZ data is correlated. The covariance matrix for the WiggleZ data is

$$\text{CovWiggleZ} = 10^3 \begin{pmatrix} 6.889 & -8.961 & 21.277 \\ & 10.201 & -13.918 \\ & & 7.396 \end{pmatrix}. \quad (4.17)$$

Note that in both case, (4.15) and (4.16), it is necessary to use the drag redshift z_d . Here, we use the best fit from [159] for z_d .

4.2.3 Type Ia Supernovae

Observations of Type Ia Supernovae led to the discovery of the accelerated expansion of the universe [160, 161]. Nowadays, they are an useful tool for studying the background dynamic. Type Ia Supernovae, which arise from the thermonuclear explosions of white dwarfs, are standard candles that allow us to measure the luminosity distance. Type Ia Supernova surveys provide the magnitude associated to the luminosity distance d_L of each supernova, where the magnitude is defined according to

$$m(z) = 5 \log_{10} \frac{d_L(z)}{10 \text{ pc}}, \quad (4.18)$$

and if one assumes flatness, i.e. $\Omega_k = 0$, the luminosity distance would be (see Appendix B for further information)

$$d_L(z) = (1 + z) \int_0^z \frac{d\tilde{z}}{H(\tilde{z})}. \quad (4.19)$$

Now, we define the χ^2 function as:

$$\chi'_{\text{SNe}}^2 = \sum_i \frac{[m_i - m(z_i) + \xi]^2}{\sigma_i^2}, \quad (4.20)$$

where the index i labels the data point and the parameter ξ is an unknown offset sum of the supernova absolute magnitude and other possible systematics. We marginalized the likelihood $\mathcal{L}'_{\text{SNe}} = \exp(-\chi'_{\text{SNe}}^2/2)$ over ξ , this drives to the marginalized χ^2 function:

$$\chi_{\text{SNe}}^2 = S_2 - \frac{S_1^2}{S_0}, \quad (4.21)$$

where we neglected a cosmology-independent normalizing constant. The quantities S_n are defined as:

$$S_n \equiv \sum_i \frac{[m_i - m(z_i)]^n}{\sigma_i^2}. \quad (4.22)$$

It is worth to stress that ξ is degenerate with $\log_{10} H_0$, then a marginalization over ξ can be thought as effectively marginalizing also over the Hubble constant. We have to mention that we will use SNe Ia data coming from JLA in its binned version [83] (including correlations).

4.2.4 Redshift space distortions

In order to be able to constrain the growth index γ , we will use redshift space distortion data which often are presented as measurements of $f\sigma_8(z)$, which are obtained from the matter power spectrum in the redshift space. Due to the peculiar velocities the power spectrum in redshift space (P_s) is distorted with respect to the power spectrum in real space (P) [162], that is:

$$P_s(\vec{k}) = P(k) [1 + \beta \mu_k^2]^2 \quad (4.23)$$

where $\beta = f/b$ and b is a parameter known as bias⁴. Then, RSD allow us to constrain $f(z)$, and so γ for the common parametrization Ω_m^γ , if a value of b is assumed. As fixing the bias could bias the results, it is more useful to measure parameters or combinations of them that do not depend on the bias b . Such combination is given by $f\sigma_8(z) = f(z)\sigma_8(z)$, where $\sigma_8(z) \equiv \sigma_8 D(z)$ and σ_8 is the variance of the matter distribution at $8h^{-1}$ Mpc. We will use the “Gold” RSD data from [8] (see the Table 4), which represent robust and independent $f\sigma_8(z)$ measurements. Figure 22 shows the “Gold” RSD data set and the function $f\sigma_8(z)$ for the fiducial Λ CDM.

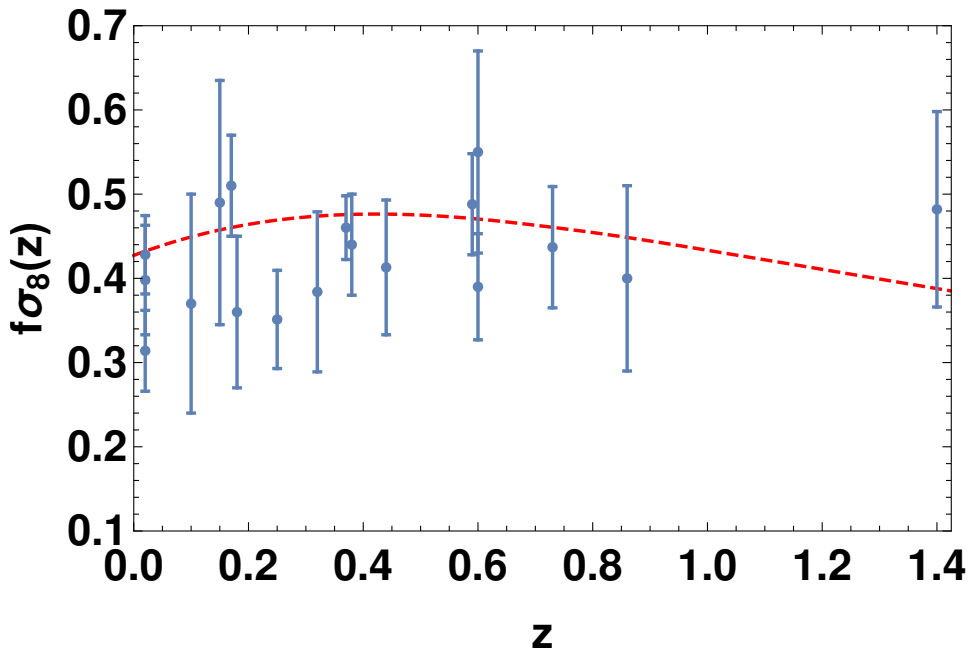


Figure 22 – Compilation of $f\sigma_8(z)$ data from [8]. Note that current RSD data is quite imprecise as it is showed by the error bars. A dashed red line corresponds to a theoretical prediction of fiducial Λ CDM model.

Thus, we build the χ'^2_{RSD} function as:

$$\chi'^2_{RSD} = (f\sigma_8^i - f\sigma_8(z_i)) \cdot \text{Cov}_{RSD}^{-1} \cdot (f\sigma_8^i - f\sigma_8(z_i))^T , \quad (4.24)$$

⁴ The bias parameter comes from the assumption that the distribution of galaxies is linearly proportional to the total matter distribution, $b \equiv \delta_g/\delta$. For large red galaxies, it is expected a bias value in the range $0.7 < (1 - b) < 1$ [163].

where $f\sigma_8(z_i)$ is the theoretical prediction for each measured redshift, $f\sigma_8^i$ represents the data listed in Table 4 and $\text{Cov}_{\text{RSD}}^{-1}$ is the inverse of the covariance matrix. Likewise to the BAO case, reference [8] shows that only the WiggleZ data is correlated:

$$\text{Cov}_{\text{WiggleZ}} = 10^{-3} \begin{pmatrix} 6.4 & 2.57 & 2.54 \\ & 3.969 & 2.54 \\ & & 5.184 \end{pmatrix}. \quad (4.25)$$

In order to adopt a more conservative position (the data was analyzed assuming the Λ CDM model), we marginalize $\mathcal{L}'_{\text{RSD}} = \exp(-\chi'^2_{\text{RSD}}/2)$ over σ_8 , so that

$$\chi^2_{\text{RSD}} = S_{dd} - \frac{S_{dt}^2}{S_{tt}}, \quad (4.26)$$

where quantities S_{dd} , S_{dt} and S_{tt} were defined as:

$$\begin{aligned} S_{dd} &\equiv f\sigma_8^i \cdot \text{Cov}_{\text{RSD}}^{-1} \cdot f\sigma_8^{i^T}, \\ S_{dt} &\equiv f\sigma_8^i \cdot \text{Cov}_{\text{RSD}}^{-1} \cdot f\sigma_8(z_i)^T, \\ S_{tt} &= f\sigma_8(z_i) \cdot \text{Cov}_{\text{RSD}}^{-1} \cdot f\sigma_8(z_i)^T. \end{aligned}$$

We have to stress that the analysis of non-marginalized ‘‘Gold’’ data sets points towards a higher-than-standard value of γ , that is $\gamma \approx 0.725$ [164]. Then, in order to confirm this result we will consider the special case of non-marginalized RSD data, where we also take away H_0^{loc} from the likelihood. Results are showed in the Appendix C.

Survey	z	$f\sigma_8$	σ
6dFGS+SnIa	0.02	0.428	0.0465
SnIa+IRAS	0.02	0.398	0.065
2MASS	0.02	0.314	0.048
SDSS-veloc	0.10	0.370	0.130
SDSS-MGS	0.15	0.490	0.145
2dFGRS	0.17	0.510	0.060
GAMA	0.18	0.360	0.090
	0.38	0.440	0.060
SDSS-LRG	0.25	0.3512	0.0583
	0.37	0.4602	0.0378
BOSS-LOWZ	0.32	0.384	0.095
SDSS-CMASS	0.59	0.488	0.060
WiggleZ	0.44	0.413	0.080
	0.60	0.390	0.063
	0.73	0.437	0.072
Vipers PDR-2	0.60	0.550	0.120
	0.86	0.400	0.110
Fast-Sound	1.40	0.482	0.116

Table 4 – ‘‘Gold’’ RSD data set from [8]

4.2.5 Local H_0

The determination of H_0^{R16} follows the same method stated in [165]. We can summarize this method in three steps. First, one measures distances of Cepheids in the Milky Way by parallax. The latter allows us to calibrate the Cepheids' brightness in order to use them as standard candles. Then, these Cepheids allow us to determine the distance to nearby galaxies where Supernovae and other Cepheids are identified. These are then used to calibrate the true brightness of Supernovae, which are standard candles. Finally, the complete Hubble diagram is obtained using the distance modulus of farthest Supernovae.

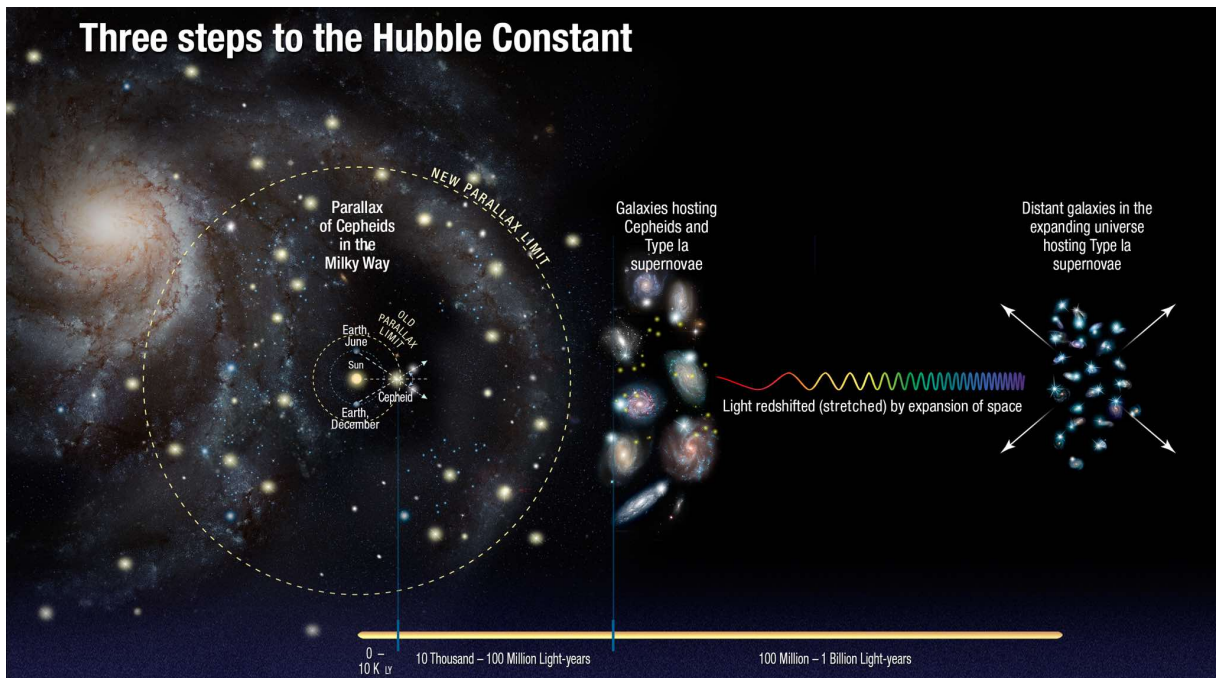


Figure 23 – This picture is from <<https://www.nasa.gov/image-feature/goddard/2016/three-steps-to-measuring-the-hubble-constant>>

The SNe recession velocities are determined via the redshift, using a Taylor expansion that takes into account the current value of the deceleration parameter q_0 and the jerk parameter, $j(z) \equiv (\ddot{a}/a)(\dot{a}/a)^{-3}$, today $j_0 = j(0)$ [166]. The recession velocities and the measured distances allow us to get the Hubble constant H_0 , basically by Hubble law. The three steps used in this method are illustrated in Figure 23.

Riess et al.[1] performed a measurement of H_0 through the method described before. Using the Wide Field Camera 3 (WFC3) on the Hubble Space Telescope (HST) they obtained H_0^{R16} . In order to build the $\chi_{H_0}^2$ function, we shall use $H_0^{\text{obs}} = H_0^{\text{R16}} = 73.24 \text{ km s}^{-1}\text{Mpc}^{-1}$ and $\sigma_{\text{obs}} = \sigma_{\text{R16}} = 1.74 \text{ km s}^{-1}\text{Mpc}^{-1}$. So, we defined the $\chi_{H_0}^2$ function

as:

$$\chi_{H_0}^2 = \frac{(H_0 - H_0^{obs})^2}{\sigma_{loc}^2} . \quad (4.27)$$

Note that before we have defined σ_{loc}^2 as (3.13). Nevertheless, in order to identify the effect of the cosmic variance in statistical inference, we will use two cases for σ_{loc} in the $\chi_{H_0}^2$ definition. First, we shall perform an analysis with $\sigma_{loc} = \sigma_{R16}$. Later, we will use $\sigma_{loc} = \sqrt{\sigma_{R16}^2 + H_0^2 \sigma_{\delta H}^2}$.

4.3 FULL LIKELIHOOD

We shall use Bayesian inference to get cosmological constraints, with and without cosmic variance and its effects. To that end, we will perform the joint analysis of the data showed before, i.e. the joint analysis of CMB, BAO, SNe Ia, RSD and local H_0 data sets. Thus, the total χ^2 , necessary to build the full likelihood $\mathcal{L} = e^{-\chi^2/2}$, is defined by:

$$\chi_{tot}^2 = \chi_{CMB}^2 + \chi_{BAO}^2 + \chi_{SNe}^2 + \chi_{RSD}^2 + \chi_{H_0}^2 . \quad (4.28)$$

It is worth to mention that the total data set has 67 data points. On the others hand, eventually we will carry out the Bayesian inference taking out the RSD data. This shall be discussed later.

5 Bayesian inference: results

In this chapter we show the results of Bayesian inference. We have performed the analysis using a Mathematica code named mBayes [167]. Also, as we have already mentioned, most of the results and discussion here showed are presented in [38].

First, we will show results corresponding to the analysis with the full likelihood of (4.28). However, we have also performed the analysis of the full likelihood without RSD data, in order to distinguish cosmic variance effects from RSD data. In both cases, we will present best fit parameters and plots of the posterior distributions. Then, we will show and discuss the value reached of the tension and the model selection criteria for each cosmological context as well as the respective error budget by cosmic variance.

Model	Free parameters
Λ CDM	H_0, Ω_{m0}, A_s
γ CDM	$H_0, \Omega_{m0}, A_s, \gamma$
γw CDM	$H_0, \Omega_{m0}, A_s, w_{de}$
γ_a CDM	$H_0, \Omega_{m0}, A_s, \gamma_0, \gamma_1$
CQ08	$H_0, \Omega_{m0}, A_s, \beta$
CQ08+ w_{de}	$H_0, \Omega_{m0}, A_s, \beta, w_{de}$
CQ10	$H_0, \Omega_{m0}, A_s, \beta$
CQ10+ w_{de}	$H_0, \Omega_{m0}, A_s, \beta, w_{de}$

Table 5 – Free parameters for each cosmological model. See the text for more details.

In order to shed light on the results, we define the relative Δ AIC and Δ BIC criteria, which are

$$\Delta\text{AIC} = \text{AIC}_{\Lambda\text{CDM}} - \text{AIC}_i , \quad (5.1)$$

$$\Delta\text{BIC} = \text{BIC}_{\Lambda\text{CDM}} - \text{BIC}_i , \quad (5.2)$$

where the subscript i represents a particular parametrization or model. Thus, a negative value of Δ AIC or Δ BIC means a preference to Λ CDM and the opposite case a preference to the particular parametrization. The value that Δ AIC or Δ BIC takes will be interpreted according to Jeffrey's scale [168]. Thus, according to this scale $\Delta X < 1$ is inconclusive, $1 < \Delta X < 2.5$ is moderate, $2.5 < \Delta X < 5$ is strong and $5 < \Delta X$ is highly significant evidence (where X represents AIC or BIC).

We use the CQ model and the γ CDM, γw CDM, γ_a CDM parameterizations, besides Λ CDM. To perform statistic inference we should use the free parameters of each model, for instance, as we have indicated in Section 1.3, the Λ CDM model has six free parameters. Nevertheless, using the whole free parameter space might be computationally expensive.

We will study only the parameters that could have an important impact on the cosmic variance, fixing the other ones to the Λ CDM fiducial value showed in Table 1. We show each model or parametrization and its free parameters in Table 5. Note that the CQ model has two more parameters than Λ CDM, α and β . In this case, as often done in the literature [19, 105, 106], we fix the value of the slope of the potential α . To avoid biased results that could be generated by this choice, we adopt two values $\alpha = 0.08$ (represented by CQ08) and $\alpha = 0.1$ (represented by CQ10).

5.1 RESULTS FOR THE FULL LIKELIHOOD

5.1.1 Best fit parameters and posteriors

$\chi^2_{H_0}$ with $\sigma_{\text{loc}}^2 = \sigma_{\mathbf{R16}}^2$								
Model	σ_8	γ_0	γ_1	H_0	Ω_{m0}	w_{de}	$\log 10^{10} A_s$	β
Λ CDM	0.842	-	-	66.42	0.326	-	3.093	-
CQ08	0.831	-	-	66.27	0.324	-	3.090	0.0124
CQ08+ w_{de}	0.833	-	-	66.28	0.324	-1.	3.094	0.0212
CQ10	0.831	-	-	66.27	0.324	-	3.090	0.
CQ10+ w_{de}	0.832	-	-	66.28	0.324	-1.	3.094	0.0106
γ CDM	0.792	0.714	-	66.42	0.326	-	3.086	-
γw CDM	0.86	0.64	-	70.46	0.307	-1.146	3.084	-
γ_a CDM	0.86	0.747	0.587	66.55	0.325	-	3.087	-
$\chi^2_{H_0}$ with $\sigma_{\text{loc}}^2 = \sigma_{\mathbf{R16}}^2 + H_0^2 \sigma_{\delta H}^2$								
Model	σ_8	γ_0	γ_1	H_0	Ω_{m0}	w_{de}	$\log 10^{10} A_s$	β
Λ CDM	0.841	-	-	66.12	0.329	-	3.084	-
CQ08	0.834	-	-	65.72	0.327	-	3.09	0.0497
CQ08+ w_{de}	0.837	-	-	65.61	0.326	-1.	3.094	0.0635
CQ10	0.833	-	-	65.72	0.327	-	3.09	0.0434
CQ10+ w_{de}	0.839	-	-	65.61	0.329	-0.998	3.094	0.0529
γ CDM	0.814	0.633	-	66.32	0.326	-	3.086	-
γw CDM	0.852	0.637	-	69.2	0.314	-1.112	3.084	-
γ_a CDM	0.852	0.661	0.202	66.37	0.325	-	3.082	-

Table 6 – Best fit parameters obtained by the full likelihood analysis for all parametrizations and models here considered. Note that we show the two cases of $\chi^2_{H_0}$ used in analysis. See the text for further information.

The minimum χ^2 gives the best fit parameters, see Table 6. Also, we display the σ_8 value for each case. One can easily note the effect of the cosmic variance over the best fit values. For instance, when $\sigma_{\delta H}$ is included in the definition of $\chi^2_{H_0}$, the value of γ decreases for all the models, meaning that the use of cosmic variance implies a universe with more structures. That also can be observed in σ_8 , where it increases for almost all

models. Similar behavior can be observed in H_0 . The inclusion of cosmic variance produces a lower values of H_0 , even lower than H_0^{Pl} . One can wonder why cosmic variance leads to lower values of H_0 , when the usual solution to the tension is to shift H_0 to higher values [18, 19, 20, 21, 22, 23, 24, 25]. The answer is due to the high correlation with Ω_{m0} . As we have pointed out before, the introduction of the cosmic variance in the analysis yields more structures in the universe and consequently more matter, that yields an increase of Ω_{m0} . Typical contour plots and PDFs are showed in Figure 25-32, where one can easily identify the effect of the cosmic variance on cosmological constraints and also note the correlation between H_0 - Ω_{m0} . On the other hand, it is important to note the effect of the cosmic variance on coupled models, especially on the parameter β . The inclusion in the error budget of the cosmic variance, $\sigma_{\delta H}$, leads to an increased coupling β .

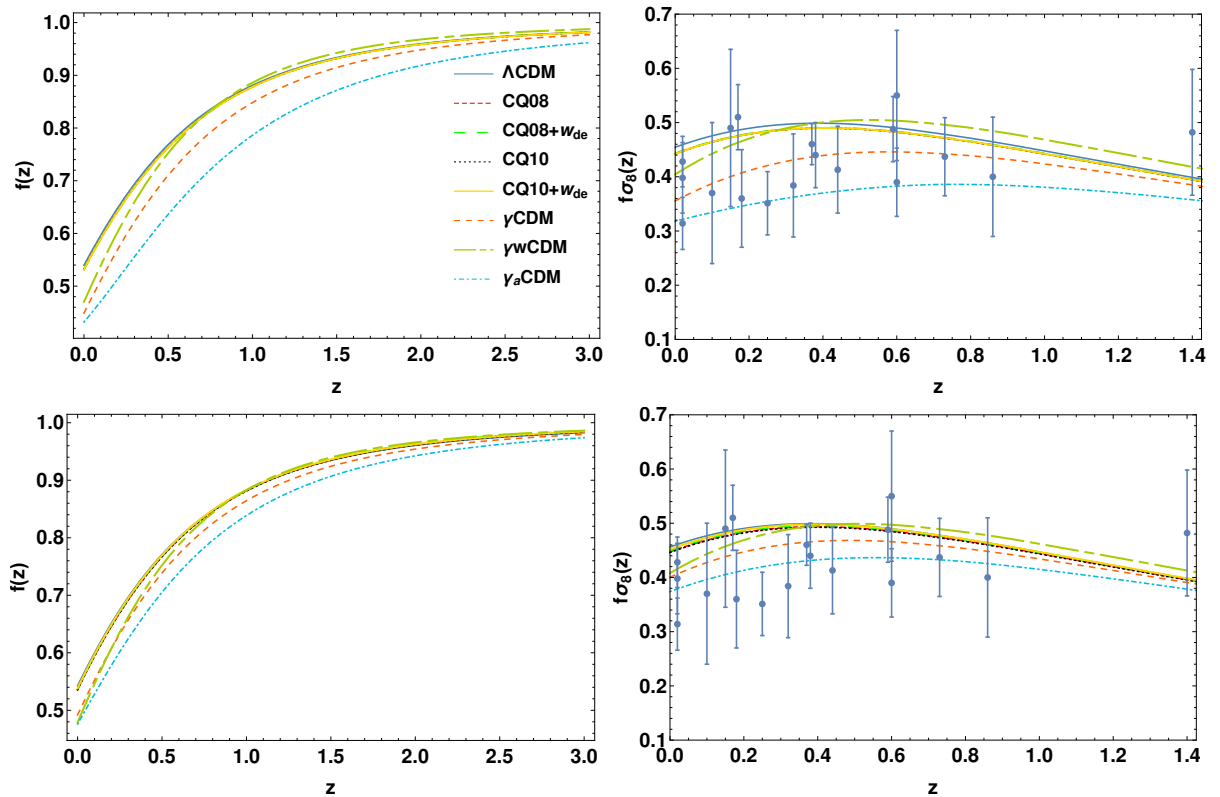


Figure 24 – **Top:** Functions $f(z)$ and $f\sigma_8(z)$ predicted for the different cosmologies when the best fit provided by $\chi^2_{H_0}$ without $\sigma_{\delta H}$ is used. **Bottom:** Functions $f(z)$ and $f\sigma_8(z)$ predicted for the different cosmologies when the best fit provided by $\chi^2_{H_0}$ with $\sigma_{\delta H}$ is used. Note that inclusion of the cosmic variance an its error budget changes the functions. See the text for further information.

Before computing the tension (3.1) for each model, we have to estimate the mean and variance of the H_0 distribution. For that, we use the $\text{PDF}(H_0)$ provided by Bayesian inference both when it is and it is not considered the effect of the cosmic variance. Results are showed in Table 7. Similar to the best fit of H_0 the inclusion of $\sigma_{\delta H}$ shifts H_0 to lower values. Instead, the variance increases when cosmic variance is included, thus widening its

posterior.

$\chi^2_{H_0}$ with $\sigma_{\text{loc}}^2 = \sigma_{\text{R16}}^2$		
Model	Mean H_0	Variance H_0
Λ CDM	66.5006	0.267491
CQ08	66.0016	0.340444
CQ08+ w_{de}	65.8316	0.401472
CQ10	65.9442	0.332064
CQ10+ w_{de}	65.8172	0.394371
γ CDM	66.4468	0.268314
γw CDM	70.365	1.79934
γ_a CDM	66.4636	0.273785
$\chi^2_{H_0}$ with $\sigma_{\text{loc}}^2 = \sigma_{\text{R16}}^2 + H_0^2 \sigma_{\delta H}^2$		
Model	Mean H_0	Variance H_0
Λ CDM	66.1793	0.273612
CQ08	65.5447	0.402547
CQ08+ w_{de}	65.2818	0.481509
CQ10	65.4985	0.390103
CQ10+ w_{de}	65.2715	0.475404
γ CDM	66.1741	0.27261
γw CDM	69.3095	2.2582
γ_a CDM	66.1801	0.285065

Table 7 – Mean and variance of H_0 , computed from the posterior obtained via Bayesian inference. Note that we show the two cases of $\chi^2_{H_0}$ used in the analysis. See the text for further information.

In order to illustrate how different are the models here considered, we plot $f(z)$ and $f\sigma_8(z)$ for each model using the best fits showed in Table 6. Thus, Figure 24 shows both $f(z)$ and $f\sigma_8(z)$ for the different models and for the two sets of best fit parameters. The most remarkable feature is how the best fit provided by the analysis with cosmic variance put all functions, both $f(z)$ and $f\sigma_8(z)$, closer.

5.1.2 Error budget $\sigma_{\delta H}$ and tension

Using the values showed in Tables 6-7 we can compute all the quantities of our interest, such as: the relative error $\sigma_{\delta H}$, the tension T , the minimum χ^2_{\min} and the relative criteria Δ AIC and Δ BIC. Theses quantities are the main results of this work and they are showed in Table 8. Before examining the values of the tension T , we will discuss the agreement of models with the data, i.e. the χ^2_{\min} for each model.

From Table 8 one can note that the analysis considering cosmic variance, i.e. $\sigma_{\text{loc}}^2 = \sigma_{\text{R16}}^2 + H_0^2 \sigma_{\delta H}^2$, produces a decrease in the minimum χ^2 . For example, the inclusion

of the cosmic variance in the statistical inference produces a $\Delta\chi_{\min}^2 \approx 8.5$ for the Λ CDM model and a $\Delta\chi_{\min}^2 \approx 9.3$ for the CQ08, with respect to the analysis without cosmic variance. Indeed, the $\chi_{H_0}^2$ would decrease after the inclusion of the systematic error $\sigma_{\delta H}$; consequently, the total χ^2 minimum also will decrease. Roughly speaking, the inclusion of the cosmic variance in the statistical inference improved the agreement of the models with the current data. The lowest values of χ_{\min}^2 are given by the γw CDM parametrization, which features $\chi_{\min}^2 = 71.71$ and $\chi_{\min}^2 = 69.68$ for the analysis without and with cosmic variance effects, respectively. We can see from Table 6 that cosmological constraints for the γw CDM extension predict a phantom dark energy, $w_{de} < -1$, with a cosmic growth index $\gamma \approx 0.64$, for the two cases of the $\chi_{H_0}^2$ analysis.

$\chi_{H_0}^2$ with $\sigma_{\text{loc}}^2 = \sigma_{\mathbf{R16}}^2$					
Model	$\sigma_{\delta H}$	T	χ_{\min}^2	ΔAIC	ΔBIC
Λ CDM	0.0297	2.56	83.82	-	-
CQ08	0.0290	2.80	83.56	-1.74	-3.95
CQ08+ w_{de}	0.0291	2.86	83.60	-3.78	-8.19
CQ10	0.0290	2.82	83.56	-1.74	-3.95
CQ10+ w_{de}	0.0291	2.87	83.60	-3.78	-8.19
γ CDM	0.0234	2.91	82.01	-0.19	-2.40
γw CDM	0.0268	1.12	71.71	8.11	3.70
γ_a CDM	0.0207	3.05	82.13	-2.31	-6.72

$\chi_{H_0}^2$ with $\sigma_{\text{loc}}^2 = \sigma_{\mathbf{R16}}^2 + H_0^2\sigma_{\delta H}^2$					
Model	$\sigma_{\delta H}$	T	χ_{\min}^2	ΔAIC	ΔBIC
Λ CDM	0.0297	2.69	75.28	-	-
CQ08	0.0293	2.97	74.29	-1.01	-3.21
CQ08+ w_{de}	0.0295	3.07	74.35	-3.07	-7.48
CQ10	0.0292	2.99	74.29	-1.01	-3.21
CQ10+ w_{de}	0.0295	3.07	74.35	-3.07	-7.48
γ CDM	0.0262	2.87	74.96	-1.68	-3.88
γw CDM	0.0269	1.54	69.68	1.60	-2.81
γ_a CDM	0.0245	2.97	75.89	-4.61	-9.02

Table 8 – Main results of the Bayesian inference with the full likelihood and, therefore, of this work. See the text for further information.

We have already discussed that it is not appropriate to perform model selection using the simple χ_{\min}^2 . Then we use the AIC and BIC criteria. In particular, in order to shed light on the results, we define the relative values with respect to the Λ CDM, see equations (5.1) and (5.2). Thus, from Table 8 it is easy to note that only the γw CDM parametrization is preferred by the data with respect to the standard Λ CDM model: most of the relative criteria values are positive. According to Jeffreys's scale, the result of the analysis with $\sigma_{\text{loc}}^2 = \sigma_{\mathbf{R16}}^2$ shows a (ΔBIC) moderate and (ΔAIC) strong evidence for the

γw CDM model. While, for the results coming from $\sigma_{loc}^2 = \sigma_{R16}^2 + \sigma_{\delta H}^2 H_0^2$ one has a weak (Δ AIC) evidence for γw CDM and a (Δ BIC) weak evidence for Λ CDM. Note that values of relative criteria do not reach neither very strong nor decisive evidence values.

$\chi_{H_0}^2$ with $\sigma_{loc}^2 = \sigma_{R16}^2$		
Model	Error $\sigma_{\delta H} H_0$	Ratio $\sigma_{R16}/(\sigma_{\delta H} H_0)$
Λ CDM	1.97523	0.880911
CQ08	1.91649	0.907909
CQ08+ w_{de}	1.91512	0.908557
CQ10	1.91375	0.909208
CQ10+ w_{de}	1.91206	0.910016
γ CDM	1.55619	1.11811
γw CDM	1.8864	0.92239
γ_a CDM	1.37935	1.26146

$\chi_{H_0}^2$ with $\sigma_{loc}^2 = \sigma_{R16}^2 + H_0^2 \sigma_{\delta H}^2$		
Model	Error $\sigma_{\delta H} H_0$	Ratio $\sigma_{R16}/(\sigma_{\delta H} H_0)$
Λ CDM	1.96556	0.885243
CQ08	1.92176	0.905419
CQ08+ w_{de}	1.92566	0.903587
CQ10	1.91558	0.908341
CQ10+ w_{de}	1.92813	0.902428
γ CDM	1.73813	1.00108
γw CDM	1.86409	0.933434
γ_a CDM	1.62117	1.0733

Table 9 – Comparison between the absolute error budget due to cosmic variance $\sigma_{\delta H} H_0$ and the error on local measurements σ_{R16} from the analysis with the full likelihood. Note that for all cosmological models $\sigma_{\delta H}$ and σ_{R16} are of the same order.

Now, we must discuss $\sigma_{\delta H}$ and T . First, the highest value of the systematic error $\sigma_{\delta H}$ is reached in the Λ CDM, which is $\sigma_{\delta H} = 0.0297$ for both the cases of $\chi_{H_0}^2$. Only the CQ models seem to produce a relative systematic error comparable to the one produced by Λ CDM. This fact also can be noted from Table 9, where we show the absolute systematic error $\sigma_{\delta H} H_0$. However, though the value of systematic error, either relative $\sigma_{\delta H}$ or absolute $\sigma_{\delta H} H_0$, has an important contribution to the tension T , its value is not fully decisive regarding the tension problem. It means, the model with the highest value of $\sigma_{\delta H}$ is not necessarily the model that provides the lowest tension. This latter can be easily noted from Table 8, where one can see that, for the two cases of $\chi_{H_0}^2$, only γw CDM produces a lower tension than Λ CDM. The γw CDM context produces the lowest tension for the analysis without cosmic variance. This is because, besides its cosmic variance contribution, it predicts a higher value of the Hubble constant $H_0 = 70.37 \text{ km s}^{-1} \text{ Mpc}^{-1}$. Nevertheless, the mean of $\text{PDF}(H_0)$ is not the only important contribution. Also, the large

standard deviation $\sigma_{H_0} \approx 1.34 \text{ km s}^{-1} \text{ Mpc}^{-1}$ is important. Similar is the case of $\gamma w\text{CDM}$ for which the analysis takes into account the systematic effect due to cosmic variance, where $H_0 = 69.31 \text{ km s}^{-1} \text{ Mpc}^{-1}$ and $\sigma_{H_0} \approx 1.50 \text{ km s}^{-1} \text{ Mpc}^{-1}$. As we have mentioned, alleviating the tension by shifting directly the Hubble constant has been largely considered in the literature [18, 21, 22, 23, 24, 25], nevertheless accommodating H_0 to a higher value modifies the early universe, which is very well constrained by the CMB [133]. Note that in all cases here presented there is remnant tension, even in the case of the $\gamma w\text{CDM}$ context.

It is worth to mention that, as showed in Table 9, the absolute systematic error produced by cosmic variance, $\sigma_{\delta H} H_0$, is always comparable to the error from local determinations, σ_{R16} . It means that $\sigma_{\delta H}$ and σ_{R16} are always of the same order. Therefore, though the tension cannot be alleviated by cosmic variance, the effects of the cosmic variance are non-negligible if one compares them with σ_{R16} . For example, for CQ08 + w_{de} when cosmic variance is introduced in analysis, we have $\sigma_{\delta H} \approx 1.1\sigma_{R16}$, therefore, the total error on local determinations is $\sigma_{loc} = 1.45\sigma_{R16}$.

5.2 RESULTS WITHOUT RSD DATA

We have showed and discussed in Chapter 3 that all non-standard dark energy models here considered are able to provide a systematic $\sigma_{\delta H}$ higher than the one in ΛCDM . However, as showed in Table 8, the systematic belonging to ΛCDM is always higher than the systematic in the non-standard dark energy context; this is due to RSD data. In Table 6 one can see that the cosmic growth index is always greater than the standard value 0.55, that is $\gamma > 0.55$. This could be a genuine effect or also signal the presence of systematics in the still very imprecise RSD measurements. Indeed, as we can note from Figure 22, or also from the right-hand side of Figure 24, the RSD data has very large error bars. Thus, in order to distinguish the effect of the cosmic variance from RSD data, we remove the RSD data from the full likelihood and re-do the analysis. Obviously, without RSD data there is not a direct way to constrain γ . Therefore it is difficult to constrain models with many parameters and here we only use the ΛCDM model and its extension γCDM . For γ we will adopt a flat prior $0 \leq \gamma \leq 2.5$.

5.2.1 Best fit parameters and posteriors

Table 10 shows the best fit parameters and σ_8 for this case. Similar to the results of the analysis with the full likelihood, the inclusion of $\sigma_{\delta H}$ leads to lower values of H_0 and higher values of Ω_{m0} . Typical contour plots and PDFs are showed in Figures 33-34, where one can appreciate that the inclusion of the cosmic variance effects allow us to constrain, at least weakly, the cosmic growth index γ . The mean and variance of the $\text{PDF}(H_0)$ are showed in Table 11. Similar to the best fit H_0 the inclusion of $\sigma_{\delta H}$ shifts H_0 to lower values,

$\chi^2_{H_0}$ with $\sigma_{\text{loc}}^2 = \sigma_{\text{R16}}^2$					
Model	σ_8	γ	H_0	Ω_{m0}	$\log 10^{10} A_s$
Λ CDM	0.838	-	66.67	0.323	3.086
γ CDM	1.06	0.	66.7	0.323	3.086

$\chi^2_{H_0}$ with $\sigma_{\text{loc}}^2 = \sigma_{\text{R16}}^2 + H_0^2 \sigma_{\delta H}^2$					
Model	σ_8	γ	H_0	Ω_{m0}	$\log 10^{10} A_s$
Λ CDM	0.839	-	66.42	0.326	3.085
γ CDM	1.059	0.	66.08	0.329	3.086

Table 10 – Best fit parameters obtained with the analysis without RSD data for Λ CDM and γ CDM. Note that we show the two cases of $\chi^2_{H_0}$. See the text for further information.

while it increases the variance.

$\chi^2_{H_0}$ with $\sigma_{\text{loc}}^2 = \sigma_{\text{R16}}^2$		
Model	Mean H_0	Variance H_0
Λ CDM	66.5032	0.269139
γ CDM	66.4522	0.269981

$\chi^2_{H_0}$ with $\sigma_{\text{loc}}^2 = \sigma_{\text{R16}}^2 + H_0^2 \sigma_{\delta H}^2$		
Model	Mean H_0	Variance H_0
Λ CDM	66.1797	0.274736
γ CDM	66.0374	0.279834

Table 11 – Mean and variance of H_0 , computed from $\text{PDF}(H_0)$ provided by cosmological constraints without RSD data. Note that we show the two cases of $\chi^2_{H_0}$. See the text for further information.

5.2.2 Error budget $\sigma_{\delta H}$ and tension

As it is showed in Table 10, the lack of RSD data in the statistical inference leads to the constraint $\gamma = 0$, even when one takes into account the error budget produced by cosmic variance in order to define the function $\chi^2_{H_0}$.¹ Then, the systematic provided by γ CDM is quite higher (~ 0.066) than the one produced in Λ CDM (~ 0.029), see Table 12. Also, one can note from Table 12 that, despite the fact that γ CDM predicts a high $\sigma_{\delta H}$, this latter is not enough to explain the whole tension. That is, even for a cosmology with enough structures to generate $\gamma = 0$, and a background dynamics equal to the Λ CDM background, there is a residual tension. Finally, due to the poor (or null) power to constrain

¹ The cosmic variance always prefers the lowest possible value of γ . This because the deviation δH_R , and consequently $\sigma_{\delta H}$, is inversely proportional to γ , see Figure 16.

γ , the γ CDM extension always offers a lower χ^2_{\min} than Λ CDM. That also occurs for the model selection criteria AIC and BIC.

$\chi^2_{H_0}$ with $\sigma_{\text{loc}}^2 = \sigma_{\text{R16}}^2$					
Model	σ_H	T	χ^2_{\min}	ΔAIC	ΔBIC
Λ CDM	0.0295	2.57	84.15	-	-
γ CDM	0.0667	1.43	70.90	11.25	9.04

$\chi^2_{H_0}$ with $\sigma_{\text{loc}}^2 = \sigma_{\text{R16}}^2 + H_0^2 \sigma_{\delta H}^2$					
Model	σ_H	T	χ^2_{\min}	ΔAIC	ΔBIC
Λ CDM	0.0296	2.69	75.87	-	-
γ CDM	0.0662	1.53	57.50	16.37	14.16

Table 12 – Main results of Bayesian inference without RSD data. See the text for further information.

Table 13 shows the absolute systematic error, $\sigma_{\delta H} H_0$, generated by the cosmic variance. Also, we show the ratio between $\sigma_{\delta H} H_0$ and σ_{R16} . Obviously, the higher values $\sigma_{\delta H}$ obtained for the γ CDM parametrization lead to an increase in σ_{loc} . For instance, for the case where $\sigma_{\text{R16}}/(\sigma_{\delta H} H_0) \approx 0.39$ (or the equivalent $\sigma_{\delta H} H_0 \approx 2.5\sigma_{\text{R16}}$) one can demonstrate that the total error on the local measurements of H_0 is given by $\sigma_{\text{loc}} \approx 1.87 \sigma_{\text{R16}}$.

$\chi^2_{H_0}$ with $\sigma_{\text{loc}}^2 = \sigma_{\text{R16}}^2$		
Model	Error $\sigma_{\delta H} H_0$	Ratio $\sigma_{\text{R16}}/(\sigma_{\delta H} H_0)$
Λ CDM	1.9623	0.886716
γ CDM	4.43312	0.3925

$\chi^2_{H_0}$ with $\sigma_{\text{loc}}^2 = \sigma_{\text{R16}}^2 + H_0^2 \sigma_{\delta H}^2$		
Model	Error $\sigma_{\delta H} H_0$	Ratio $\sigma_{\text{R16}}/(\sigma_{\delta H} H_0)$
Λ CDM	1.9595	0.887981
γ CDM	4.37337	0.397862

Table 13 – Comparison between the absolute error budget due to cosmic variance $\sigma_{\delta H} H_0$ and the error on local measurements σ_{R16} from the analysis without RSD data.

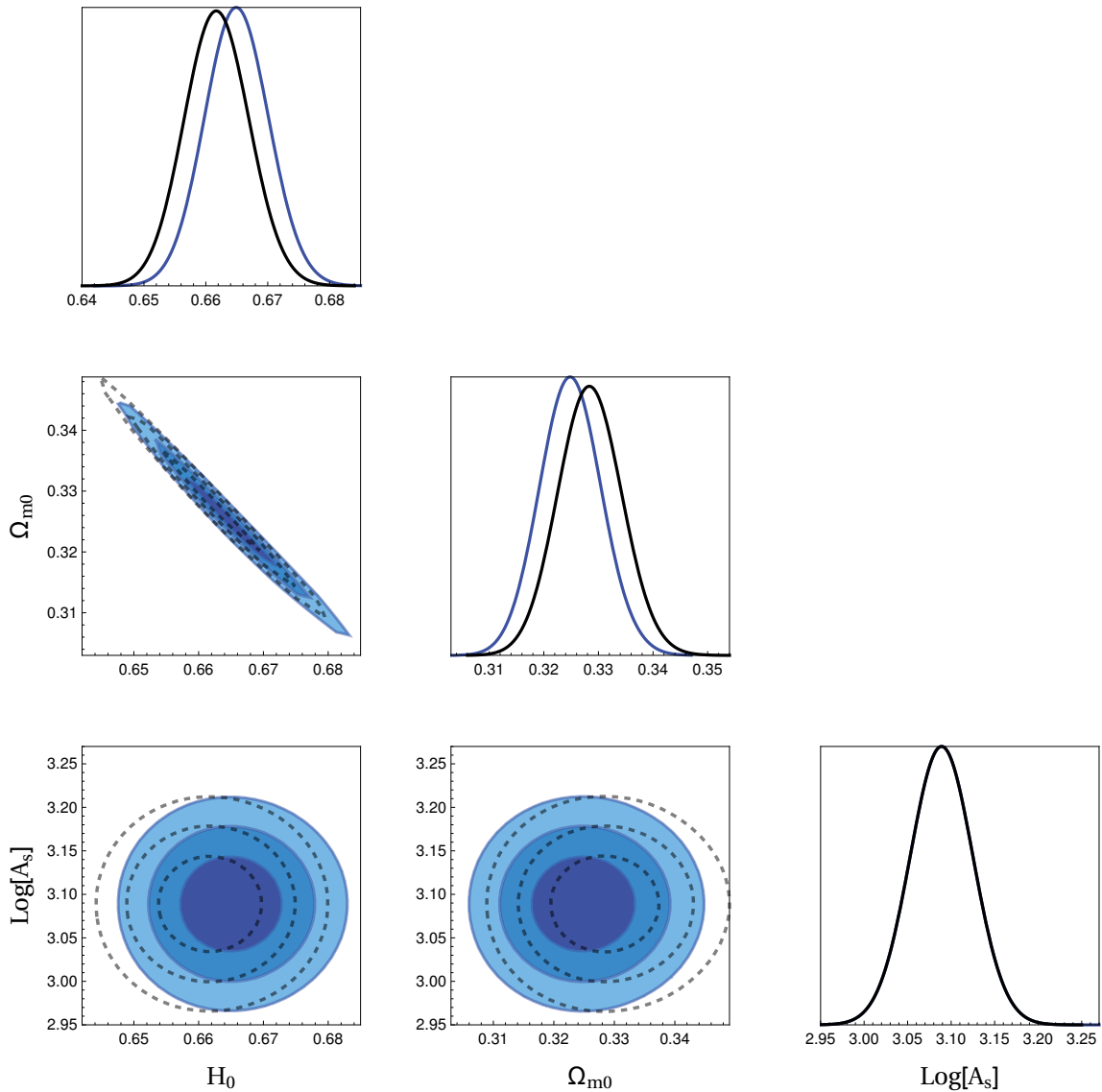


Figure 25 – Cosmological constraints, with the full likelihood, for the Λ CDM model, where the contours are 68.3%, 95.4% and 99.7% confidence levels. One can note that the inclusion of the cosmic variance into the analysis (dashed black contours) shifts the usual constraints (blue contours). Higher values of Ω_{m0} and lower values of H_0 are preferred if the cosmic variance is included. Note the high correlation between $\Omega_{m0} - H_0$.

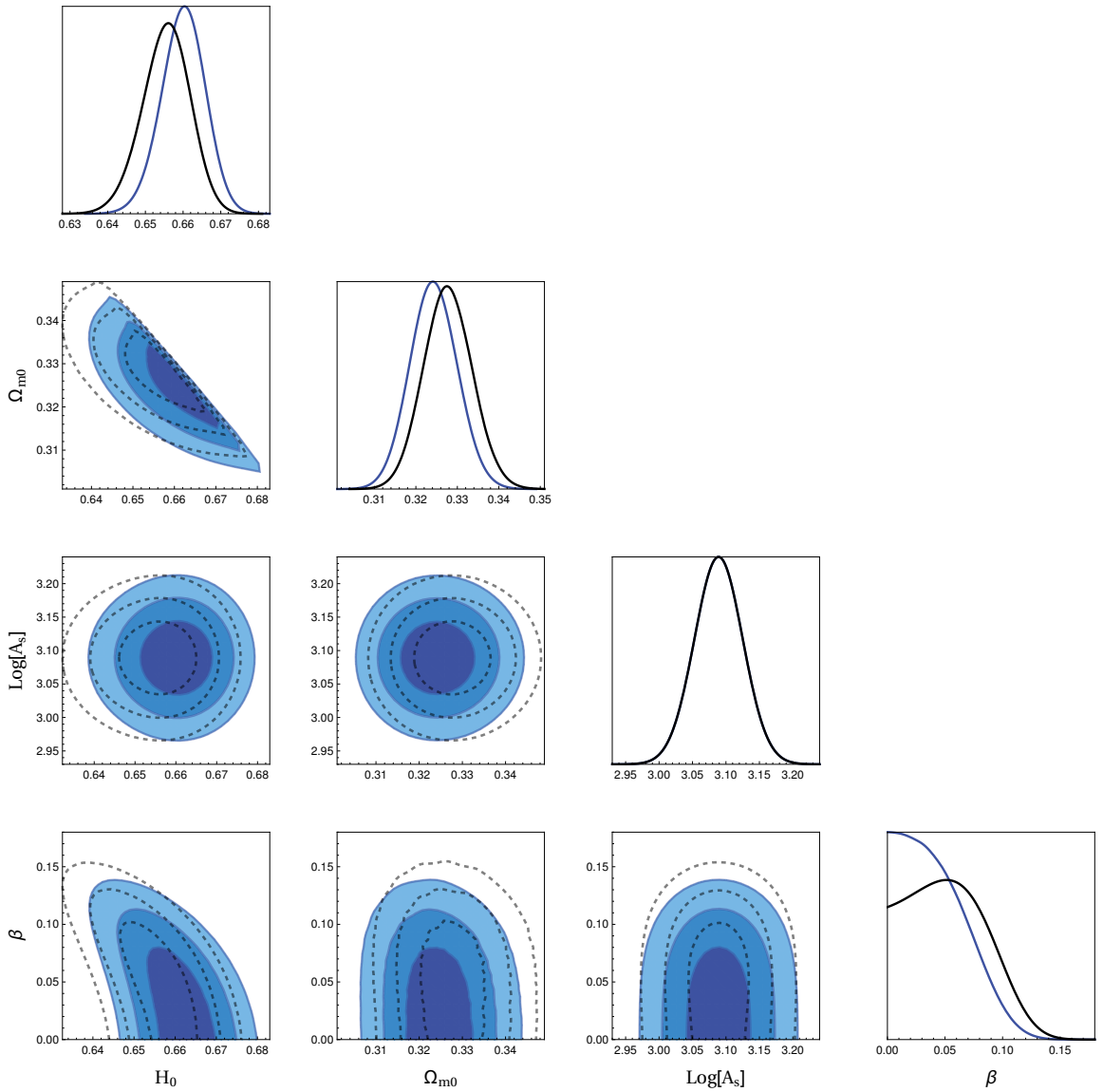


Figure 26 – Cosmological constraints, with the full likelihood, for the CQ08 model, where the contours are 68.3%, 95.4% and 99.7% confidence levels. One can note that the inclusion of the cosmic variance into the analysis (dashed black contours) shifts the usual constraint (blue contours). Higher values of Ω_{m0} , lower values of H_0 and non-null couplings β are preferred if the cosmic variance is included. Note the high correlation between $\Omega_{m0} - H_0$.

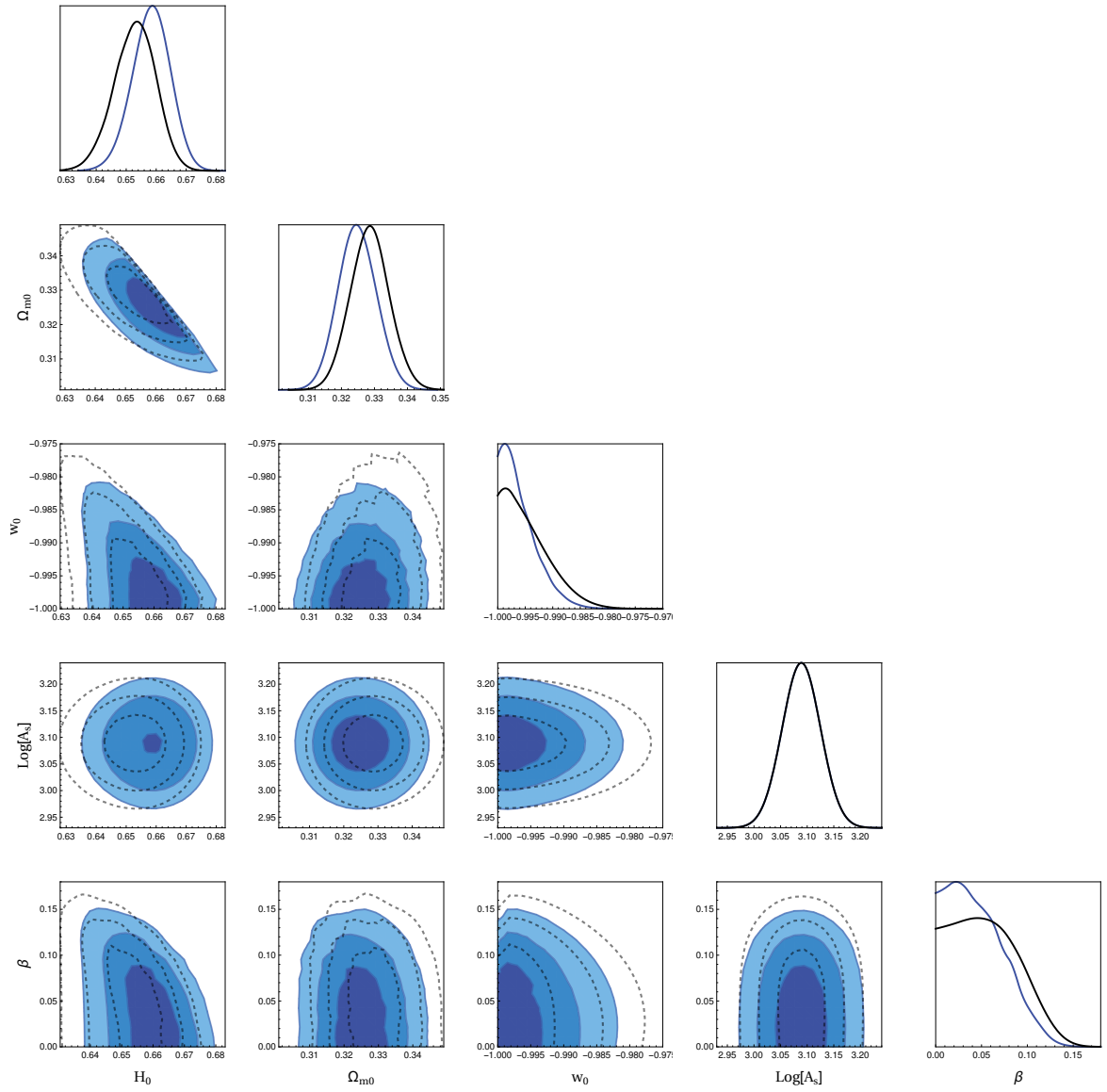


Figure 27 – Cosmological constraints, with the full likelihood, for the CQ08 + w_{de} model, where the contours are 68.3%, 95.4% and 99.7% confidence levels. One can note that the inclusion of the cosmic variance into the analysis (dashed black contours) shifts the usual constraint (blue contours). Higher values of Ω_{m0} , lower values of H_0 and non-null couplings β are preferred if the cosmic variance is included. Also, the cosmic variance extends the confidence levels for w_{de} . Note the high correlation between $\Omega_{m0} - H_0$.

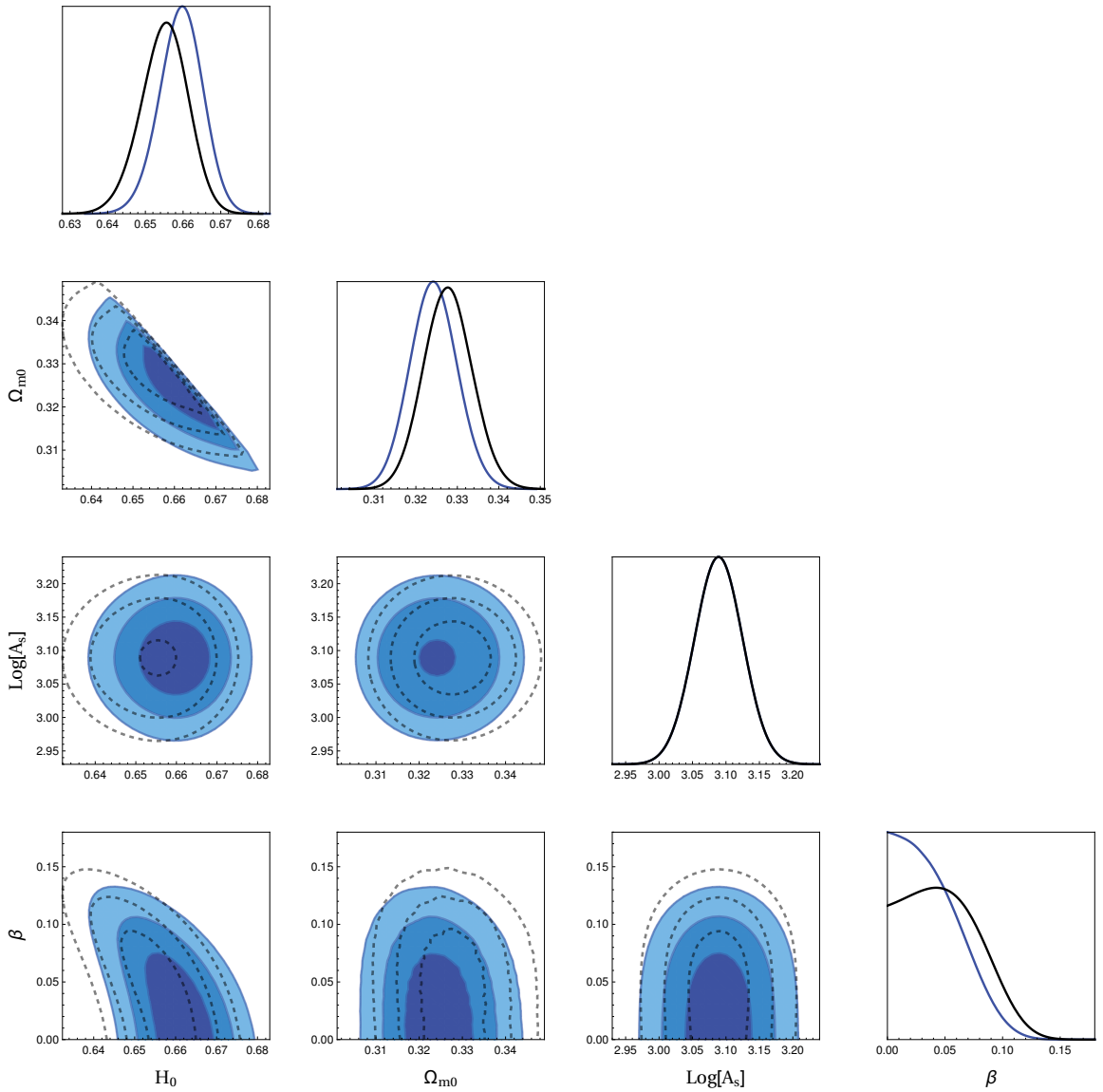


Figure 28 – Cosmological constraints, with full the likelihood, for the CQ10 model, where the contours are 68.3%, 95.4% and 99.7% confidence levels. One can note that the inclusion of the cosmic variance into the analysis (dashed black contours) shifts the usual constraint (blue contours). Higher values of Ω_{m0} , lower values of H_0 and non-null couplings β are preferred if the cosmic variance is included. Note the high correlation between $\Omega_{m0} - H_0$.

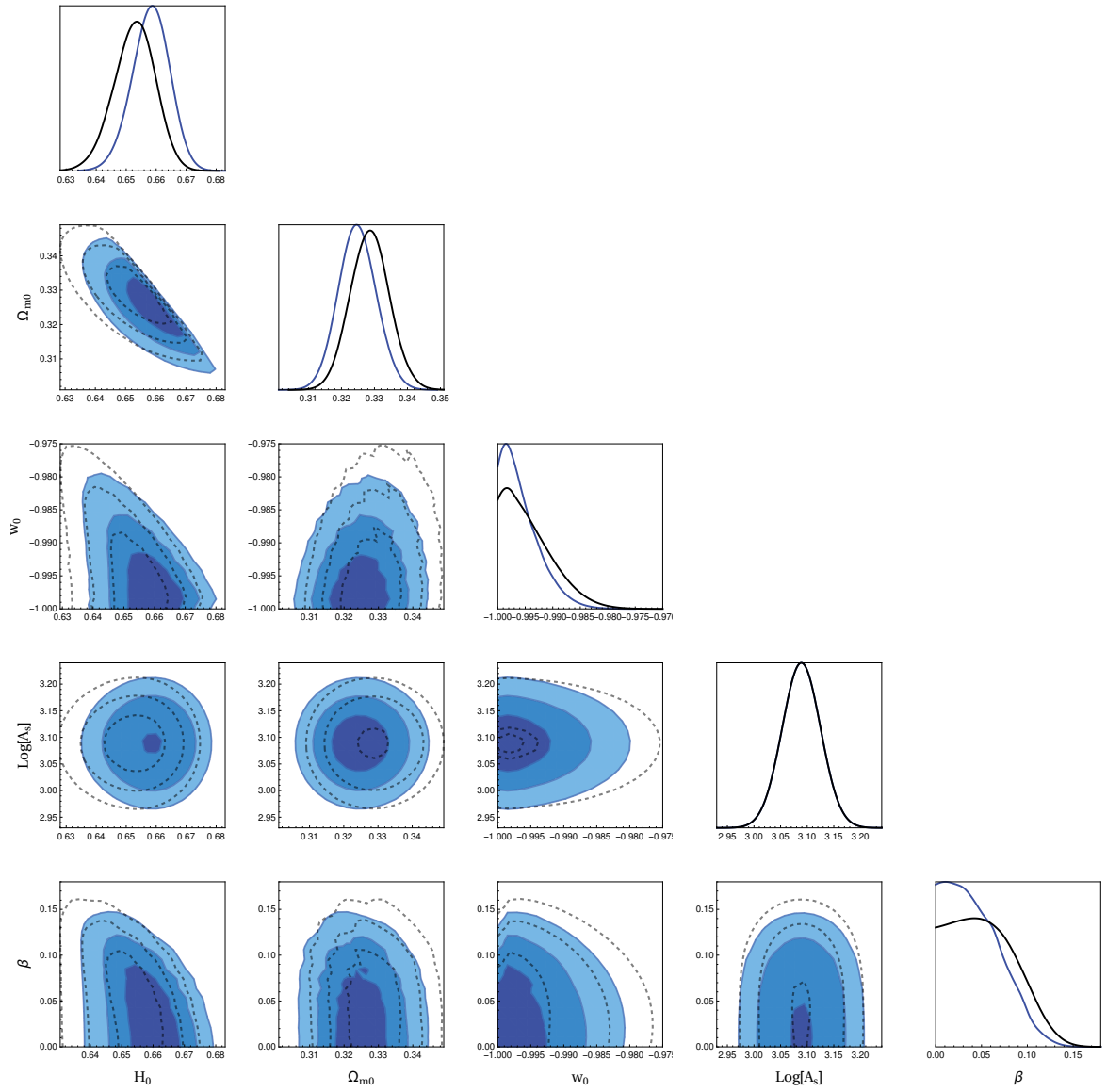


Figure 29 – Cosmological constraints, with full the likelihood, for the CQ10 + w_{de} model, where the contours are 68.3%, 95.4% and 99.7% confidence levels. One can note that the inclusion of the cosmic variance into the analysis (dashed black contours) shifts the usual constraint (blue contours). Higher values of Ω_{m0} , lower values of H_0 and non-null couplings β are preferred if the cosmic variance is included. Also, the cosmic variance extends the confidence levels for w_{de} . Note the high correlation between $\Omega_{m0} - H_0$.

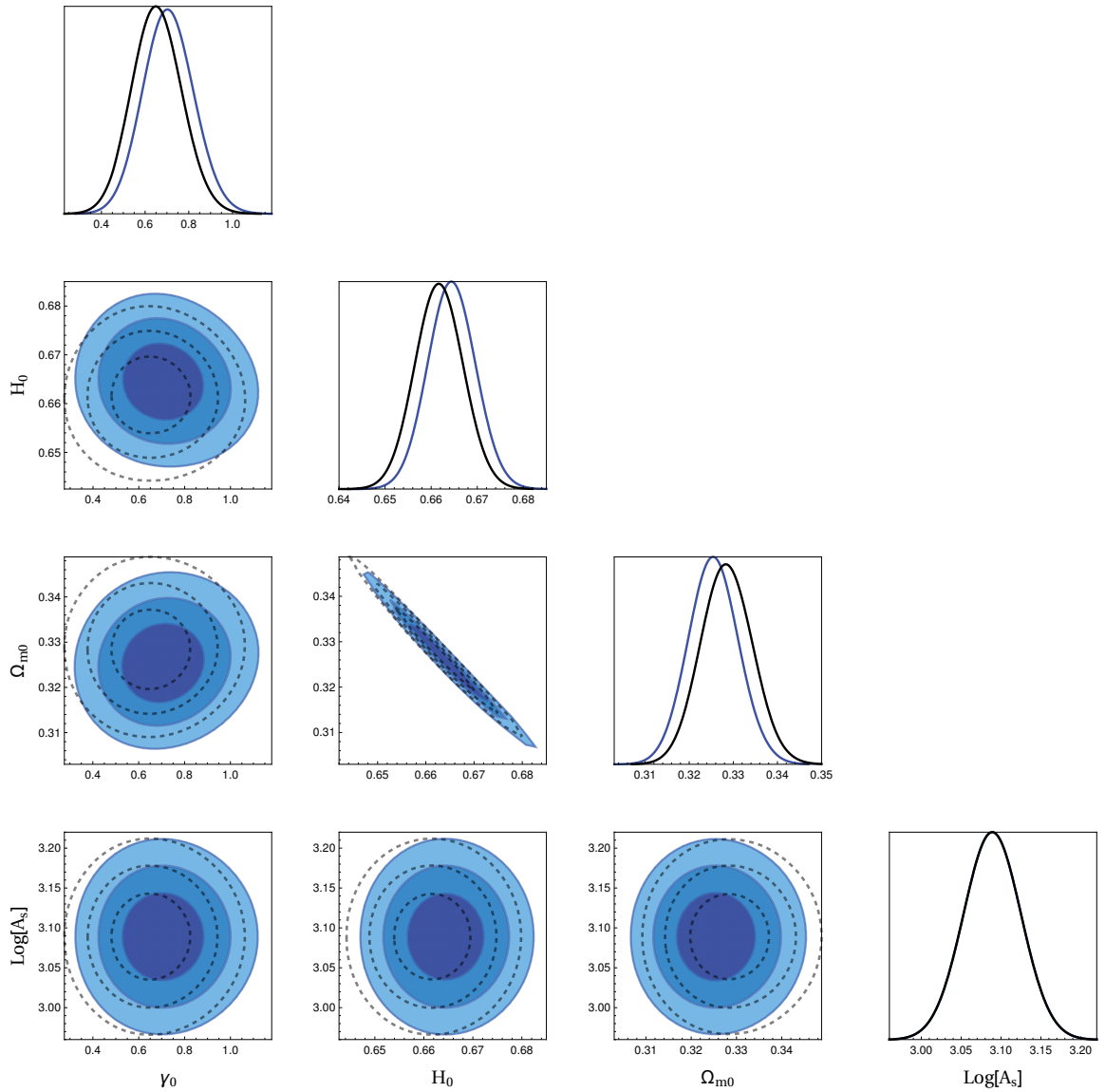


Figure 30 – Cosmological constraints, with the full likelihood, for the γ CDM extension, where the contours are 68.3%, 95.4% and 99.7% confidence levels. One can note that the inclusion of the cosmic variance into analysis (dashed black contours) shifts the usual constraint (blue contours). Higher values of Ω_{m0} and lower values of H_0 and γ are preferred if the cosmic variance is included. Note the high correlation between $\Omega_{m0} - H_0$.

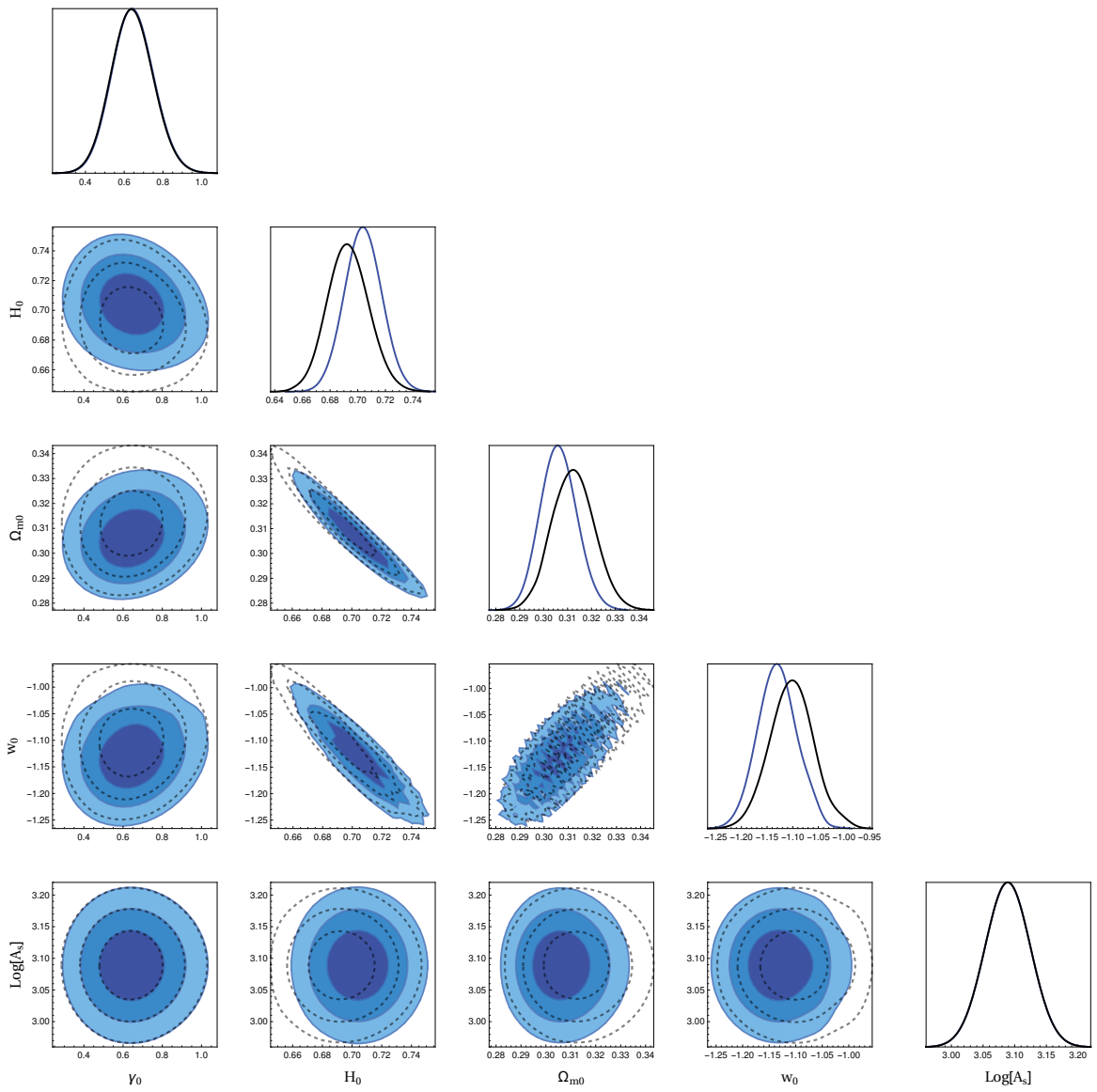


Figure 31 – Cosmological constraint, with the full likelihood, to the γw CDM extension, where the contours are 68.3%, 95.4% and 99.7% confidence levels. One can note that the inclusion of the cosmic variance into the analysis (dashed black contours) shifts the usual constraint (blue contours). Lower values of H_0 and higher values of Ω_{m0} and w_{de} are preferred if the cosmic variance is included. Here, the cosmic variance does not change markedly constraint on γ . Note the high correlation between $\Omega_{m0} - H_0$.

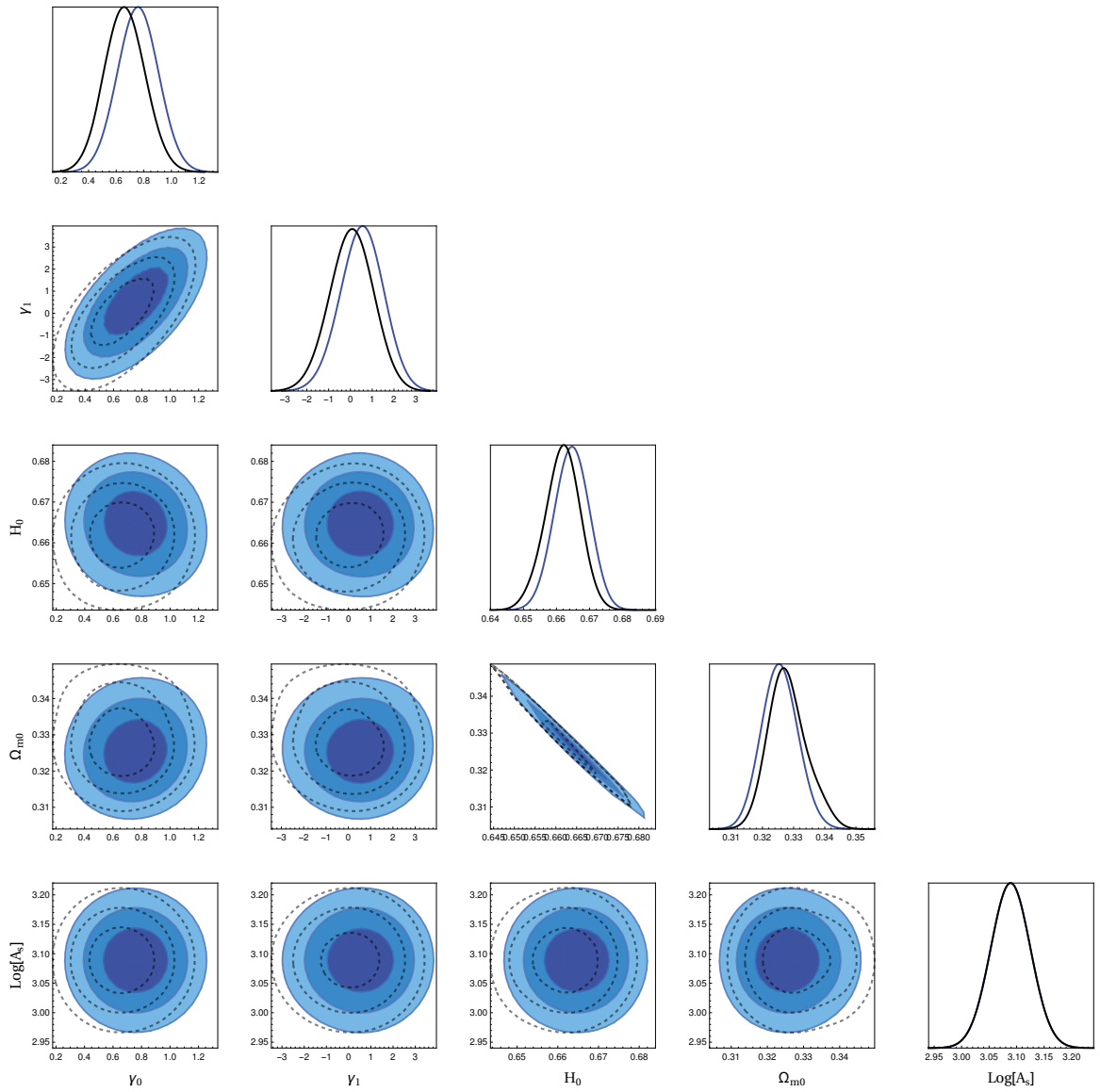


Figure 32 – Cosmological constraints, with the full likelihood, for the γ_a CDM extension, where the contours are 68.3%, 95.4% and 99.7% confidence levels. One can note that the inclusion of the cosmic variance into the analysis (dashed black contours) shifts the usual constraint (blue contours). Higher values of Ω_{m0} and lower values of H_0 , γ_0 and γ_1 are preferred if the cosmic variance is included. Note the high correlation between $\Omega_{m0} - H_0$.

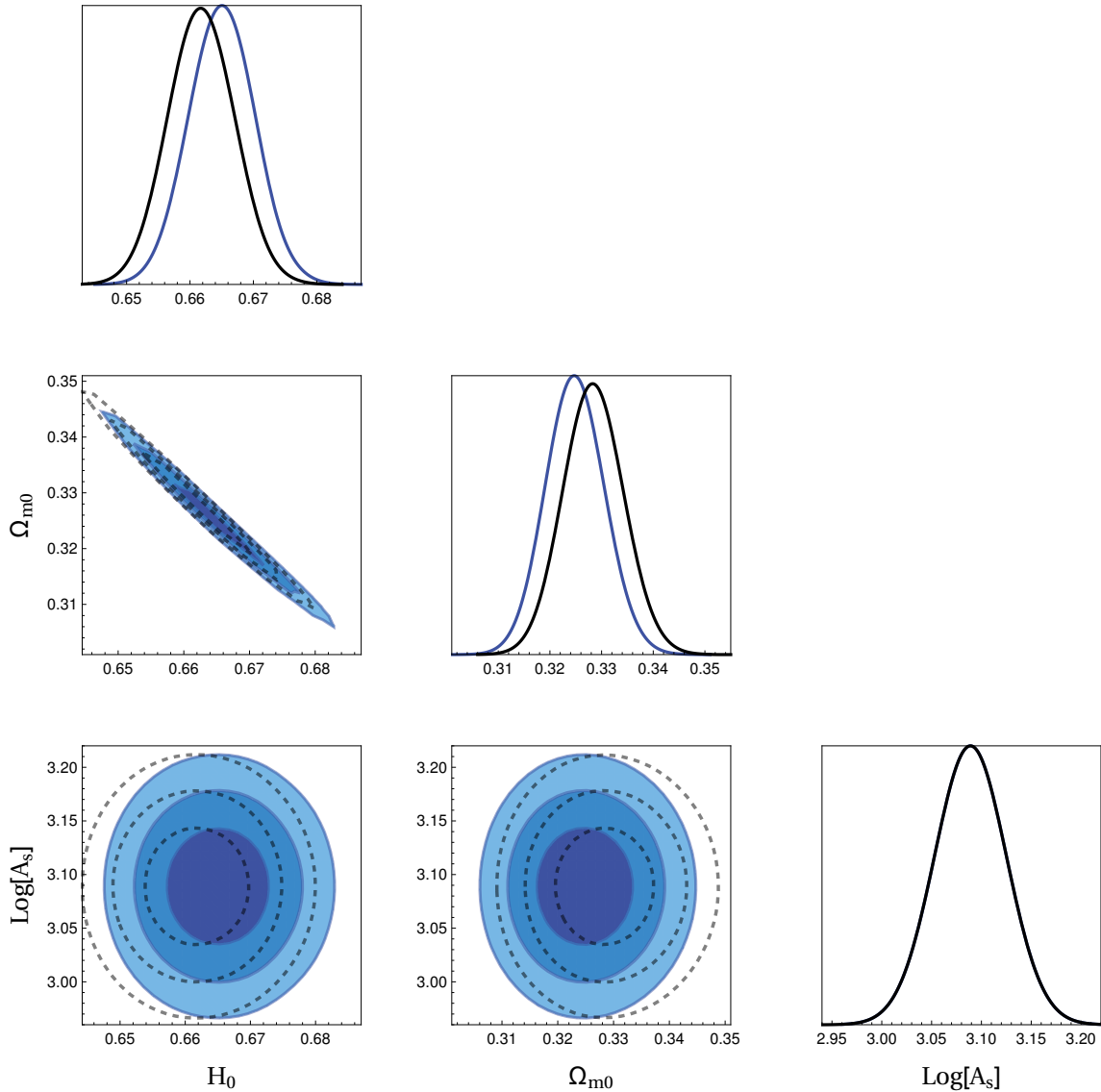


Figure 33 – Cosmological constraints, without RSD data, to the Λ CDM model, where the contours are 68.3%, 95.4% and 99.7% confidence levels. One can note that the inclusion of the cosmic variance into the analysis (dashed black contours) shifts the usual constraint (blue contours). Higher values of Ω_{m0} and lower values of H_0 are preferred if the cosmic variance is included. Note the high correlation between $\Omega_{m0} - H_0$.

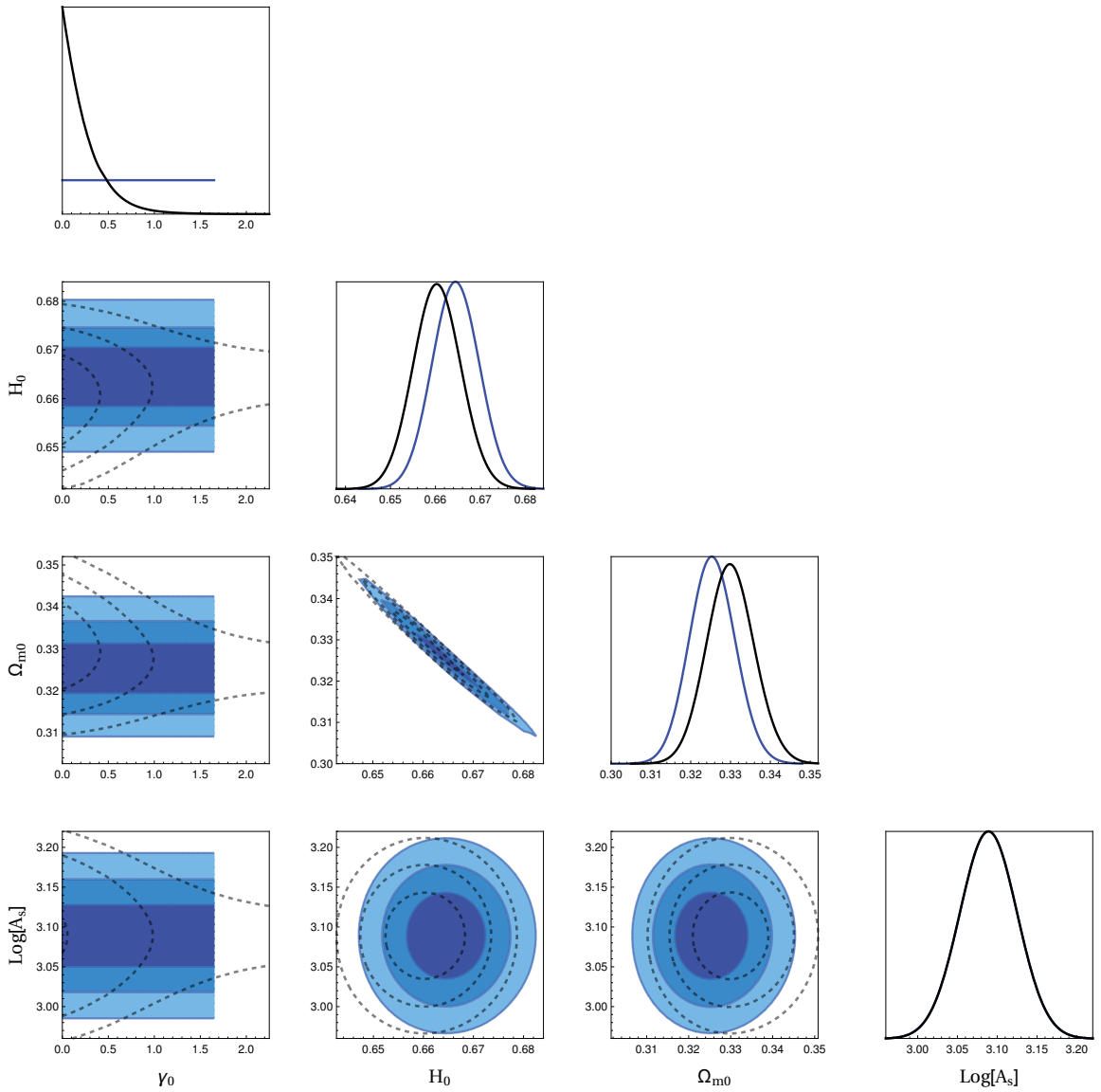


Figure 34 – Cosmological constraints, without RSD data, for the γ CDM extension, where the contours are 68.3%, 95.4% and 99.7% confidence levels. One can note that the inclusion of the cosmic variance into the analysis (dashed black contours) shifts the usual constraint (blue contours). Higher values of Ω_{m0} and lower values of H_0 are preferred if the cosmic variance is included. Also, the cosmic variance is able to constraint, weakly, the cosmic growth index γ . Note the high correlation between $\Omega_{m0} - H_0$.

6 Conclusions

We have investigated if a non-standard dark energy model is able to alleviate the current tension through the cosmic variance on local determinations of H_0 and its budget error. For that, we have used the CQ model and the γ CDM, γw CDM and γ_a CDM extensions. Also, we have studied the impact of cosmic variance in the analysis of the current cosmological data. For that, we have used Bayesian inference and data coming from CMB, BAO, SNe Ia, RSD and local H_0 . It is worth to stress, that, we have also performed cosmological constraints without RSD data in order to distinguish between effects of RSD data and the systematic error $\sigma_{\delta H}$ produced by the cosmic variance.

First, we have found that, for all the models and cases here considered, the absolute systematic error $\sigma_{\delta H}H_0$, induced by local structures and peculiar velocities, is always comparable to σ_{R16} and, in most cases, $\sigma_{\delta H}H_0 \approx \sigma_{R16}$. Consequently, given the definition of the total local error, $\sigma_{loc}^2 \equiv \sigma_{R16}^2 + \sigma_{\delta H}^2 H_0^2$, one obtains that the total local error is $\sigma_{loc} \approx 1.4\sigma_{R16}$. So, the effect of cosmic variance, in these cases, is non-negligible.

In addition, we have observed that there is an important decrease in the χ^2_{min} when the cosmic variance is considered. All cosmological models improve their concordance with the cosmological data if one takes into account the systematic error $\sigma_{\delta H}$. The lowest values of χ^2_{min} , for the full likelihood analysis, are achieved by a cosmology with a phantom dark energy $w_{de} < -1$ and a growth cosmic index $\gamma \approx 0.64$. Using AIC and BIC criteria, we have found that cosmological data show a strong and moderate evidence for γw CDM when the cosmic variance is neglected in $\chi^2_{H_0}$. Also, when the definition of $\chi^2_{H_0}$ includes the error $\sigma_{\delta H}$, the data provides a weak evidence for both Λ CDM and γw CDM through BIC and AIC, respectively.

Besides that, our results show that the tension between H_0^{Pl} and H_0^{R16} is partially cured by the cosmic variance. It means, there exists a residual tension. The better scenario is provided by a γw CDM cosmology where the tension is $T = 1.12\sigma$. This remnant tension could be produced by a simple statistical fluke or by systematics in the cosmic distance ladder used to measure H_0 locally or another unknowns systematics either in local and global measurements. On the other hand, we also have performed the analysis for Λ CDM and γ CDM without the RSD noting that the cosmic variance always prefers the lowest allowed value for γ . In this case γ CDM produces a higher $\sigma_{\delta H}H_0$ that leads to $\sigma_{loc} \approx 1.87\sigma_{R16}$. Even in this case, there exists a remnant tension, about $T = 1.52\sigma$, that cannot be ascribed to cosmic variance.

Therefore, we conclude that although the whole tension cannot be explained by cosmic variance, even if RSD data is discounted, the systematic error $\sigma_{\delta H}$ induced by

the cosmic variance is always comparable to σ_{R16} , and so, it should be considered in the results of local determinations of H_0 . This is also because considering the error budget $\sigma_{\delta H}$ improved the concordance of the model with the cosmological data. Finally, we report that the current cosmological data gives evidence for the γw CDM cosmology, where constraints suggest a phantom dark energy $w_{de} < -1$ and a growth index $\gamma \approx 0.64$. This cosmological scenario also seems to be able to explain the actual tension.

Bibliography

- 1 RIESS, A. G. et al. A 2.4% Determination of the Local Value of the Hubble Constant. *Astrophys. J.*, v. 826, n. 1, p. 56, 2016. Citado 9 vezes nas páginas [4](#), [5](#), [14](#), [29](#), [54](#), [57](#), [60](#), [61](#), and [77](#).
- 2 AGHANIM, N. et al. Planck intermediate results. XLVI. Reduction of large-scale systematic effects in HFI polarization maps and estimation of the reionization optical depth. *Astron. Astrophys.*, v. 596, p. A107, 2016. Citado 5 vezes nas páginas [4](#), [5](#), [14](#), [30](#), and [54](#).
- 3 HUBBLE, E. A relation between distance and radial velocity among extra-galactic nebulae. *Proc. Nat. Acad. Sci.*, v. 15, p. 168–173, 1929. Citado 4 vezes nas páginas [6](#), [14](#), [28](#), and [29](#).
- 4 KOWALSKI, M. et al. Improved Cosmological Constraints from New, Old and Combined Supernova Datasets. *Astrophys. J.*, v. 686, p. 749–778, 2008. Citado 2 vezes nas páginas [6](#) and [30](#).
- 5 FREEDMAN, W. L. Cosmology at Crossroads: Tension with the Hubble Constant. *Nat. Astron.*, v. 1, p. 0169, 2017. Citado 3 vezes nas páginas [7](#), [14](#), and [55](#).
- 6 ADE, P. A. R. et al. Planck 2015 results. XIII. Cosmological parameters. *Astron. Astrophys.*, v. 594, p. A13, 2016. Citado 10 vezes nas páginas [7](#), [11](#), [14](#), [29](#), [31](#), [33](#), [44](#), [49](#), [70](#), and [71](#).
- 7 EISENSTEIN, D. J. et al. Detection of the Baryon Acoustic Peak in the Large-Scale Correlation Function of SDSS Luminous Red Galaxies. *Astrophys. J.*, v. 633, p. 560–574, 2005. Citado 2 vezes nas páginas [7](#) and [72](#).
- 8 NESSERIS, S.; PANTAZIS, G.; PERIVOLAROPOULOS, L. Tension and constraints on modified gravity parametrizations of $G_{\text{eff}}(z)$ from growth rate and Planck data. 2017. Citado 5 vezes nas páginas [7](#), [11](#), [38](#), [75](#), and [76](#).
- 9 FREEDMAN, W. L.; MADORE, B. F. The Hubble Constant. *Ann. Rev. Astron. Astrophys.*, v. 48, p. 673–710, 2010. Citado 2 vezes nas páginas [14](#) and [29](#).
- 10 HUMPHREYS, E. M. L. et al. Toward a New Geometric Distance to the Active Galaxy NGC 4258. III. Final Results and the Hubble Constant. *Astrophys. J.*, v. 775, p. 13, 2013. Citado na página [14](#).
- 11 FERNÁNDEZ-ARENAS, D. et al. An independent determination of the local Hubble constant. 2017. Citado na página [14](#).
- 12 WU, P.-X.; LI, Z.-X.; YU, H.-W. Determining H_0 using a model-independent method. *Front. Phys.(Beijing)*, v. 12, n. 1, p. 129801, 2017. Citado na página [14](#).
- 13 WANG, D.; MENG, X.-H. Model-independent determination on H_0 using the latest cosmic chronometer data. *Sci. China Phys. Mech. Astron.*, v. 60, n. 11, p. 110411, 2017. Citado na página [14](#).

- 14 BONVIN, V. et al. H0LiCOW - V. New COSMOGRAIL time delays of HE 0435-1223: H_0 to 3.8 per cent precision from strong lensing in a flat Λ CDM model. *Mon. Not. Roy. Astron. Soc.*, v. 465, n. 4, p. 4914–4930, 2017. Citado 2 vezes nas páginas [14](#) and [29](#).
- 15 ABBOTT, T. M. C. et al. Dark Energy Survey Year 1 Results: A Precise H_0 Measurement from DES Y1, BAO, and D/H Data. 2017. Citado 2 vezes nas páginas [14](#) and [29](#).
- 16 ABBOTT, B. P. et al. A gravitational-wave standard siren measurement of the Hubble constant. *Nature*, v. 551, n. 7678, p. 85–88, 2017. Citado 2 vezes nas páginas [14](#) and [30](#).
- 17 VERDE, L.; PROTOPAPAS, P.; JIMENEZ, R. Planck and the local Universe: Quantifying the tension. *Phys. Dark Univ.*, v. 2, p. 166–175, 2013. Citado 2 vezes nas páginas [14](#) and [57](#).
- 18 VALENTINO, E. D.; MELCHIORRI, A.; MENA, O. Can interacting dark energy solve the H_0 tension? *Phys. Rev.*, D96, n. 4, p. 043503, 2017. Citado 6 vezes nas páginas [14](#), [15](#), [45](#), [55](#), [81](#), and [85](#).
- 19 ODDERSKOV, I.; BALDI, M.; AMENDOLA, L. The effect of interacting dark energy on local measurements of the Hubble constant. *JCAP*, v. 1605, n. 05, p. 035, 2016. Citado 6 vezes nas páginas [14](#), [15](#), [45](#), [55](#), [80](#), and [81](#).
- 20 VALENTINO, E. D.; MELCHIORRI, A.; SILK, J. Reconciling Planck with the local value of H_0 in extended parameter space. *Phys. Lett.*, B761, p. 242–246, 2016. Citado 3 vezes nas páginas [14](#), [55](#), and [81](#).
- 21 VALENTINO, E. D.; LINDER, E. V.; MELCHIORRI, A. A Vacuum Phase Transition Solves H_0 Tension. 2017. Citado 4 vezes nas páginas [14](#), [55](#), [81](#), and [85](#).
- 22 ZHAO, M.-M. et al. Search for sterile neutrinos in holographic dark energy cosmology: Reconciling Planck observation with the local measurement of the Hubble constant. *Phys. Rev.*, D96, n. 4, p. 043520, 2017. Citado 4 vezes nas páginas [14](#), [55](#), [81](#), and [85](#).
- 23 PUTTEN, M. H. P. M. van. Accelerated cosmological expansion without tension in the Hubble parameter. In: . [s.n.], 2017. Disponível em: <<https://inspirehep.net/record/1609204/files/arXiv:1707.02588.pdf>>. Citado 4 vezes nas páginas [14](#), [55](#), [81](#), and [85](#).
- 24 SOLÀ, J.; GÓMEZ-VALENT, A.; PÉREZ, J. de C. The H_0 tension in light of vacuum dynamics in the Universe. *Phys. Lett.*, B774, p. 317–324, 2017. Citado 4 vezes nas páginas [14](#), [55](#), [81](#), and [85](#).
- 25 HUANG, Q.-G.; WANG, K. How the dark energy can reconcile Planck with local determination of the Hubble constant. *Eur. Phys. J.*, C76, n. 9, p. 506, 2016. Citado 4 vezes nas páginas [14](#), [55](#), [81](#), and [85](#).
- 26 EFSTATHIOU, G. H_0 Revisited. *Mon. Not. Roy. Astron. Soc.*, v. 440, n. 2, p. 1138–1152, 2014. Citado 2 vezes nas páginas [14](#) and [55](#).
- 27 ODDERSKOV, I.; HANNESTAD, S.; HAUGBØLLE, T. On the local variation of the Hubble constant. *JCAP*, v. 1410, n. 10, p. 028, 2014. Citado 2 vezes nas páginas [14](#) and [55](#).

- 28 DHAWAN, S.; JHA, S. W.; LEIBUNDGUT, B. Measuring the Hubble constant with Type Ia supernovae as near-infrared standard candles. 2017. Citado 2 vezes nas páginas [14](#) and [55](#).
- 29 ZHANG, B. R. et al. A blinded determination of H_0 from low-redshift Type Ia supernovae, calibrated by Cepheid variables. *Mon. Not. Roy. Astron. Soc.*, v. 471, p. 2254, 2017. Citado 2 vezes nas páginas [14](#) and [55](#).
- 30 WU, H.-Y.; HUTERER, D. Sample variance in the local measurements of the Hubble constant. *Mon. Not. Roy. Astron. Soc.*, v. 471, p. 4946, 2017. Citado 2 vezes nas páginas [14](#) and [55](#).
- 31 CARDONA, W.; KUNZ, M.; PETTORINO, V. Determining H_0 with Bayesian hyper-parameters. *JCAP*, v. 1703, n. 03, p. 056, 2017. Citado 2 vezes nas páginas [14](#) and [55](#).
- 32 ODDERSKOV, I.; HANNESTAD, S.; BRANDBYGE, J. The variance of the locally measured Hubble parameter explained with different estimators. *JCAP*, v. 1703, n. 03, p. 022, 2017. Citado 3 vezes nas páginas [14](#), [55](#), and [60](#).
- 33 MARRA, V. et al. Cosmic variance and the measurement of the local Hubble parameter. *Phys. Rev. Lett.*, v. 110, n. 24, p. 241305, 2013. Citado 4 vezes nas páginas [15](#), [55](#), [56](#), and [61](#).
- 34 WOJTAK, R. et al. Cosmic variance of the local Hubble flow in large-scale cosmological simulations. *Mon. Not. Roy. Astron. Soc.*, v. 438, n. 2, p. 1805–1812, 2014. Citado 3 vezes nas páginas [15](#), [55](#), and [56](#).
- 35 JOUDAKI, S. et al. KiDS-450: Testing extensions to the standard cosmological model. *Mon. Not. Roy. Astron. Soc.*, v. 471, n. 2, p. 1259–1279, 2017. Citado 3 vezes nas páginas [15](#), [56](#), and [57](#).
- 36 Akaike, H. A New Look at the Statistical Model Identification. *IEEE Transactions on Automatic Control*, v. 19, p. 716–723, 1974. Citado 2 vezes nas páginas [15](#) and [69](#).
- 37 SCHWARZ, G. Estimating the Dimension of a Model. *Annals Statist.*, v. 6, p. 461–464, 1978. Citado 2 vezes nas páginas [15](#) and [69](#).
- 38 CAMARENA, D.; MARRA, V. In preparation... 2018. Citado 2 vezes nas páginas [16](#) and [79](#).
- 39 BATTERMAN, R. *The Oxford Handbook of Philosophy of Physics*. OUP USA, 2013. (Oxford Handbooks in Philosophy). ISBN 9780195392043. Disponível em: <<https://books.google.com.pe/books?id=HX1iPDdj61EC>>. Citado 2 vezes nas páginas [17](#) and [26](#).
- 40 ARCHIDIACONO, M. et al. Neutrino properties from cosmology. In: *Prospects in Neutrino Physics (NuPhys2016) London, London, United Kingdom, December 12-14, 2016*. [s.n.], 2017. Disponível em: <<https://inspirehep.net/record/1597380/files/arXiv:1705.00496.pdf>>. Citado na página [17](#).

- 41 WEINBERG, S. *Gravitation and cosmology: principles and applications of the general theory of relativity*. Wiley, 1972. ISBN 9780471925675. Disponível em: <<https://books.google.com.br/books?id=XLbvAAAAMAAJ>>. Citado 5 vezes nas páginas 17, 22, 25, 112, and 113.
- 42 WHITTAKER, E. *A History of the Theories of Aether and Electricity from the Age of Descartes to the Close of the Nineteenth Century*. Longmans, Green and Company, 1910. (Dublin University Press series). Disponível em: <<https://books.google.com.pe/books?id=CGJDAAAAIAAJ>>. Citado na página 17.
- 43 NEWTON, I. *Philosophiae naturalis principia mathematica*. J. Societatis Regiae ac Typis J. Streater, 1687. Disponível em: <<https://books.google.com.br/books?id=-dVKAQAAIAAJ>>. Citado na página 17.
- 44 MICHELSON, A. A.; MORLEY, E. W. On the relative motion of the earth and the luminiferous ether. *American Journal of Science*, v. 34, p. 333–345, 1887. Citado 2 vezes nas páginas 17 and 18.
- 45 Lorentz, H. A. Simplified Theory of Electrical and Optical Phenomena in Moving Systems. *Koninklijke Nederlandse Akademie van Wetenschappen Proceedings Series B Physical Sciences*, v. 1, p. 427–442, 1898. Citado na página 18.
- 46 EINSTEIN, A. Zur elektrodynamik bewegter körper. *Annalen der Physik*, WILEY-VCH Verlag, v. 322, n. 10, p. 891–921, 1905. ISSN 1521-3889. Disponível em: <<http://dx.doi.org/10.1002/andp.19053221004>>. Citado na página 18.
- 47 EINSTEIN, A. Die grundlage der allgemeinen relativitätstheorie. *Annalen der Physik*, WILEY-VCH Verlag, v. 354, n. 7, p. 769–822, 1916. ISSN 1521-3889. Disponível em: <<http://dx.doi.org/10.1002/andp.19163540702>>. Citado na página 18.
- 48 CHOUDHURY, T. R.; PADMANABHAN, T. Cosmological parameters from supernova observations: A Critical comparison of three data sets. *Astron. Astrophys.*, v. 429, p. 807, 2005. Citado na página 18.
- 49 NESSERIS, S.; PERIVOLAROPOULOS, L. A Comparison of cosmological models using recent supernova data. *Phys. Rev.*, D70, p. 043531, 2004. Citado na página 18.
- 50 WALD, R. *General Relativity*. University of Chicago Press, 1984. ISBN 9780226870328. Disponível em: <<https://books.google.com.br/books?id=ibSdQgAACAAJ>>. Citado 2 vezes nas páginas 19 and 22.
- 51 CARROLL, S. M. *Spacetime and geometry: An introduction to general relativity*. [s.n.], 2004. ISBN 0805387323, 9780805387322. Disponível em: <<http://www.slac.stanford.edu/spires/find/books/www?cl=QC6:C37:2004>>. Citado 4 vezes nas páginas 20, 21, 22, and 23.
- 52 Eötvös, R. V.; Pekár, D.; Fekete, E. Beiträge zum Gesetze der Proportionalität von Trägheit und Gravität. *Annalen der Physik*, v. 373, p. 11–66, 1922. Citado na página 22.
- 53 WILL, C. M. The Confrontation between General Relativity and Experiment. *Living Rev. Rel.*, v. 17, p. 4, 2014. Citado na página 22.
- 54 Baßler, S. et al. Improved Test of the Equivalence Principle for Gravitational Self-Energy. *Physical Review Letters*, v. 83, p. 3585–3588, nov. 1999. Citado na página 22.

- 55 SCHLAMMINGER, S. et al. Test of the equivalence principle using a rotating torsion balance. *Phys. Rev. Lett.*, v. 100, p. 041101, 2008. Citado na página [23](#).
- 56 SOTIRIOU, T. P.; FARAONI, V. f(R) Theories Of Gravity. *Rev. Mod. Phys.*, v. 82, p. 451–497, 2010. Citado 2 vezes nas páginas [23](#) and [45](#).
- 57 OLMO, G. J. Palatini Approach to Modified Gravity: f(R) Theories and Beyond. *Int. J. Mod. Phys.*, D20, p. 413–462, 2011. Citado na página [23](#).
- 58 Einstein, A. Kosmologische Betrachtungen zur allgemeinen Relativitätstheorie. *Sitzungsberichte der Königlich Preußischen Akademie der Wissenschaften (Berlin)*, Seite 142-152., 1917. Citado 2 vezes nas páginas [24](#) and [32](#).
- 59 EDDINGTON, A. S. On the Instability of Einstein's Spherical World. *Mon. Not. Roy. Astron. Soc.*, v. 90, p. 668–678, 1930. Citado na página [24](#).
- 60 SOLA, J. Cosmological constant and vacuum energy: old and new ideas. *J. Phys. Conf. Ser.*, v. 453, p. 012015, 2013. Citado na página [24](#).
- 61 PEEBLES, P. J. E.; RATRA, B. The Cosmological constant and dark energy. *Rev. Mod. Phys.*, v. 75, p. 559–606, 2003. Citado na página [24](#).
- 62 BEISBART, C. Can We Justifiably Assume the Cosmological Principle in Order to Break Model Underdetermination in Cosmology? *J. Gen. Phil. Sci.*, v. 40, n. 2, p. 175–205, 2009. Citado na página [25](#).
- 63 GONÇALVES, R. S. et al. Cosmic homogeneity: a spectroscopic and model-independent measurement. 2017. Citado na página [25](#).
- 64 ABBOTT, B. P. et al. Binary Black Hole Mergers in the first Advanced LIGO Observing Run. *Phys. Rev.*, X6, n. 4, p. 041015, 2016. Citado na página [28](#).
- 65 ABBOTT, B. P. et al. GW151226: Observation of Gravitational Waves from a 22-Solar-Mass Binary Black Hole Coalescence. *Phys. Rev. Lett.*, v. 116, n. 24, p. 241103, 2016. Citado na página [28](#).
- 66 ABBOTT, B. P. et al. GW170104: Observation of a 50-Solar-Mass Binary Black Hole Coalescence at Redshift 0.2. *Phys. Rev. Lett.*, v. 118, n. 22, p. 221101, 2017. Citado na página [28](#).
- 67 ABBOTT, B. P. et al. GW170814: A Three-Detector Observation of Gravitational Waves from a Binary Black Hole Coalescence. *Phys. Rev. Lett.*, v. 119, n. 14, p. 141101, 2017. Citado na página [28](#).
- 68 ABBOTT, B. et al. GW170817: Observation of Gravitational Waves from a Binary Neutron Star Inspiral. *Phys. Rev. Lett.*, v. 119, n. 16, p. 161101, 2017. Citado na página [28](#).
- 69 DODELSON, S. Book. *Modern Cosmology*. [S.l.]: Academic Press, Elsevier Science, 2003. Citado 5 vezes nas páginas [28](#), [38](#), [41](#), [43](#), and [70](#).
- 70 Lemaître, G. Un Univers homogène de masse constante et de rayon croissant rendant compte de la vitesse radiale des nébuleuses extra-galactiques. *Annales de la Société Scientifique de Bruxelles*, v. 47, p. 49–59, 1927. Citado na página [28](#).

- 71 SLIPHER, V. M. Nebulae. *Proc. Am. Phil. Soc.*, v. 56, p. 403–409, 1917. Citado na página 28.
- 72 Lundmark, K. The Motions and the Distances of Spiral Nebulæ. *Mon. Not. Roy. Astron. Soc.*, v. 85, p. 865, jun. 1925. Citado na página 28.
- 73 WAY, M. J.; NUSSBAUMER, H. Lemaître's Hubble relationship. *Phys. Today*, v. 64N8, p. 8, 2011. Citado na página 28.
- 74 BERGH, S. van den. The Curious Case of Lemaitre's Equation No. 24. *J. Roy. Astron. Soc. Canada*, v. 105, p. 151, 2011. Citado na página 28.
- 75 PATUREL, G.; TEERIKORPI, P.; BARYSHEV, Y. Hubble Law: Measure and Interpretation. *Found. Phys.*, v. 47, n. 9, p. 1208–1228, 2017. Citado na página 28.
- 76 WEINBERG, S. *Cosmology*. OUP Oxford, 2008. (Cosmology). ISBN 9780191523601. Disponível em: <<https://books.google.com.br/books?id=nqQZdg020fsC>>. Citado 2 vezes nas páginas 29 and 43.
- 77 MOHAPATRA, R. N. et al. Theory of neutrinos: A White paper. *Rept. Prog. Phys.*, v. 70, p. 1757–1867, 2007. Citado na página 31.
- 78 DOLGOV, A. D. Neutrinos in cosmology. *Phys. Rept.*, v. 370, p. 333–535, 2002. Citado na página 31.
- 79 ABAZAJIAN, K.; FULLER, G. M.; PATEL, M. Sterile neutrino hot, warm, and cold dark matter. *Phys. Rev.*, D64, p. 023501, 2001. Citado na página 32.
- 80 BERTONE, G.; HOOPER, D.; SILK, J. Particle dark matter: Evidence, candidates and constraints. *Phys. Rept.*, v. 405, p. 279–390, 2005. Citado na página 32.
- 81 PROFUMO, S. Astrophysical Probes of Dark Matter. In: *Proceedings, Theoretical Advanced Study Institute in Elementary Particle Physics: Searching for New Physics at Small and Large Scales (TASI 2012): Boulder, Colorado, June 4-29, 2012*. [s.n.], 2013. p. 143–189. Disponível em: <<https://inspirehep.net/record/1209480/files/arXiv:1301.0952.pdf>>. Citado na página 32.
- 82 BAUMANN, D. Inflation. In: *Physics of the large and the small, TASI 09, proceedings of the Theoretical Advanced Study Institute in Elementary Particle Physics, Boulder, Colorado, USA, 1-26 June 2009*. [s.n.], 2011. p. 523–686. Disponível em: <<https://inspirehep.net/record/827549/files/arXiv:0907.5424.pdf>>. Citado na página 33.
- 83 BETOULE, M. et al. Improved cosmological constraints from a joint analysis of the SDSS-II and SNLS supernova samples. *Astron. Astrophys.*, v. 568, p. A22, 2014. Citado 2 vezes nas páginas 33 and 74.
- 84 Amendola, L.; Tsujikawa, S. *Dark Energy: Theory and Observations*. [S.l.]: Cambridge University Press, 2010. Citado 4 vezes nas páginas 36, 37, 43, and 45.
- 85 Lifshitz, E. M. On the gravitational stability of the expanding universe. *Zhurnal Eksperimentalnoi i Teoreticheskoi Fiziki*, v. 16, p. 587–602, 1946. Citado na página 36.
- 86 MUKHANOV, V. *Physical Foundations of Cosmology*. Cambridge University Press, 2005. ISBN 9780521563987. Disponível em: <<https://books.google.com.pe/books?id=1TXO7GmwZFgC>>. Citado na página 36.

- 87 BARDEEN, J. M. Gauge Invariant Cosmological Perturbations. *Phys. Rev.*, D22, p. 1882–1905, 1980. Citado na página 37.
- 88 LAUREIJS, R. et al. Euclid Definition Study Report. 2011. Citado 2 vezes nas páginas 38 and 54.
- 89 PEEBLES, P. J. E. *The large-scale structure of the universe*. [S.l.]: Princeton university press, 1980. Citado na página 41.
- 90 WEINBERG, S. The cosmological constant problem. *Rev. Mod. Phys.*, American Physical Society, v. 61, p. 1–23, Jan 1989. Disponível em: <<https://link.aps.org/doi/10.1103/RevModPhys.61.1>>. Citado na página 43.
- 91 ZLATEV, I.; WANG, L.-M.; STEINHARDT, P. J. Quintessence, cosmic coincidence, and the cosmological constant. *Phys. Rev. Lett.*, v. 82, p. 896–899, 1999. Citado na página 43.
- 92 POPOLI, A. D.; DELLIQU, M. L. Small scale problems of the Λ CDM model: a short review. *Galaxies*, v. 5, n. 1, p. 17, 2017. Citado na página 43.
- 93 RYAN, S. G. et al. Primordial Lithium and Big Bang Nucleosynthesis. *Astrophys. J.*, v. 530, p. L57–L60, 2000. Citado na página 43.
- 94 SCHWARZ, D. J. et al. CMB Anomalies after Planck. *Class. Quant. Grav.*, v. 33, n. 18, p. 184001, 2016. Citado na página 43.
- 95 VELTEN, H. E. S.; MARTTENS, R. F. vom; ZIMDAHL, W. Aspects of the cosmological “coincidence problem”. *Eur. Phys. J.*, C74, n. 11, p. 3160, 2014. Citado na página 44.
- 96 BIANCHI, E.; ROVELLI, C. Why all these prejudices against a constant? 2010. Citado na página 44.
- 97 COPELAND, E. J.; SAMI, M.; TSUJIKAWA, S. Dynamics of dark energy. *Int. J. Mod. Phys.*, D15, p. 1753–1936, 2006. Citado na página 45.
- 98 TSUJIKAWA, S. Dark energy: investigation and modeling. v. 370, n. 2010, p. 331–402, 2011. Citado na página 45.
- 99 CAPOZZIELLO, S.; LAURENTIS, M. D. Extended Theories of Gravity. *Phys. Rept.*, v. 509, p. 167–321, 2011. Citado na página 45.
- 100 BAMBA, K. et al. Dark energy cosmology: the equivalent description via different theoretical models and cosmography tests. *Astrophys. Space Sci.*, v. 342, p. 155–228, 2012. Citado na página 45.
- 101 CALDWELL, R. R.; DAVE, R.; STEINHARDT, P. J. Cosmological imprint of an energy component with general equation of state. *Phys. Rev. Lett.*, v. 80, p. 1582–1585, 1998. Citado na página 45.
- 102 TSUJIKAWA, S. Quintessence: A Review. *Class. Quant. Grav.*, v. 30, p. 214003, 2013. Citado na página 45.
- 103 AMENDOLA, L. Coupled quintessence. *Phys. Rev.*, D62, p. 043511, 2000. Citado 4 vezes nas páginas 45, 46, 48, and 49.

- 104 AMENDOLA, L.; QUERCELLINI, C. Tracking and coupled dark energy as seen by WMAP. *Phys. Rev.*, D68, p. 023514, 2003. Citado 2 vezes nas páginas [45](#) and [46](#).
- 105 PETTORINO, V. et al. Constraints on coupled dark energy using CMB data from WMAP and SPT. *Phys. Rev.*, D86, p. 103507, 2012. Citado 3 vezes nas páginas [45](#), [46](#), and [80](#).
- 106 BALDI, M. et al. Hydrodynamical N-body simulations of coupled dark energy cosmologies. *Mon. Not. Roy. Astron. Soc.*, v. 403, p. 1684–1702, 2010. Citado 4 vezes nas páginas [45](#), [46](#), [50](#), and [80](#).
- 107 BALDI, M. Time dependent couplings in the dark sector: from background evolution to nonlinear structure formation. *Mon. Not. Roy. Astron. Soc.*, v. 411, p. 1077, 2011. Citado 3 vezes nas páginas [45](#), [48](#), and [49](#).
- 108 PETTORINO, V.; BACCIGALUPI, C. Coupled and Extended Quintessence: theoretical differences and structure formation. *Phys. Rev.*, D77, p. 103003, 2008. Citado 2 vezes nas páginas [45](#) and [49](#).
- 109 PETTORINO, V. Testing modified gravity with Planck: the case of coupled dark energy. *Phys. Rev.*, D88, p. 063519, 2013. Citado na página [45](#).
- 110 CASAS, S. et al. Fitting and forecasting coupled dark energy in the non-linear regime. *JCAP*, v. 1601, n. 01, p. 045, 2016. Citado na página [45](#).
- 111 ELAHI, P. J. et al. Hidden from view: Coupled Dark Sector Physics and Small Scales. *Mon. Not. Roy. Astron. Soc.*, v. 452, n. 2, p. 1341–1352, 2015. Citado na página [45](#).
- 112 MACCIO, A. V. et al. N-body simulations for coupled dark energy: Halo mass function and density profiles. *Phys. Rev.*, D69, p. 123516, 2004. Citado na página [45](#).
- 113 AMENDOLA, L. et al. Testing coupled dark energy with next-generation large-scale observations. *Phys. Rev.*, D85, p. 103008, 2012. Citado na página [45](#).
- 114 HONOREZ, L. L. Coupled quintessence through dark energy density. *J. Phys. Conf. Ser.*, v. 375, p. 032007, 2012. Citado na página [45](#).
- 115 XIA, J.-Q. Constraint on coupled dark energy models from observations. *Phys. Rev.*, D80, p. 103514, 2009. Citado na página [45](#).
- 116 KODAMA, H.; SASAKI, M. Cosmological perturbation theory. *Progress of Theoretical Physics Supplement*, v. 78, p. 1–166, 1984. Disponível em: <[+http://dx.doi.org/10.1143/PTPS.78.1](http://dx.doi.org/10.1143/PTPS.78.1)>. Citado na página [46](#).
- 117 AMENDOLA, L.; TOCCHINI-VALENTINI, D. Stationary dark energy: The Present universe as a global attractor. *Phys. Rev.*, D64, p. 043509, 2001. Citado na página [46](#).
- 118 XIA, J.-Q. New Limits on Coupled Dark Energy from Planck. *JCAP*, v. 1311, p. 022, 2013. Citado 2 vezes nas páginas [46](#) and [63](#).
- 119 COPELAND, E. J.; LIDDLE, A. R.; WANDS, D. Exponential potentials and cosmological scaling solutions. *Phys. Rev.*, D57, p. 4686–4690, 1998. Citado 2 vezes nas páginas [48](#) and [49](#).

- 120 TOCCHINI-VALENTINI, D.; AMENDOLA, L. Stationary dark energy with a baryon dominated era: Solving the coincidence problem with a linear coupling. *Phys. Rev.*, D65, p. 063508, 2002. Citado 2 vezes nas páginas [48](#) and [49](#).
- 121 AMENDOLA, L. Linear and non-linear perturbations in dark energy models. *Phys. Rev.*, D69, p. 103524, 2004. Citado na página [49](#).
- 122 LINDER, E. V.; CAHN, R. N. Parameterized Beyond-Einstein Growth. *Astropart. Phys.*, v. 28, p. 481–488, 2007. Citado na página [51](#).
- 123 DVALI, G. R.; GABADADZE, G.; PORRATI, M. 4-D gravity on a brane in 5-D Minkowski space. *Phys. Lett.*, B485, p. 208–214, 2000. Citado na página [51](#).
- 124 DEFFAYET, C.; DVALI, G. R.; GABADADZE, G. Accelerated universe from gravity leaking to extra dimensions. *Phys. Rev.*, D65, p. 044023, 2002. Citado na página [51](#).
- 125 WANG, L.-M.; STEINHARDT, P. J. Cluster abundance constraints on quintessence models. *Astrophys. J.*, v. 508, p. 483–490, 1998. Citado na página [52](#).
- 126 POLARSKI, D.; STAROBINSKY, A. A.; GIACOMINI, H. When is the growth index constant? *JCAP*, v. 1612, n. 12, p. 037, 2016. Citado na página [52](#).
- 127 STEIGERWALD, H.; BEL, J.; MARINONI, C. Probing non-standard gravity with the growth index: a background independent analysis. *JCAP*, v. 1405, p. 042, 2014. Citado na página [53](#).
- 128 WU, P.; YU, H. W.; FU, X. A Parametrization for the growth index of linear matter perturbations. *JCAP*, v. 0906, p. 019, 2009. Citado na página [53](#).
- 129 PORTO, C. D.; AMENDOLA, L.; BRANCHINI, E. Growth factor and galaxy bias from future redshift surveys: a study on parametrizations. *Mon. Not. Roy. Astron. Soc.*, v. 419, p. 985, 2012. Citado na página [53](#).
- 130 BELLOSO, A. B.; GARCIA-BELLIDO, J.; SAPONE, D. A parametrization of the growth index of matter perturbations in various Dark Energy models and observational prospects using a Euclid-like survey. *JCAP*, v. 1110, p. 010, 2011. Citado na página [53](#).
- 131 BENITEZ, N. et al. J-PAS: The Javalambre-Physics of the Accelerated Universe Astrophysical Survey. 2014. Citado na página [54](#).
- 132 TROXEL, M. A. et al. Dark Energy Survey Year 1 Results: Cosmological Constraints from Cosmic Shear. 2017. Citado na página [54](#).
- 133 EVSLIN, J.; SEN, A. A.; RUCHIKA. The Price of Shifting the Hubble Constant. 2017. Citado 2 vezes nas páginas [56](#) and [85](#).
- 134 ABBOTT, T. M. C. et al. Dark Energy Survey Year 1 Results: Cosmological Constraints from Galaxy Clustering and Weak Lensing. 2017. Citado 2 vezes nas páginas [56](#) and [64](#).
- 135 HENNING, J. W. et al. Measurements of the Temperature and E-Mode Polarization of the CMB from 500 Square Degrees of SPTpol Data. *Astrophys. J.*, v. 852, n. 2, p. 97, 2018. Citado na página [56](#).

- 136 LIN, W.; ISHAK, M. Cosmological discordances: A new measure, marginalization effects, and application to geometry versus growth current data sets. *Phys. Rev.*, D96, n. 2, p. 023532, 2017. Citado na página 57.
- 137 SHI, X.; WIDROW, L. M.; DURSI, L. J. Measuring hubble's constant in our inhomogeneous universe. *Mon. Not. Roy. Astron. Soc.*, v. 281, p. 565, 1996. Citado na página 59.
- 138 WANG, Y.; SPERGEL, D. N.; TURNER, E. L. Implications of cosmic microwave background anisotropies for large scale variations in Hubble's constant. *Astrophys. J.*, v. 498, p. 1, 1998. Citado na página 59.
- 139 Lesgourges, J. The Cosmic Linear Anisotropy Solving System (CLASS) I: Overview. *ArXiv e-prints*, abr. 2011. Citado 2 vezes nas páginas 61 and 70.
- 140 EISENSTEIN, D. J.; HU, W. Power spectra for cold dark matter and its variants. *Astrophys. J.*, v. 511, p. 5, 1997. Citado na página 61.
- 141 SMITH, R. E. et al. Stable clustering, the halo model and nonlinear cosmological power spectra. *Mon. Not. Roy. Astron. Soc.*, v. 341, p. 1311, 2003. Citado na página 61.
- 142 AAD, G. et al. Observation of a new particle in the search for the Standard Model Higgs boson with the ATLAS detector at the LHC. *Phys. Lett.*, B716, p. 1–29, 2012. Citado na página 66.
- 143 TROTTA, R. Bayesian Methods in Cosmology. In: . [s.n.], 2017. Disponível em: <<https://inspirehep.net/record/1507974/files/arXiv:1701.01467.pdf>>. Citado 3 vezes nas páginas 66, 67, and 68.
- 144 VERDE, L. Statistical methods in cosmology. *Lect. Notes Phys.*, v. 800, p. 147–177, 2010. Citado 3 vezes nas páginas 66, 67, and 68.
- 145 SELJAK, U.; ZALDARRIAGA, M. A Line of sight integration approach to cosmic microwave background anisotropies. *Astrophys. J.*, v. 469, p. 437–444, 1996. Citado na página 70.
- 146 LEWIS, A.; BRIDLE, S. Cosmological parameters from CMB and other data: A Monte Carlo approach. *Phys. Rev.*, D66, p. 103511, 2002. Citado na página 70.
- 147 WANG, Y.; MUKHERJEE, P. Observational Constraints on Dark Energy and Cosmic Curvature. *Phys. Rev.*, D76, p. 103533, 2007. Citado na página 71.
- 148 KOSOWSKY, A.; MILOSAVLJEVIC, M.; JIMENEZ, R. Efficient cosmological parameter estimation from microwave background anisotropies. *Phys. Rev.*, D66, p. 063007, 2002. Citado na página 71.
- 149 EFSTATHIOU, G.; BOND, J. R. Cosmic confusion: Degeneracies among cosmological parameters derived from measurements of microwave background anisotropies. *Mon. Not. Roy. Astron. Soc.*, v. 304, p. 75–97, 1999. Citado na página 71.
- 150 HU, W.; SUGIYAMA, N. Small scale cosmological perturbations: An Analytic approach. *Astrophys. J.*, v. 471, p. 542–570, 1996. Citado na página 71.

- 151 ADE, P. A. R. et al. Planck 2015 results. XIV. Dark energy and modified gravity. *Astron. Astrophys.*, v. 594, p. A14, 2016. Citado na página 71.
- 152 ALAM, S. et al. The clustering of galaxies in the completed SDSS-III Baryon Oscillation Spectroscopic Survey: cosmological analysis of the DR12 galaxy sample. *Submitted to: Mon. Not. Roy. Astron. Soc.*, 2016. Citado 2 vezes nas páginas 72 and 73.
- 153 BASSETT, B. A.; HLOZEK, R. Baryon Acoustic Oscillations. 2009. Citado na página 72.
- 154 BEUTLER, F. et al. The 6dF Galaxy Survey: Baryon Acoustic Oscillations and the Local Hubble Constant. *Mon. Not. Roy. Astron. Soc.*, v. 416, p. 3017–3032, 2011. Citado na página 73.
- 155 PADMANABHAN, N. et al. A 2 per cent distance to $z=0.35$ by reconstructing baryon acoustic oscillations - I. Methods and application to the Sloan Digital Sky Survey. *Mon. Not. Roy. Astron. Soc.*, v. 427, n. 3, p. 2132–2145, 2012. Citado na página 73.
- 156 ROSS, A. J. et al. The clustering of the SDSS DR7 main Galaxy sample – I. A 4 per cent distance measure at $z = 0.15$. *Mon. Not. Roy. Astron. Soc.*, v. 449, n. 1, p. 835–847, 2015. Citado na página 73.
- 157 ANDERSON, L. et al. The clustering of galaxies in the SDSS-III Baryon Oscillation Spectroscopic Survey: baryon acoustic oscillations in the Data Releases 10 and 11 Galaxy samples. *Mon. Not. Roy. Astron. Soc.*, v. 441, n. 1, p. 24–62, 2014. Citado na página 73.
- 158 KAZIN, E. A. et al. The WiggleZ Dark Energy Survey: improved distance measurements to $z = 1$ with reconstruction of the baryonic acoustic feature. *Mon. Not. Roy. Astron. Soc.*, v. 441, n. 4, p. 3524–3542, 2014. Citado na página 73.
- 159 EISENSTEIN, D. J.; HU, W. Baryonic features in the matter transfer function. *Astrophys. J.*, v. 496, p. 605, 1998. Citado na página 74.
- 160 RIESS, A. G. et al. Observational evidence from supernovae for an accelerating universe and a cosmological constant. *Astron. J.*, v. 116, p. 1009–1038, 1998. Citado na página 74.
- 161 PERLMUTTER, S. et al. Measurements of Omega and Lambda from 42 high redshift supernovae. *Astrophys. J.*, v. 517, p. 565–586, 1999. Citado na página 74.
- 162 KAISER, N. Clustering in real space and in redshift space. *Mon. Not. Roy. Astron. Soc.*, v. 227, p. 1–27, 1987. Citado na página 75.
- 163 ADE, P. A. R. et al. Planck 2013 results. XX. Cosmology from Sunyaev–Zeldovich cluster counts. *Astron. Astrophys.*, v. 571, p. A20, 2014. Citado na página 75.
- 164 BASILAKOS, S.; NESSERIS, S. Conjoined constraints on modified gravity from the expansion history and cosmic growth. *Phys. Rev.*, D96, n. 6, p. 063517, 2017. Citado 2 vezes nas páginas 76 and 116.
- 165 RIESS, A. G. et al. A Redetermination of the Hubble Constant with the Hubble Space Telescope from a Differential Distance Ladder. *Astrophys. J.*, v. 699, p. 539–563, 2009. Citado na página 77.

- 166 VISSER, M. Jerk and the cosmological equation of state. *Class. Quant. Grav.*, v. 21, p. 2603–2616, 2004. Citado na página [77](#).
- 167 MARRA, V. In preparation... 2018. Citado na página [79](#).
- 168 JEFFREYS, H. *Theory of Probability*. Third. Oxford, England: Oxford, 1961. Citado na página [79](#).

APPENDIX A – Maximally symmetric space

In order to solve the Einstein equations, it is necessary to specify the matter content of the universe via $T_{\mu\nu}$. Yet, solutions to the field equations, or at least some features of them, can be obtained without solving directly the Einstein equations. For that, it is necessary to identify some geometrical features of our pseudo-Riemannian manifold, for instance symmetries. Here, we use the cosmological principal and its geometrical consequences in order to obtain some characteristics of the solution of the Einstein equations.

A symmetry is defined when the metric $g_{\mu\nu}$ is form-invariant under coordinate transformations $x \rightarrow x'$, that is

$$g'_{\mu\nu}(y) = g_{\mu\nu}(y) , \quad (\text{A.1})$$

for any y , where $g'_{\mu\nu}(x')$ and $g_{\mu\nu}(x)$ are the metric tensor according to the coordinate systems x' and x , respectively. The set of transformation that leaves form-invariant the metric is dubbed isometries. It is often assumed an infinitesimal transformation, given by

$$x'^{\mu} = x^{\mu} + \varepsilon \xi^{\mu}(x), \quad (\text{A.2})$$

with $|\varepsilon| \ll 1$. If one uses this infinitesimal transformation in the law of transformation of tensor and demands (A.1), obtains:

$$\nabla_{\sigma} \xi_{\rho} + \nabla_{\rho} \xi_{\sigma} = 0 , \quad (\text{A.3})$$

where ξ_{μ} is named Killing vector.

An n -dimensional space that has the maximum number of Killing vectors, that is $n(n+1)/2$ vectors, is called maximally symmetric space. It is obvious that we are interested in four-dimensional spaces, which are maximally symmetric if they have 10 Killing vectors. Also, it can be demonstrated that for a maximally symmetric n -dimensional space, with $n \geq 3$, the curvature tensor is defined by:

$$R_{\lambda\rho\sigma\nu} = K \{ g_{\sigma\rho}g_{\lambda\nu} - g_{\nu\rho}g_{\lambda\sigma} \} , \quad (\text{A.4})$$

and the Ricci tensor

$$R_{\sigma\rho} = -(N-1)Kg_{\sigma\rho} , \quad (\text{A.5})$$

where the constant K is defined as $K \equiv -R^{\mu}_{\mu}/N(N-1)$ [41].

One can think of an extension of these properties to spaces that are not maximally symmetric but rather have a maximally symmetric sub-space. Indeed, results shown before

can be used for such cases. Then, we focus our attention on the restrictions that symmetries set on the metric. For example, consider an n -dimensional space with an m -dimensional maximally symmetric sub-space. It is always possible to choose a coordinate system, with coordinates v and u for the $(n - m)$ -dimensional sub-space and maximally symmetric space, respectively, where the world lines are defined according to [41]:

$$ds^2 = g_{ab}dv^a dv^b + f(v)\bar{g}_{ij}du^i du^j , \quad (\text{A.6})$$

where the indexes $a, b = 1, 2, \dots, (N - M)$ e $i, j = 1, 2, \dots, M$. It is interesting to consider a four-dimensional space, that is $n = 4$, with a three-dimensional maximally symmetric subspace, i.e. $m = 3$. Then, as it is always possible to introduce locally Euclid coordinates, the line element (A.6) becomes:

$$ds^2 = h(t)dt^2 + f(t) \left[dx^2 + \frac{k(\vec{x} \cdot d\vec{x})}{1 - kx^2} \right] , \quad (\text{A.7})$$

where the function $f(t)$ is always positive and k is a constant whose value is associated to the sign of the curvature constant of the maximally symmetric sub-space. That is:

$$k = \begin{cases} +1 & \text{se a constante de curvatura } K > 0 , \\ 0 & \text{se a constante de curvatura } K = 0 , \\ -1 & \text{se a constante de curvatura } K < 0 . \end{cases} \quad (\text{A.8})$$

APPENDIX B – Cosmological distances

There are two ways to measure distances in cosmology: considering or not the expansion of the universe. Distances that are measured not considering the expansion are dubbed comoving distances, which, obviously, do not depend on time. As we will see later, all distance are built from comoving distance. The FLRW metric (1.23) allows us to define the comoving distance. Under assumption of $d\Omega = 0$, it is defined by:

$$d_c = \int_0^r \frac{dr'}{\sqrt{1 - kr'^2}} .$$

We can recast this latter integral as

$$d_c = \frac{1}{H_0} \int_0^\chi \frac{d\chi'}{\sqrt{1 - \Omega_{k0}\chi^2}} ,$$

where we have defined the quantities $\Omega_{k0} \equiv -kd_H^2$, $\chi \equiv r/d_H$ and $d_H \equiv 1/H_0$. Then, it is straightforward to demonstrate that

$$d_c = \begin{cases} \frac{d_H}{\sqrt{\Omega_{k0}}} \sinh[\sqrt{\Omega_{k0}} \frac{r}{d_H}] & \text{for } \Omega_{k0} > 0 , \\ r & \Omega_{k0} = 0 , \\ \frac{d_H}{\sqrt{|\Omega_{k0}|}} \sin[\sqrt{|\Omega_{k0}|} \frac{r}{d_H}] & \text{for } \Omega_{k0} < 0 . \end{cases} \quad (\text{B.1})$$

As it has been mentioned before, in the present work we consider $\Omega_{k0} = 0$, and so, the comoving distance is $d_c = r$. Note that the distance of the radial coordinate, r , will be obtained from the geodesic equations (or simply by the line element). Thus, for a photon, which follows null geodesics (that is $ds^2 = 0$), we have

$$r = \int_t^{t_0} \frac{dt'}{d(t')} = d_H \int_0^z \frac{dz'}{E(z')} ,$$

where $E(z)$ is the normalized Hubble rate defined in Subsection 1.3.4. As all data sets here used are obtained via the observations of photons, the comoving distance is:

$$d_c = \int_0^z \frac{dz'}{H(z')} . \quad (\text{B.2})$$

Analogously, we define the comoving distance travelled by a sound wave of speed c_s as:

$$r_s = \int_0^z \frac{c_s dz}{H(z)} . \quad (\text{B.3})$$

Also, we can define another distances that are related to d_c . For instance, we can define the proper distance, which, unlike the comoving distance, does take into account the expansion of the universe. It is given by:

$$d_p = ad_c = (1 + z)^{-1}d_c . \quad (\text{B.4})$$

and is often called physical distance.

The use of standard candles force us to define a distance related to the intrinsic luminosity, L , and flux, F , of a source. This distance, dubbed luminosity distance, is defined so as to satisfy the relationship $d_L \equiv \sqrt{L/4\pi F}$. Then, it is

$$d_L = (1 + z)d_c . \quad (\text{B.5})$$

Similar is the case of the angular diameter distance. The presence of standard rulers in the universe leads us to define a distance that relates the object's physical transverse size and its angular sizes, which is known as the angular diameter distance. It is defined as:

$$d_A = (1 + z)^{-1}d_c . \quad (\text{B.6})$$

Finally, it is also useful to define the volume averaged distance D_v , which is

$$D_v = \left[d_H(1 + z)^2 z \frac{d_A^2}{E} \right]^{1/3} . \quad (\text{B.7})$$

When cosmological data is used it could be problematic to keep $c = 1$. So, to reinsert the speed of light into the definitions of cosmological distances it is only necessary to perform $d_H = 1/H_0 \rightarrow d_H = c/H_0$.

APPENDIX C – RSD data not marginalized over σ_8

Here we consider the non-marginalized RSD data in order to confirm results from [164]. For that, we also remove the H_0^{loc} from the full likelihood. Thus, we obtain the cosmological constraints under the assumption that $\sigma_8 = 0.815$. From Figure 35 one can

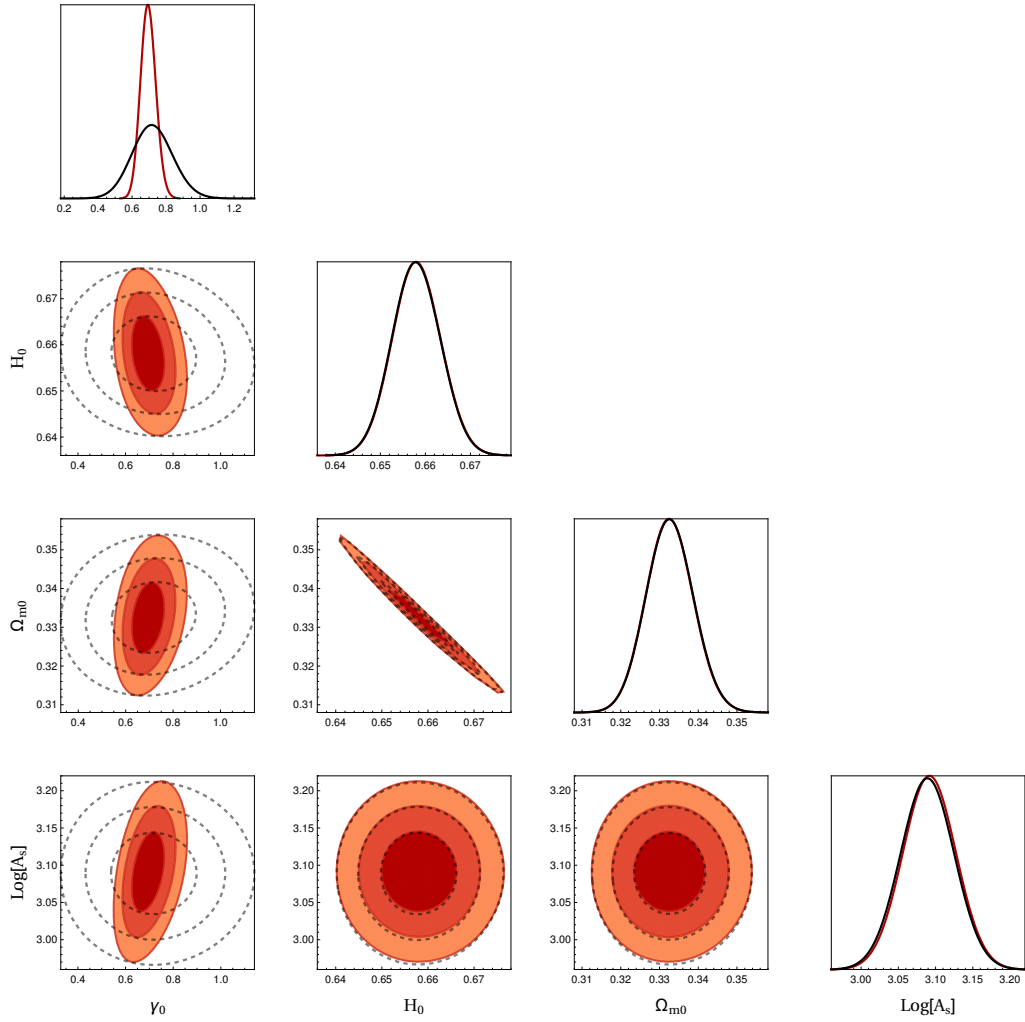


Figure 35 – Cosmological constraints, with non-marginalized RSD data and without the local determination of H_0 , where the contours are 68.3%, 95.4% and 99.7% confidence levels. Note that in the absence of cosmic variance (red contours) $\gamma = 0.55$ is ruled out at about 99.7% confidence level. The best fit of the cosmic growth index is $\gamma = 0.699$.

note that the cosmic index growth rate $\gamma = 0.55$, predicted by Λ CDM, is excluded at about 99.7% confidence level and $\gamma = 0.699$ is quite higher, in concordance with $\gamma = 0.725$ from [164]. When the systematic error, due to the cosmic variance, is considered the values

of the best fit remain practically invariant but the error on γ increases dramatically and so allowing for the value predicted by Λ CDM, $\gamma = 0.55$.